

**IDENTIFICATION AND TARGETING OF
DEREGULATED METABOLIC PATHWAYS
IN METASTATIC PROSTATE CANCER CELLS**

A THESIS SUBMITTED TO
THE GRADUATE SCHOOL OF ENGINEERING AND SCIENCE
OF BILKENT UNIVERSITY
IN PARTIAL FULFILLMENT OF THE REQUIREMENTS FOR
THE DEGREE OF
MASTER OF SCIENCE
IN
MOLECULAR BIOLOGY AND GENETICS

By

Irmak Kaysudu

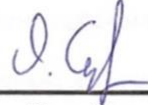
January 2023

**IDENTIFICATION AND TARGETING OF
DEREGULATED METABOLIC PATHWAYS
IN METASTATIC PROSTATE CANCER CELLS**

By Irmak Kaysudu

January 2023

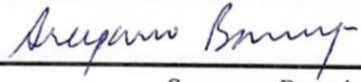
We certify that we have read this thesis and that in our opinion it is fully adequate, in scope and quality, as a thesis for the degree of Master of Science.



Onur Çizmecioglu (Advisor)



Özlen Konu Karakayalı



Sreeparna Banerjee

Approved for the Graduate School of Engineering and Science:



Orhan Arıkan
Director of the Graduate School

ABSTRACT

IDENTIFICATION AND TARGETING OF DEREGULATED METABOLIC PATHWAYS IN METASTATIC PROSTATE CANCER CELLS

“Irmak Kaysudu”

M.S. in Molecular Biology and Genetics

Advisor: Asst. Prof. Onur Çizmecioglu

January 2023

Prostate cancer is the most diagnosed cancer type and the second leading cause of death in men globally. The pathogenesis of prostate cancer mainly relies on the androgen signaling axis. Therefore, androgen deprivation therapy is the primary treatment for prostate cancer. Nevertheless, the disease progression proceeds, followed by castration resistance and androgen independence. Aberrant androgen signaling activity intertwined with the hyperactivated PI3K-Akt signaling pathway has important oncogenic consequences for castration resistance mechanisms. PTEN, a negative regulator of the PI3K/Akt pathway, is one of the most altered tumor suppressor genes in prostate cancer. PTEN loss occurs in the initial stages of prostate cancer and the frequency of its alteration increases in metastatic and castration-resistant prostate cancer. PTEN has both lipid and protein phosphatase activity, with the former antagonizing the PI3K-Akt pathway by converting membrane-associated PIP3 to PIP2. PTEN loss may cause metabolic rewiring in metastatic prostate cancer cells and the associated metabolic vulnerabilities may be tackled for the disease therapy. To understand the impact of PTEN loss in metastatic prostate cancer cells, we created a dox-inducible system in PTEN-null metastatic and castration-naïve LNCaP cells to re-express WT-PTEN and various PTEN functional mutants, and we employed targeted

metabolomics to investigate the direct effects of PTEN loss on selected metabolite levels. We also performed RNA-sequencing to reveal transcriptomic alterations upon PTEN loss to better understand the metabolic deregulations and mechanisms underlying the castration resistance in metastatic prostate cancer. Our multidirectional omics studies suggest that the acquisition of resistance to castration depends on the deregulation of the sphingolipid metabolism in metastatic prostate cancer cells. Furthermore, we showed that PTEN re-expression in metastatic and castration-naïve LNCaP cells attenuated sphingosine kinase levels, which might switch the sphingolipid metabolism towards increased sphingomyelin biosynthesis and ceramide phosphorylation. Moreover, we showed decreased PI3K/Akt pathway activity when we inhibited sphingosine kinase with opaganib in LNCaP cells. Our results also showed a significant upregulation in sphingolipid metabolism in castration-resistant C4-2 cells compared to castration-naïve LNCaP. We treated these cells with several sphingolipid metabolism inhibitors and discovered that castration-resistant prostate cancer cells were more sensitive to opaganib or ARN14988, but not to fingolimod, than castration-naïve prostate cancer cells. These findings suggest that sphingolipid metabolism might be a promising target for the treatment of metastatic and castration-resistant prostate cancer. Understanding changes in sphingolipid metabolism may be critical for developing rational combinatorial targeting strategies for prostate cancer in the long run.

Keywords: Prostate cancer, castration-naïve, castration-resistant, AR, PI3K, PTEN-null, metabolomics, transcriptomics, sphingolipid metabolism, opaganib, ARN14988, fingolimod

ÖZET

METASTATİK PROSTAT KANSERİ HÜCRELERİNDE DEREGÜLE EDİLEN METABOLİK MEKANİZMALARI ORTAYA ÇIKARMAK VE HEDEFLEMEK

“Irmak Kaysudu”

Moleküler Biyoloji ve Genetik, Yüksek Lisans

Tez Danışmanı: Dr. Öğr. Üyesi Onur Çizmecioğlu

Ocak, 2023

Prostat kanseri, dünya çapında, erkeklerde en çok teşhis konulan ve ikinci önde gelen kansere bağlı ölüm nedenidir. Prostat kanserinin patogenezi esas olarak androjen sinyal eksenine dayanır. Bu nedenle, androjen yoksunluğu tedavisi prostat kanserine karşı birincil tedavidir. Bununla birlikte, hastalık ilerlemesi devam eder, ardından kastrasyon direnci ve androjen bağımsızlığı gelir. Hiperaktifleştirilmiş PI3K-Akt sinyal yolu ile iç içe geçmiş anormal androjen sinyal aktivitesi, kastrasyon direnç mekanizmaları için önemli onkojenik sonuçlara sahiptir. PI3K/Akt yolunun negatif düzenleyicisi olan PTEN, prostat kanserinde en çok değiştirilmiş tümör baskılayıcı genlerden biridir. PTEN kaybı, prostat kanserinin ilk evrelerinde meydana gelir ve metastatik ve kastrasyona dirençli prostat kanserinde değişim sıklığı artar. PTEN, hem lipid hem de protein fosfataz aktivitesine sahiptir; birincisi, membranla ilişkili PIP3'ü PIP2'ye dönüştürerek PI3K-Akt yolunu antagonize eder. PTEN kaybı, metastatik prostat kanseri hücrelerinde metabolik yeniden programlanmaya neden olabilir ve ilişkili metabolik zayıflıklar, hastalık tedavisi için ele alınabilir. PTEN kaybının metastatik prostat kanseri hücrelerindeki etkisini anlamak için, WT-PTEN'i ve çeşitli PTEN işlevsel mutantlarını yeniden ifade etmek için PTEN-yoksun metastatik ve kastrasyon-naif LNCaP hücrelerinde doksisisiklin ile indüklenebilir bir sistem oluşturduk ve PTEN

kaybının seçilen metabolit seviyeleri üzerindeki doğrudan etkilerini arařtırmak için hedeflenen metabolomik aracını kullandık. Metastatik prostat kanserinde kastrasyon direncinin altında yatan metabolik düzensizlikleri ve mekanizmaları daha iyi anlamak için PTEN kaybı üzerine transkriptomik deęişiklikleri ortaya çıkarmak için RNA dizilimi de yaptık. Çok yönlü omik arařtırmalarımız, kastrasyona direnç kazanılmasının, metastatik prostat kanseri hücrelerinde sfingolipid metabolizmasının dereęülasyonuna baęlı olduğunu göstermektedir. Ayrıca, metastatik ve kastrasyon-naif LNCaP hücrelerinde PTEN yeniden ekspresyonunun, sfingolipid metabolizmasını artan sfingomyelin biyosentezi ve seramid fosforilasyonuna doęru deęiřtirebilecek sfingosin kinaz seviyelerini zayıflattığını gösterdik. Ayrıca, LNCaP hücrelerinde opaganib ile sfingosin kinazı inhibe ettiğimizde azalmıř PI3K/Akt yolu aktivitesi gösterdik. Sonuçlarımız kastrasyona dirençli C4-2 hücrelerinde, kastrasyona naif LNCaP hücrelerine kıyasla sfingolipid metabolizmasında önemli bir artış gösterdi. Bu hücreleri birkaç sfingolipid metabolizma inhibitörü ile tedavi ettik ve kastrasyona dirençli prostat kanseri hücrelerinin opaganib veya ARN14988'e, kastrasyon-naif prostat kanseri hücrelerine göre fingolimod'a karşı daha duyarlı olduğunu keřfettik. Bu bulgular, sfingolipid metabolizmasının metastatik ve kastrasyona dirençli prostat kanserinin tedavisi için umut verici bir hedef olabileceğini düşündürmektedir. Sfingolipid metabolizmasındaki deęişiklikleri anlamak, uzun vadede prostat kanseri için rasyonel kombinatoriyal hedefleme stratejileri geliřtirmek için kritik olabilir.

Anahtar Sözcükler: Prostat kanser, kastrasyona hassas, kastrasyona dirençli, AR, PI3K, PTEN-yoksun, metabolomik, transkriptomik, sfingolipid metabolizması, opaganib, ARN14988, fingolimod

To the future
With the beloved ones

ACKNOWLEDGEMENT

I would like to give my biggest thanks to my advisor, Asst. Prof. Onur Çizmecioglu. He is a brilliant scientist and an amazing mentor. He has been very supportive throughout my master's journey. I feel very lucky and honored to be his student.

I would like to thank our collaboration group at Boğaziçi University, Prof. Berat Haznedaroğlu, and his research team. They performed mass spectrometry for the targeted metabolomics assay.

I would like to thank OC Lab members. They are the sweetest and the most fun people to work with. I am very lucky to be part of this lovely research environment. I would like to thank Mahnoor Sulaiman for her help in our project and her motivating existence and friendship throughout these years. I would like to promise her a great breakfast in Switzerland. I also would like to thank Şevval Yılmaz for her support and friendship. She has been an amazing colleague. I would like to thank Melda Özge Oğuz for being such a hardworking and brilliant senior student and intern. I am very glad that I worked with each of our group members, exchanging great thoughts and sharing wonderful memories. I also would like to thank Bilkent University MBG family for the collaborative and friendly environment.

I would like to thank Taha Buğra Güngül, who is an alumnus of OC Lab and the best project mate forever. He had been the most wonderful colleague and the best friend to me. I appreciate how much he contributed to me and how much fun we had for two straight years. I am also angry with him to put my standards at the highest level for my prospective colleagues.

I would like to thank Kübra Çalışır for being such a lovely colleague, amazing friend, and wonderful roommate. I am grateful for her support, motivational speeches, and patience with my bioinformatical questions.

I would like to thank my family, Hatice and İsmail Kaysudu. They have been the best parents to me, and I feel their support all the time. I could not succeed without them. I also would like to thank Mehmet Onat. He makes everything beautiful as he did Ankara for me. Without him, I would be lost and what I do is much more meaningful with him. I am extremely thankful to have the most supportive best friends, Berfu Unay and İlayda Mırmır. They have been there for me for anything and anytime.

I would like to thank TUBITAK for Bideb 2210A National M.Sc. Scholarship. This study was granted by two different TUBITAK projects, which are 1001-118Z976 and 1002-121Z791.

TABLE OF CONTENTS

ABSTRACT	ii
ÖZET	iv
ACKNOWLEDGEMENT	vii
LIST OF FIGURES	xi
LIST OF TABLES	xiii
ABBREVIATIONS	xiv
1. INTRODUCTION	1
1.1. Prostate Cancer	1
1.2. PI3K/PTEN/Akt Pathway and its Regulations in Prostate Cancer	3
1.3. PTEN Functions in Prostate Cancer	5
1.4. Sphingolipid Metabolism and its Implications in Prostate Cancer	9
1.5. Aim of the Research	12
2. MATERIALS AND METHODS	13
2.1. MATERIALS	13
2.1.1. Cell Lines.....	13
2.1.2. Cell Culture Reagents.....	14
2.1.3. Solutions.....	15
2.1.4. Western Blot Reagents.....	17
2.1.5. Western Blot Antibodies	18
2.1.6. qPCR Reagents	19
2.1.7. qPCR Primers.....	19
2.1.8. Vectors	20
2.1.9 Kits	21
2.1.10. Equipment.....	21
2.2. METHODS	22
2.2.1. Cell Maintenance, thawing, and freezing	22
2.2.2. Generation of stable cell lines.....	23
2.2.3. Westernblotting Analysis	24
2.2.4. Immunofluorescence assay	26
2.2.5. Cellular Proliferation Assays	27
2.2.6. RT-qPCR.....	28
2.2.7. Targeted Metabolomics	30
2.2.8. RNA-sequencing.....	31
2.2.9. Statistical Analysis	33
3. RESULTS	33
3.1. Introduction of Tet-on Gene Expression System to LNCaP Cell Lines.....	33
3.2. Confirmation of PTEN Functionality in LNCaP PTEN Variants	35

3.3. Determination of the Viability of Dox-inducible LNCaP PTEN variants	38
3.4. Characterization of PI3K/PTEN/Akt pathway in LNCaP PTEN variants	39
3.5. Determination of the metabolome of LNCaP Cells upon different PTEN conditions.....	41
3.6. Identification of the Transcriptome Profile of Castration-Naïve and Castration-Resistant Prostate Cancer Cells.....	49
3.7. Targeting Prostate Cancer Cells with Sphingolipid Metabolism Inhibitors.....	60
3.8. Regulation of PI3K/Akt Pathway upon Sphingolipid Metabolism Inhibition in Castration-naïve Prostate Cancer Cells.....	62
4. DISCUSSION	65
5. CONCLUSION AND FUTURE PERSPECTIVES	78
6. BIBLIOGRAPHY.....	79
7. APPENDIX.....	93
7.1. COPYRIGHT PERMISSIONS	93

LIST OF FIGURES

FIGURE 1.1. AR SIGNALING IN PROSTATE CANCER	2
FIGURE 1.2. PI3K/PTEN/AKT SIGNALING CASCADE.....	4
FIGURE 1.3. PTEN STRUCTURE.....	6
FIGURE 1.4. PHOSPHATASE-DEPENDENT OR -INDEPENDENT PTEN FUNCTIONS	8
FIGURE 1.5. SPHINGOLIPID METABOLISM AND ITS TARGETED INHIBITORS.....	10
FIGURE 3.1. PTEN EXPRESSION IN DOX-INDUCIBLE LNCAP PTEN VARIANTS.....	35
FIGURE 3.2. PH ^{BTK} -GFP FUSION PROTEIN EXPRESSION IN DOX-INDUCIBLE LNCAP PTEN VARIANTS.	36
FIGURE 3.3. PH ^{BTK} -GFP REPORTER INDICATES MEMBRANE-BOUND PIP3 ABUNDANCE IN LNCAP PTEN VARIANTS	37
FIGURE 3.4. THE LIPID PHOSPHATASE FUNCTION OF PTEN DIMINISHES THE CELLULAR VIABILITY IN LNCAP CELLS	39
FIGURE 3.5. CHARACTERIZATION OF PI3K/AKT PATHWAY IN DOX-INDUCIBLE LNCAP PTEN VARIANTS	40
FIGURE 3.6. WORKFLOW OF TARGETED METABOLOMICS.	42
FIGURE 3.7. DISTRIBUTION OF DETECTED METABOLITES BASED ON THEIR METABOLIC CLASSES	43
FIGURE 3.8. SELECTED METABOLITE QUANTIFICATIONS FOR LNCAP CELLS EXPRESSING WILDTYPE PTEN OR PTEN-C124S UPON DOXYCYCLINE INDUCTION	44
FIGURE 3.9. METABOLITE SET ENRICHMENT ANALYSIS IN PTEN-NULL VS PTEN- REplete LNCAP CELLS	46
FIGURE 3.10. THE CONCENTRATIONS OF SPHINGOLIPIDS DECREASE IN LNCAP CELLS UPON PTEN LOSS.....	47
FIGURE 3.11. RELATIVE MRNA EXPRESSION LEVELS OF THE GENES IN SPHINGOLIPID METABOLISM IN PTEN-NULL AND PTEN-REplete LNCAP CELLS	48

FIGURE 3.12. THE MOST SIGNIFICANTLY UPREGULATED PATHWAYS UPON PTEN LOSS IN METASTATIC PROSTATE CANCER CELLS.....	52
FIGURE 3.13.THE MOST SIGNIFICANTLY ENRICHED CANONICAL PATHWAYS IN LNCAP CELLS UPON PTEN LOSS.....	53
FIGURE 3.14. THE MOST SIGNIFICANTLY UPREGULATED PATHWAYS IN C4-2 CELLS COMPARED TO LNCAP CELLS.....	59
FIGURE 3.15. DOSE-RESPONSE CURVES OF LNCAP OR C4-2 CELLS FOR OPAGANIB, ARN14988, AND FINGOLIMOD.....	61
FIGURE 3.16. OPAGANIB INHIBITS LNCAP PROLIFERATION BY DOWNREGULATING THE PI3K/AKT PATHWAY.....	64

LIST OF TABLES

TABLE 2.1 RECIPES FOR RESOLVING AND STACKING GELS	25
TABLE 2.2. CONDITIONS FOR CDNA SYNTHESIS.....	29
TABLE 2.3. CONDITIONS FOR QPCR.....	30
TABLE 2.4. THERMAL CYCLING CONDITIONS FOR QPCR.....	30
TABLE 3.1. DIFFERENT PTEN FUNCTIONS EXPRESSED IN DOX-INDUCIBLE LNCAP CELLS	34
TABLE 3.2. SIGNIFICANT DEGS IN SPHINGOLIPID METABOLISM IN LNCAP CELLS UPON PTEN LOSS.....	50
TABLE 3.3. SIGNIFICANT DEGS IN SPHINGOLIPID METABOLISM IN C4-2 CELLS UPON PTEN LOSS.....	55

ABBREVIATIONS

mCRPC metastatic and castration-resistant prostate cancer

PTEN Phosphatase and tensin homolog

AR Androgen receptor

PSA Prostate-specific antigen

PI3K Phosphatidylinositol-3 kinase

PIP3 Phosphatidylinositol-3,4,5-triphosphate

PIP2 Phosphatidylinositol-4,5-bisphosphate

AKT Serine/threonine kinase

PDK1 3-phosphoinositide-dependent protein kinase 1

mTOR Mammalian target of rapamycin

PH Pleckstrin homology

Btk Bruton's tyrosine kinase

GFP Green fluorescent protein

DEGs Differentially expressed genes

SPT Serine palmitoyltransferase

DES Dihydroceramide desaturase

CERS Ceramide synthase

CERK Ceramide kinase

C1P Ceramide-1-phosphate

SPHK or SK Sphingosine kinase

S1P Sphingosine-1-Phosphate

SGMS Sphingomyeline synthase

ASAH Acid ceramidase (N-acylsphingosine amidohydrolase 1)

LPC Lysophosphotidylcholine

PC Phosphatidylcholine

PC-O Glycerophosphocholine

SM Sphingomyelin

Cer Ceramide

1. INTRODUCTION

1.1. Prostate Cancer

Prostate cancer is the most diagnosed cancer type in males, and it causes over 350.000 deaths each year [1]. Prostate carcinogenesis depends on inherited or somatic gene alterations and environmental factors. Oxidative stress-induced DNA damage by chronic infection and inflammations, or accumulation of genetic and epigenetic arrangements in the genome drive to occur prostate adenocarcinoma [2]. Highly heterogeneous prostate cancer harbors combinations of TMPRSS2-ERG gene fusions, loss of function mutations in the SPOP gene, p53 mutations, or PTEN deletions in the primary and localized stage of the disease, and the alteration frequencies of these genes increase in the advanced-stage prostate cancer (Fraser et al., 2017).

Gain of function mutations in the androgen receptor gene together with the activating mutations in AR-regulating genes or inactivating mutations in AR-repressing genes are the most common alterations in metastatic and castration-resistant prostate cancer [3]. In normal prostate epithelium or castration-sensitive prostate cancer, when AR binds to androgen, they are translocated to the nucleus where it is dimerized and bound to the androgen response element (ARE) in the AR-regulated gene, leading to the gene transcription (**Figure 1.1**). However, aberrant activation of androgen signaling occurs in castration-resistant prostate cancer after androgen deprivation therapy accompanied by AR activating mutations, expression of AR splice variants (AR SVs), or excessive non-specific ligand binding to AR together with intracrine androgen synthesis, thus AR-dependent transcription is upregulated (**Figure 1.1**) [1], [4]–[6].

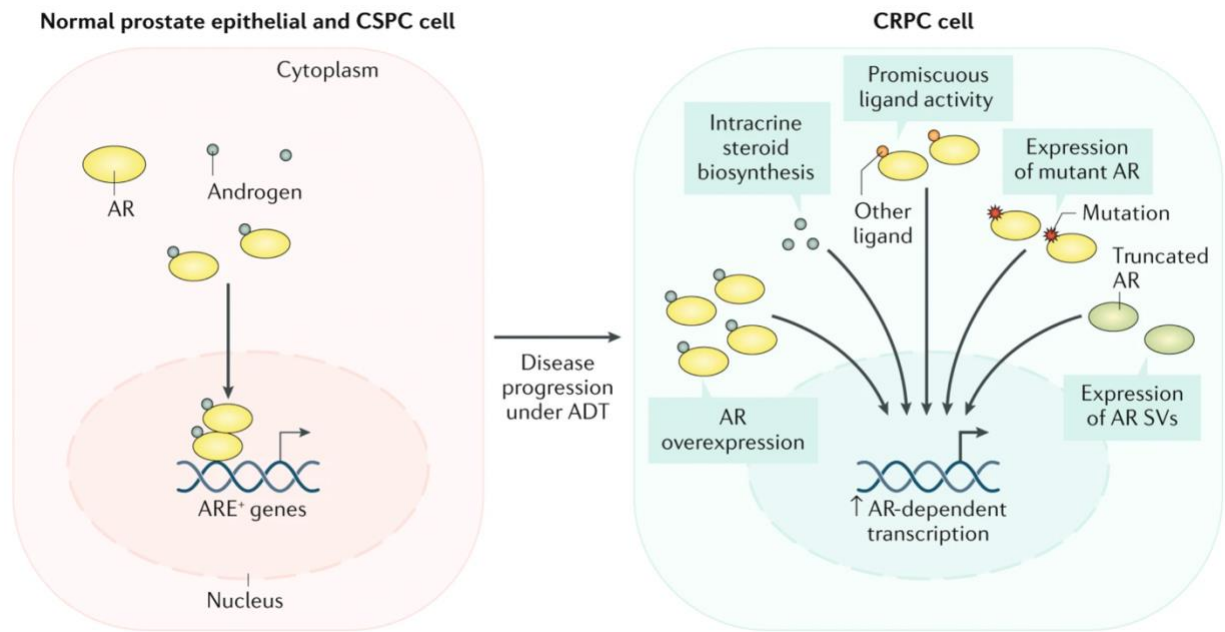


Figure 1.1. AR signaling in prostate cancer. AR can bind to androgen, then it is translocated to the nucleus. When it is dimerized, it is recruited to ARE of the target genes. AR overexpression, AR mutations, expression of AR splice variants, steroid biosynthesis, and binding other ligands to AR can lead to aberrant AR signaling in castration-resistant prostate cancer [1].

During prostate cancer progression, hyperactivation of AR signaling and increases in PSA levels are acquired after androgen deprivation therapy (ADT) or anti-androgen therapy [7]. Additionally, cross-regulation of the hyperactivated PI3K/Akt/mTOR pathway is also an important parameter for prostate cancer progression. Activating mutations in PIK3CA, PIK3CB, or AKT1 with homozygous PTEN deletion facilitates a feedback mechanism with AR signaling, leading to castration-resistant prostate cancer progression [3]. Since these mechanisms are not mutually exclusive, they lead to switching the behavior of androgen signaling inhibitors, such as Enzalutamide (MDV3100), to become AR-agonists for metastatic and castration-resistant prostate cancer [8]. Therefore, it removes available therapeutic options causing a significantly lower chance of survival.

1.2. PI3K/PTEN/Akt Pathway and its Regulations in Prostate Cancer

PI3K/Akt/mTOR pathway is one of the most significant signaling pathways in the event of carcinogenesis. It modulates the proliferation, migration, survival, metabolism, and angiogenesis in tumor cells [9]. This pathway is very frequently mutated in around 40% of primary prostate cancers, and around 70% of metastatic prostate cancers, including amplifications and activating mutations in PIK3CA or PIK3CB and activating mutations in AKT, and homozygous PTEN deletion as well [10].

PI3Ks, which are membrane-associated lipid kinases, have three different classes (class I, II, or III) based on their variable structures and substrates. Class I PI3Ks are divided into two subclasses, which are class IA or class IB PI3Ks. Class IA PI3Ks are composed of p110 catalytic subunits, which are encoded by PIK3CA, PIK3CB, or PIK3CD genes, and p85 regulatory subunits, which are encoded by PIK3R1, PIK3R2, or PIK3R3 genes [11].

Extracellular signals such as growth factors (EGF, insulin, insulin-like growth factor 1) and peptide hormones stimulate PI3K phosphorylation. PI3K phosphorylates phosphatidylinositol (4,5)-bisphosphate (PIP₂) to produce phosphatidylinositol (3,4,5)-trisphosphate (PIP₃) (**Figure 1.2**). Membrane-bound secondary messenger PIP₃ recruits PH-domain containing kinases AKT (PKB) and PDK1 to the cell membrane, and PDK1 phosphorylates AKT at T308 residue. AKT is also phosphorylated at S473 residue by mTORC2, and it becomes fully activated, thus it phosphorylates downstream effectors for further regulations in proliferation, survival, migration, nutrient metabolism, or angiogenesis [9].

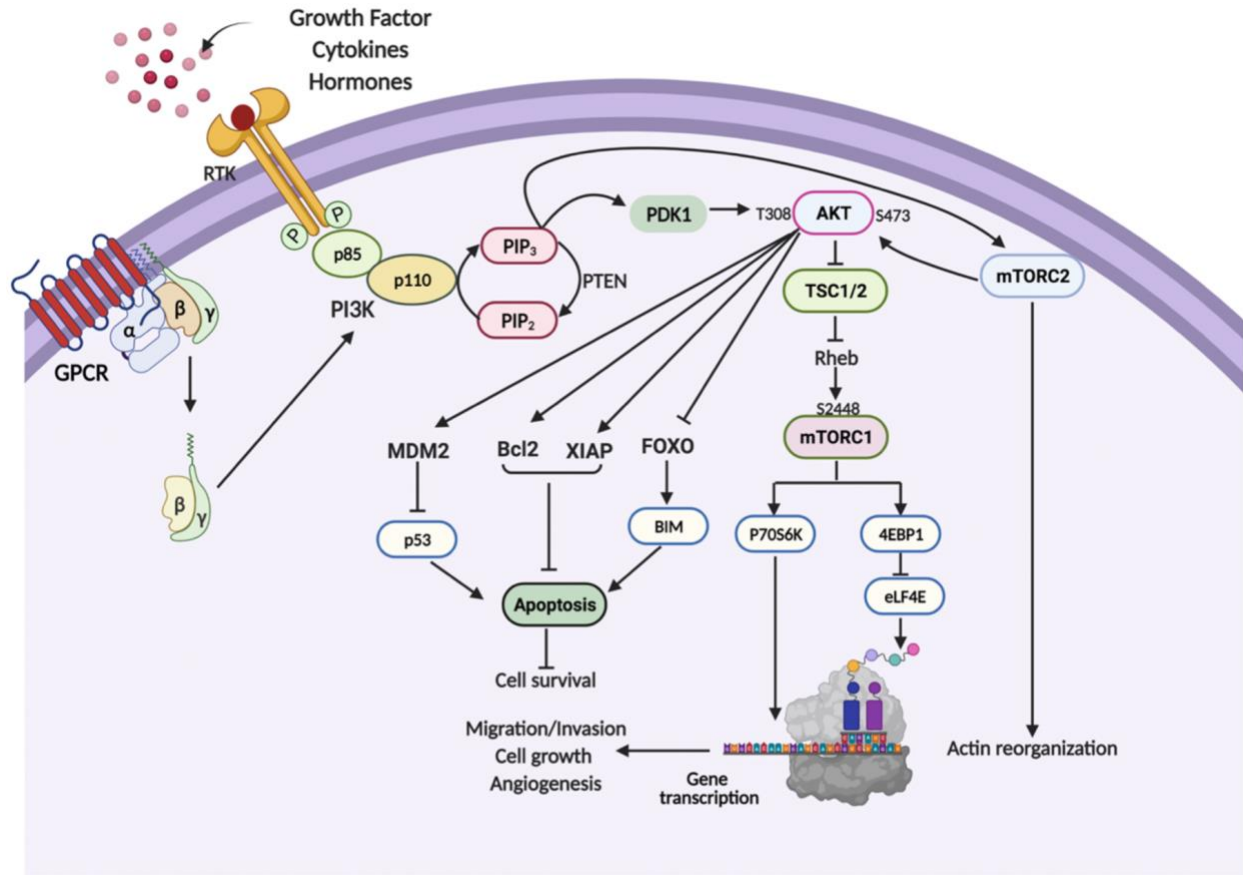


Figure 1.2. PI3K/PTEN/Akt Signaling Cascade. Growth factors, cytokines, and hormones can bind to RTKs or GPCRs. When the receptors are activated, PIP3 is produced, which recruits and promotes AKT activation. Activated AKT phosphorylates downstream mediators to promote survival, migration, cell growth, angiogenesis, and protein synthesis [12].

The most important regulator of the pathway is PTEN, a tumor suppressor gene, which is frequently altered in prostate cancer. It dephosphorylates membrane-bound PIP3 to convert it back to PIP2, thus it negatively regulates PI3K/Akt pathway by antagonizing the PI3K activity (**Figure 1.2**) [13]. Genetic alterations of PTEN are accounted for as the primary factor in the activation of the PI3K/Akt signaling cascade. PTEN is inactivated in 16% of primary prostate cancer and 40% of metastatic prostate cancer by harboring biallelic deletion in its phosphatase domain, whereas

12% of primary prostate cancer and 17% of advanced prostate cancer have PI3K and AKT amplification mutations [3], [14].

1.3. PTEN Functions in Prostate Cancer

Phosphatase and tensin homolog deleted on chromosome 10 (PTEN) is a very frequently mutated tumor suppressor gene, which has both protein and lipid phosphatase functions. PTEN encodes a protein consisting of 403 amino acids and five domains, which are the N-terminal PIP2 binding domain (PBD), the phosphatase domain catalyzing dephosphorylation function, the C2 domain facilitating lipid and membrane binding, the C-tail domain and the PDZ-binding domain (**Figure 1.3**) [15], [16].

PTEN was found to cause PTEN hamartoma tumor syndromes (PHTS) by harboring rare autosomal dominant germline mutations which lead to multiple hamartomatous lesions and susceptibility to cancer development [17], [18].

PTEN is a haploinsufficient tumor suppressor gene, which means that a deletion of an allele leads to improper functionality [19]. Previous research on human samples or mice bearing partial PTEN loss displayed that the incidence of tumor formations correlated with the PTEN loss in a dose-dependent manner. Additionally, it was shown that PTEN is indispensable for embryonic development, and complete PTEN loss caused embryonic lethality in genetically engineered mouse models [20]. Studies on hypermorphic PTEN mice demonstrated that a little reduction in PTEN protein levels caused transcriptional changes in proliferation-related genes and enhanced cancer susceptibility, while hypomorphic PTEN mice models showed accelerated cancer progression and severity in the diseases in various types of cancer [21], [22]. These findings suggest a continuum model for PTEN functionality, indicating that even a minor downregulation

of the expression levels, even though it has both alleles, is sufficient to weaken tumor suppressor functionality of PTEN in a dose-dependent manner [23].

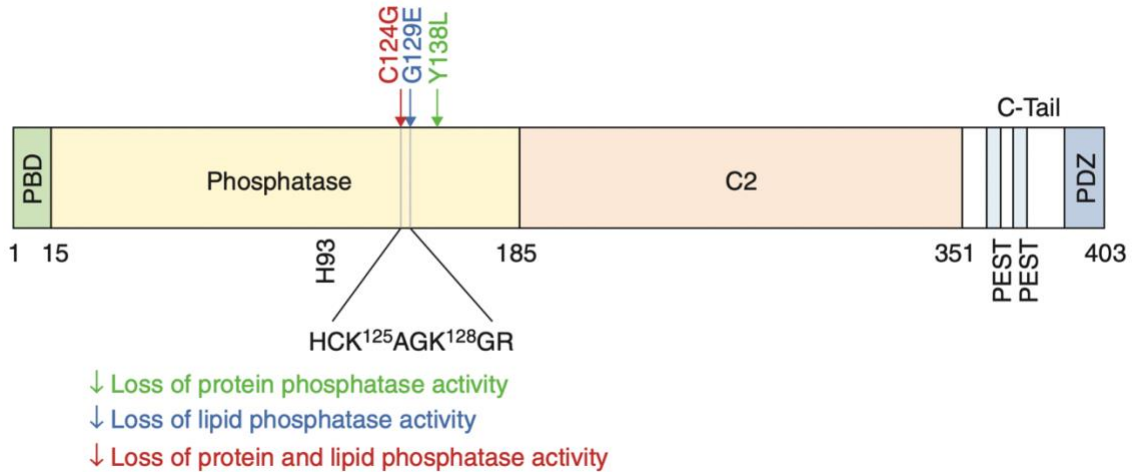


Figure 1.3. PTEN structure. PTEN consists of five domains, which are the PIP2-binding domain (PBD), phosphatase domain, C2 domain, C-tail domain, and PDZ domain. Indicated point mutations in the phosphatase domain lead to inactivation of either protein phosphatase, lipid phosphatase, or dual phosphatase functions [24] “© Cold Spring Harbor Laboratory Press”.

PTEN has a dual-specificity phosphatase function, which can dephosphorylate lipid and protein substrates. The lipid phosphatase function of PTEN dominates PI3K/Akt pathway regulation, dephosphorylating PIP3, and converting it to PIP2. It exerts its tumor suppressor activity by negatively regulating the pathway and hinders cell growth, survival, and migration [17].

PTEN also shows protein phosphatase activity on phosphorylated tyrosine, threonine, and serine residues, as well as residues on itself [16]. To date, the focal adhesion kinase 1 (FAK1), cAMP-responsive element-binding protein 1 (CREBP1), protein-tyrosine kinase SRC, insulin receptor substrate 1 (IRS1), glucocorticoid receptor (GR) were found to be some of the protein substrates for PTEN to act as a tumor suppressor [25]–[28]. The protein phosphatase function of PTEN

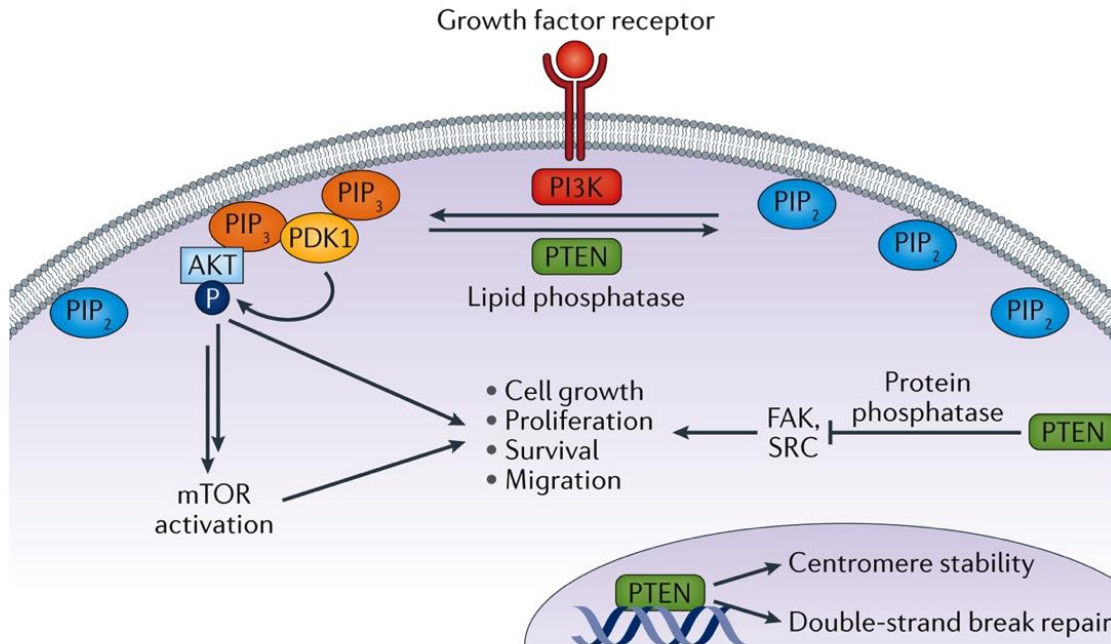
facilitates the active and open conformation of PTEN and increases its stability, modulates cell migration, invasion, and gene transcription, and preserves the genome stability [16].

Additionally, some studies showed the phosphatase-independent function of PTEN to exert its tumor suppressive activity by scaffold functions in the nucleus and cytoplasm. PTEN can bind to centromere protein C (CENPC) to sustain the centromere stability and also contributes to the double-strand break repair mechanism by RAD51 induction in the nucleus [29]. The same study suggests that PTEN loss is associated with impaired genomic stability. Importantly, other studies also demonstrated that nuclear PTEN loss was also associated with cancer aggressiveness, which indicates the contribution of nuclear PTEN to its tumor suppression function [30], [31].

Characterization of point mutations in the phosphatase domain of PTEN enabled the identification of different roles of PTEN phosphatase function (**Figure 1.3**). G129E mutation in PTEN causes lipid phosphatase deficiency, but it displays protein phosphatase functionality. In contrast to this, the Y138L mutation in PTEN shows impaired protein phosphatase function but intact lipid phosphatase function. Besides, the C124S mutation of PTEN exhibits phosphatase-dead function, where both lipid and protein phosphatase functions are lost [32], [33]. Although these mutations identified different active roles of PTEN in many experimental setups, the physiological relevance of these mutations has not been elusive yet.

PTEN deficiency in cancer can regulate a variety of physiological processes including proliferation and motility, genome stability, stem cell maintenance, senescence, tumor microenvironment, as well as metabolism [15]. Loss of PTEN or hyperactivation of the PI3K/Akt pathway can alter the metabolic needs of cancer cells to maintain their growth and survival [34]. Primarily, cancer cells can go through a metabolic switch from oxidative phosphorylation to aerobic glycolysis, which is termed by the Warburg effect, to sustain their growth and proliferation [35]. They can also regulate

glutamine uptake and glutaminolysis to cover the needs for intermediates in the tricarboxylic acid cycle, NADPH, phospholipid synthesis, and nucleotide synthesis [36].



Nature Reviews | Urology

Figure 1.4. Phosphatase-dependent or -independent PTEN functions. PTEN negatively regulates PI3K/Akt pathway by its lipid phosphatase function, dephosphorylating PIP₃ into PIP₂. Protein phosphatase function can dephosphorylate protein substrates, e.g., FAK, and Src. Phosphatase-independent/scaffold functions provide centromere stability and contribute genome stability [37].

PTEN loss also increases protein synthesis by the regulation of mTOR pathway components, which are eukaryotic translation initiation factor 4E-binding protein (4EBP1) and p70S6K [38]. The studies in heterozygous PTEN inactivation mice showed upregulated insulin-mediated glucose uptake by enhanced GLUT4 translocation to the plasma membrane [39], [40]. PTEN deficiency also mediates insulin-induced hepatic gluconeogenesis through the hyperactivated

PI3K/Akt pathway by inhibiting downstream effectors like FOXO1 and PGC1 α [15]. Moreover, increased activity of PI3K/Akt pathway with PTEN loss also demonstrated upregulation in lipid biosynthesis via the activity of sterol regulatory element-binding proteins (SREBPs) in metastatic prostate cancer [41], [42]. A recent study also showed that prostate-specific PTEN-null mice exhibited metabolic deregulation in polyamine biosynthesis via the mTORC1-dependent AMD1 stability [43]. Considering these findings, it would be crucial to elucidate metabolic deregulation and target metabolic vulnerabilities upon PTEN inactivation in cancer.

1.4. Sphingolipid Metabolism and its Implications in Prostate Cancer

Sphingolipids, which are one of the main components of the plasma membrane and responsible for preserving the fluidity and barrier of the membrane, modulate cell signaling, proliferation, migration, and metastasis [44], [45].

The main lipid molecule of the sphingolipid metabolism pathway is ceramide, which is composed of an amide-linked fatty acyl chain and a sphingosine long-chain base. It can be synthesized by *de novo* synthesis, hydrolysis of sphingomyelin, glucosylceramides or galactosyl ceramides, or the salvage pathway (**Figure 1.5**) [45].

The *de novo* synthesis of ceramides, which occurs in the endoplasmic reticulum, begins with the condensation reaction of serine and palmitoyl-CoA by serine palmitoyl-transferase (SPT) activity, which yields the production of 3-ketosphinganine. Then, it is reduced to sphinganine by the 3-ketosphinganine reductase enzyme. After this step, dihydroceramide is produced by ceramide synthases (CERS1-6), which are the rate-limiting enzymes for ceramide production by the *de novo* synthesis. Then, dihydroceramide desaturase (DES) produces ceramide from dihydroceramide by desaturation reaction through the addition of a double bond between C4 and C5 in the long chain base (**Figure 1.5**) [46].

On the other hand, ceramides are also produced by either sphingomyelinase, which hydrolyzes sphingomyelins, or by glucoceramidase (GlcCDase) and galactoceramidase (GCDase) hydrolyzing glucosylceramides and galactosyl ceramides, respectively (**Figure 1.5**) [47]. The salvage pathway is another way to generate ceramides from sphingosine by ceramide synthase enzymes (CERS1-6) (**Figure 1.5**) [48].

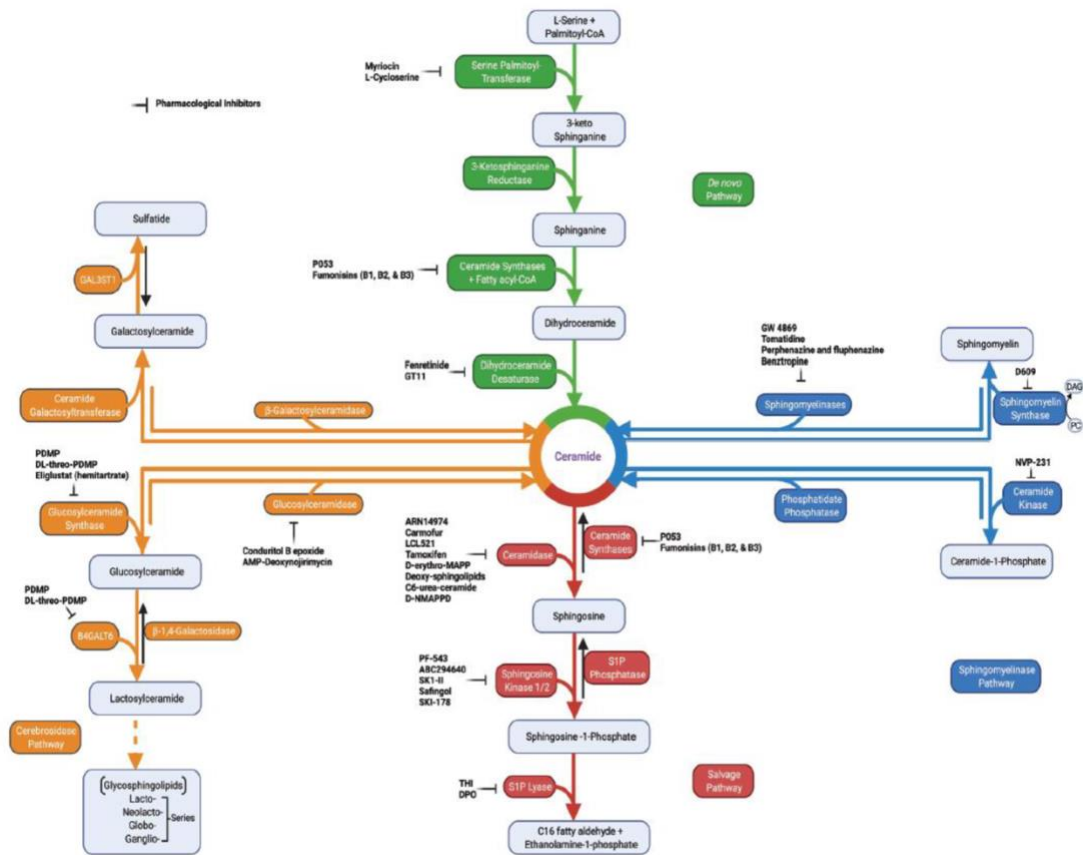


Figure 1.5. Sphingolipid Metabolism and its targeted inhibitors. Ceramides are the main lipid molecules in the pathway. They can be synthesized by de novo biosynthesis, the salvage pathway, the sphingomyelinase pathway, and the cerebrosidase pathway [49].

Ceramides can be utilized for the production of ceramide-1-phosphate or sphingomyelins by ceramide kinases (CERK) or sphingomyelin synthases (SMS1 or SMS2), respectively (**Figure 1.5**) [50], [51].

Glucosylceramide or galactosyl ceramides, which are produced by glucosylceramide synthase (GCS) from ceramides, are further processed to the complex sphingolipids, such as glycosphingolipids or gangliosides in Golgi (**Figure 1.5**) [52].

Furthermore, ceramidases (CDases) hydrolyze ceramides to generate sphingosines, which are further phosphorylated to sphingosine-1-phosphate (S1P) by sphingosine kinases (SPHK1/SK1 or SPHK2/SK2) (**Figure 1.5**). S1P can interact with S1P receptors (S1PR1-5), which are G protein-coupled receptors evoking survival signals in cancer cells [53]. Then, S1P lyase 1 (SPL) catalyzes the reaction converting S1P to ethanolamine-1-phosphate and C16 fatty aldehyde, whereas sphingosine-1-phosphate phosphatase (SGPP) dephosphorylates S1P to yield sphingosine (**Figure 1.5**) [54].

Prostate cancer can be regulated via alterations in sphingolipid metabolism, which may control cell cycle, survival, or drug resistance mechanisms. To date, ceramides are shown to be associated mostly with anti-survival responses of cancer cells, whereas the generation of sphingosine-1-phosphate leads to cancer progression, survival, and therapy resistance [55]. Studies in androgen-responsive LNCaP cells showed cell cycle arrest and increased apoptosis by building up the ceramides in the androgen deprivation therapy [56]. Although ceramides have been shown to be upregulated by radiation therapy and led to anti-cancer effects, some studies also demonstrated boosted resistance to radiation therapy or chemotherapy by ceramides [57], [58].

The enzymes of sphingolipid metabolism are shown to be regulated in prostate cancer. A recent study showed that DES1 is an AR-regulated gene, and the downregulation of DES1 led to a

diminished migration ability in metastatic and castration-resistant C4-2 cells [59]. The study also demonstrated a correlation between high DES1 expression and poor prognosis in the prostate cancer [59]. ASAH1, which is one of the ceramidases that generate sphingosine from ceramide, was observed to be increased in prostate tumor samples and was associated with an enhanced Akt phosphorylation [60]. It also promotes sphingosine kinase 1 activity for the sphingosine-1-phosphate production, activating PI3K, and promoting PTEN nuclear export [60]. Furthermore, sphingosine kinase genes were found to be positively associated with metastatic prostate cancer. SPHK gene expression is increased in metastatic prostate cancer tumors, compared to primary tumors [48]. Besides, sphingomyelin biosynthesis by the catalysis of sphingomyelin synthase enzymes (SGMS1 or SGMS2) has pleiotropic effects on the cancer development [61].

For the last few decades, sphingolipid metabolism has been a highlight to elucidate the mechanism behind carcinogenesis. How sphingolipid metabolism is regulated in various types of cancer remains elusive. The development of therapeutic substances against the enzymes involved in sphingolipid metabolism and targeting them became a promising approach for anti-cancer treatments and overcoming drug resistance mechanisms in cancer (**Figure 1.5**).

1.5. Aim of the Research

Prostate cancer is the most commonly diagnosed cancer type and the second leading cause of death in men annually and globally [2]. Hyperactivation of the PI3K/Akt signaling pathway has important oncogenic consequences in prostate cancer [13]. PTEN, a negative regulator of the pathway, is one of the most frequently altered tumor suppressor genes in metastatic and castration-resistant prostate cancer [14]. PTEN has both protein and lipid phosphatase activity, with the latter antagonizing the PI3K/Akt pathway by converting PIP3 to PIP2 [37]. PTEN loss occurs at the very

early stages of prostate carcinogenesis [3], thus it may cause metabolic rewiring in metastatic prostate cancer cells. These metabolic vulnerabilities may allow for the identification of new therapeutic target genes for prostate cancer. In this research, we wanted to understand the impact of PTEN loss on prostate cancer metabolism. For this purpose, we created a doxycycline-inducible system in PTEN-null metastatic prostate cancer cells to re-express wild-type PTEN and various PTEN function mutants, then we utilized targeted metabolomics and transcriptomics to reveal the direct effects of PTEN loss on the metabolome and transcriptome profiles of PTEN-null metastatic prostate cancer cells. Then, we aimed to target the candidate metabolic genes and/or pathways with the appropriate inhibitors and discover their mechanistic consequences on metastatic prostate cancer cells.

2. MATERIALS AND METHODS

2.1. MATERIALS

2.1.1. Cell Lines

Cell Line	Complete Medium
LNCaP (parental)	RPMI-1640; 8% FBS; 1% P/S
LNCaP with Tet-on system expression (LNCaP-rtTA, LNCaP-rtTA-pRXTN, LNCaP-rtTA-pRXTN-pBabe-PH-Btk-GFP)	RPMI-1640; 8% Tet-Free FBS; 1% P/S
C4-2 (parental)	RPMI-1640; 8% FBS; 1% P/S
HEK293	DMEM; 8% FBS; 1% P/S

2.1.2. Cell Culture Reagents

Catalog Number	Product Name	Brand
P04-17500	RPMI	Pan-Biotech, Germany
41966-029	DMEM	Gibco, US
S1810-500	Fetal Bovine Serum (FBS)	Biowest, US
S181T-500	Tetracycline-Free FBS	Biowest, US
15140-122	Penicillin-Streptomycin	Gibco,US
25300-054	Trypsin-EDTA (0.05%)	Gibco,US
L3000-008	Lipofectamine 3000	Thermo Scientific, US
631455	Retro-X Concentrator	Takara Bio, US
AB-101L	Nourseothricin (NAT)	Jena Bioscience, Germany
10131-035	Geneticin (G418 Sulfate)	Gibco, US
A111138-03	Puromycin	Gibco, US
D9891-1G	Doxycycline Hyclate	Sigma-Aldrich, US
10587	ABC294640 (Opaganib)	Cayman Chemical, US
24284	ARN14988	Cayman Chemical, US
10006292	Fingolimod (Hydrochloride)	Cayman Chemical, US
1H72652	PBS, 10X pH 7.4	BioShop, Canada
P36931	ProLong Gold Antifade reagent with DAPI	Invitrogen, US
5100-0001	Mr. Frosty Freezing Container	Thermo Scientific, US

2.1.3. Solutions

Solutions	Ingredients
10X TBS	80 g NaCl 2 g KCl 30 g Trizma-Base pH adjusted 7.4 with HCl Complete with ddH ₂ O up to 1L
1X TBS-T	1 mL Tween-20 100 ml 10X TBS Complete with ddH ₂ O up to 1L
Cell Lysis Buffer	1X RIPA 1X Protease inhibitor 1X Phosphatase inhibitor mix 1 μ M DTT 1 mM Na ₃ VO ₄
Resolving Gel Buffer (pH=8.8)	187 g Trizma-Base pH adjusted to 8.8 with HCl Complete volume up to 1 liter with ddH ₂ O
Stacking Gel Buffer (pH=6.8)	60.5 g Trizma-Base pH adjusted to 6.8 with HCl Complete volume up to 1 liter with ddH ₂ O
10X Running Buffer (Western Blot)	30 g Trizma-Base

	144 g Glycine
	10 g SDS
	Complete volume up to 1 liter with ddH ₂ O
10X Transfer Buffer (Western Blot)	30.3 g Trizma-Base
	144.1 Glycine
	Complete volume up to 1 liter with ddH ₂ O
1X Transfer Buffer (Western Blot)	100 ml 10X Transfer Buffer
	200 ml Methanol
	700 ml ddH ₂ O
5% Milk Blocking Solution (Western Blot)	5 mg milk powder
	100 ml 1X TBS-T
5% BSA Blocking Solution (Western Blot)	5 mg BSA Fraction V
	100 ml 1X TBS-T
Cell Fixation Solution (4% PFA)	4 g Paraformaldehyde
	100 ml 1X PBS
Crystal Violet Staining Solution	0.4% crystal violet powder
	20% Ethanol
	Complete with ddH ₂ O
Destaining Solution	10% Acetic Acid
	0.5% SDS
	Complete with ddH ₂ O
50% Trichloroacetic acid (TCA) (w/v)	50 g TCA

	100 ml ddH ₂ O
0.4% SRB (w/v)	400 mg SRB 100 ml 1% Acetic Acid
1% Acetic Acid	1% Acetic Acid Complete with ddH ₂ O
50X TAE	242 g Trizma-base 57.1 mL acetic acid 100 mL 0.5M EDTA

2.1.4. Western Blot Reagents

Catalog Number	Product Name	Brand
161-0747	Laemmli Sample Buffer (4x)	Bio-Rad, US
10688.01	Acrylamide/Bisacrylamide Solution (30w/v)	Serva, Germany
K-12045-D20	WesternBright ECL kit	Advansta, US
11930.03	Albumin Bovine Fraction V, pH 7.0	Serva, Germany
773301	Prime-Step Protein Ladder	BioLegend, US
23391.02	Glycine	Serva, Germany
39055.01	Phosphatase Inhibitor Mix	Serva, Germany
P0758S	Sodium Orthovanadate	New England Biolabs, US
PIC002.1	Protease Inhibitor Cocktail, Powder without EDTA	BioShop, Canada

2502	ReBlot Plus Mild Stripping Solution, 10X	Merck, Germany
2504	ReBlot Plus Strong Stripping Solution, 10X	Merck, Germany
GE10600003	Nitrocellulose Blotting Membrane	Merck, Germany
PS05	ClearBand Ponceau S Tween 20	EcoTech, Turkey Serva, Germany

2.1.5. Western Blot Antibodies

Catalog Number	Product Name	Brand
7076S	Anti-Mouse IgG, HRP-linked	Cell Signaling Technology, US
7074S	Anti-Rabbit IgG, HRP-linked	Cell Signaling Technology, US
2118S	GAPDH (14C10) Rabbit mAb	Cell Signaling Technology, US
9559S	PTEN (138G6) Rabbit mAb	Cell Signaling Technology, US
9272S	Akt Rabbit mAb	Cell Signaling Technology, US
9018P	Phospho-Akt1 (Ser473) Rabbit mAb	Cell Signaling Technology, US
4056S	Phospho-Akt (Thr308) Rabbit mAb	Cell Signaling Technology, US
2072S	mTOR Rabbit mAb	Cell Signaling Technology, US
2974S	Phospho-mTOR (Ser2481) Rabbit mAb	Cell Signaling Technology, US

2317S	S6 Ribosomal Protein Mouse mAb	Cell Signaling Technology, US
2215S	Phospho-S6 Ribosomal Protein (Ser240/244) Rabbit mAb	Cell Signaling Technology, US
4858S	Phospho-S6 Ribosomal Protein (Ser235/236) Rabbit mAb	Cell Signaling Technology, US
9452S	4EBP1 Rabbit mAb	Cell Signaling Technology, US
9451S	Phospho-4EBP1 (Ser65) Rabbit mAb	Cell Signaling Technology, US
SC-271616	SREBP2 Mouse mAb	Santa Cruz Biotechnology, US
40659S	SQLE Antibody	Cell signaling Technology, US
9101	Phospho-p44/42 MAPK (Erk1/2) T202/Y204	Cell Signaling Technology, US

2.1.6. qPCR Reagents

Catalog Number	Product Name	Brand
170-8891	iScript cDNA Synthesis Kit	Bio-Rad, US
L003037B	SSoAdvanced Universal IT SYBR Green Supermix	Bio-Rad, US
04729692001	LightCycler 480 Multiwell Plate 96, White	Roche Life Sciences, US

2.1.7. qPCR Primers

Gene (Human)	Forward Primer	Reverse Primer
--------------	----------------	----------------

RPL19	CGGAAGGGCAGGCACAT	GGCGCAAATCCTCATTCTC
ACTB	CACTCTTCCAGCCTTCCTT	CTCGTCATACTCCTGCTTGCT
SPHK1	TATGAATGCCCTACTTGGTATTG	GCCTCGCTAACCATCAATTCC
SGMS2	CTTAGCCCTCCACTCCC	CAGAATCTGCGTCCCAC
CERK	CACCTTAGCCTCCATCACCCTG	AACATACCATCTCCGCCGACAC
DES1	CTATGCGTTTGGCAGTTGCA	CAGTTGCCAAAGGCAGCATT
SPTLC1	CAGAACCTCTTGTTCCCTCCTGTC	TTTTGTGGCTTGGAGGGC
CERS2	AGATCATCCACCATGTGGCC	TGATTAGAGTCCCAGCTCGGA
ASAH1	AGTTGCGTCGCCTTAGTCCT	TGCACCTCTGTACGTTGGTC

2.1.8. Vectors

Catalog Number	Vectors	Brand
Addgene plasmid #8454	pCMV-VSV-G	Addgene, USA
Addgene plasmid #14887	Gag/pol	Addgene, USA
Addgene plasmid #47916	pRXTN expression plasmid	Addgene, USA
	pRXTN-PTEN-WT	Generated in-house
	pRXTN-PTEN-Y138L	Generated in-house
	pRXTN-PTEN-G129E	Generated in-house
	pRXTN-PTEN-C124S	Generated in-house
	pBabe-puro-PH-Btk-GFP	Generated in-house

2.1.9 Kits

Catalog Number	Product Name	Brand
169014875	Plasmid Midi Kit	Qiagen, Germany
11922402	NucleoSpin RNA Isolation Kit	Macherey-Nagel, Germany
21071	SMART BCA Protein Assay Kit	Intron Biotechnology, South Korea
21018.1	AbsoluteIDQ® p400 HR Kit	Biocrates, Austria

2.1.10. Equipment

Equipment	Brand
Mini-Protean Tetra Cell	Bio-Rad, US
Amersham Imager 600	GE Healthcare, US
Centrifuges	Hettich, Germany
	Nuve, Turkey
Cell Culture Hood	Nuaire, US
CO ₂ Incubator	Thermo Scientific, US
Nanodrop one	Thermo Scientific, US
Synergy HT Microplate Reader	Biotek, US
LightCycler 96 Sytem for qPCR	Roche Life Sciences, US
Thermocycler for PCR	Bio-Rad, US
Fluorescence Microscope AX10 Imager.A1	Zeiss, Germany

2.2. METHODS

2.2.1. Cell Maintenance, thawing, and freezing

LNCaP parental or LNCaP-rtTA-pRXTN-PTEN variants or LNCaP-rtTA-pRXTN-pBabe-PH-Btk-GFP cell lines were used in this study. Only for the transfection protocol, the HEK293 cell line was used. The cells were sub-cultured when they reached around 80% confluency. They were washed with sterile 1X PBS, then detached by trypsinization for 5 minutes at 37°C and 5% CO₂. Next, the cells were collected with complete media in a falcon tube. They were centrifuged for 5 minutes at 1500 rpm. After discarding the supernatant, the cells were resuspended with complete media and seeded on a 10-cm culture dish with a 1:6 dilution ratio. LNCaP-rtTA-pRXTN cells were maintained with the appropriate amount of geneticin (50 ug/ml) and noursethricin (50 ug/ml). LNCaP-rtTA-pRXTN-pBabe cells were maintained with the appropriate amount of geneticin (50 ug/ml), noursethricin (50 ug/ml), and puromycin (0.2 ug/ml). The cells were incubated at 37°C and 5% CO₂.

For the freezing procedure, the cells were trypsinized, then centrifuged as passaging protocol. After the centrifugation, the supernatant was discarded and the cells were resuspended with a freezing medium consisting of 50% FBS, 40% RPMI-1640 (or DMEM for the HEK293 cell line), and 10% DMSO. The cells were put into the cryovials and then the cryovials were placed into Mr. Frosty freezing container and incubated at -80°C for at least 5 hours. Then, the cryovials were transferred to nitrogen for longer cryopreservation.

The cells were thawed in the water bath at 37°C for 2-3 minutes for the thawing procedure. Then, they were transferred to a falcon tube containing a complete medium. They were centrifuged for 5

minutes at 1500 rpm. After centrifugation, the supernatant was discarded, and the cells were resuspended with a complete medium without antibiotics and seeded on 6-cm culture dishes. The cells were incubated at 37°C and 5% CO₂.

2.2.2. Generation of stable cell lines

Doxycycline-inducible Tet-on gene expression systems were stably generated in LNCaP cells.

LNCaP cells expressing rtTA plasmid (TetR expression plasmid) were transduced with pRXTN, pRXTN-PTEN-WT, pRXTN-PTEN-Y138L, pRXTN-PTEN-G129E, pRXTN-PTEN-C124S retroviral expression plasmids separately. Additionally, dox-inducible LNCaP PTEN variants were stably transduced with pBabe-PH-Btk-GFP retroviral expression plasmid. First, HEK293 cells were seeded at a density of 0.2×10^6 per well on 6-well plates. The next day, the cells were triple-transfected with 2 µg of DNA-of-interest, 1 µg of pCMV-VSV-G, and 1 µg of gag/pol according to the manufacturer's protocol (Lipofectamine 3000, ThermoScientific). The next day, the medium was replenished. At 48-hour and 72-hour post-transfection, the supernatants were collected in sterile falcon tubes, wrapped with aluminum foil, and incubated at 4°C until the infection. At 24-hour pre-infection, the supernatant was sterile filtered by a 0,45 µm syringe filter. The Retro-X Concentrator (Takara Bio, USA) was added to the supernatant at a volume of one-third of the supernatant volume and incubated at 4°C overnight in the dark. On the day of infection, the supernatant and concentrator mixture was centrifuged at 1500g for 45 minutes at 4°C to precipitate the viral particles. After centrifugation, the supernatant was discarded, and the pellet was resuspended with growth media. Then, the media was given to the infecting LNCaP cell lines with 10µg/ml polybrene. The next day, the media was replenished. At 48 hours post-infection, the selection was started with appropriate antibiotics. The selection marker for pRXTN retroviral

expression plasmid is nourseothricin (NAT). Transduced LNCaP cell lines were selected with 250 ug/ml NAT until non-transduced LNCaP cells were completely dead. The selection marker for pBabe-PH-Btk-GFP retroviral expression plasmid is puromycin. Transduced LNCaP cell lines were selected with 1.1 ug/ml puromycin until non-transduced LNCaP cells were completely dead. For the maintenance of the retroviral-transduced LNCaP cell lines, appropriate amounts of selection markers were added to the growth media as indicated.

2.2.3. Westernblotting Analysis

2.2.3.1. Cell Harvest and Cell Lysis

The media of the cells were discarded and washed with 1X cold PBS on ice. Then, 1 ml of 1X cold PBS was added to the plates, and the cells were scraped by the scrapers. The cells were collected to the Eppendorf tubes and centrifuged at 4000 rpm for 10 minutes at 4°C. Then, the supernatant was discarded, and the pellet was snap-frozen by liquid nitrogen, and stored at -80°C.

Just before the cell lysis, a lysis buffer was freshly prepared on ice. The lysis buffer was added three times the volume of the pellet and incubated on ice for 30 minutes. Then, they were centrifuged at 13000 rpm for 15 minutes at 4°C. After the centrifugation, the supernatant was collected into new tubes, and the pellets were discarded. The lysates were snap-frozen by liquid nitrogen and stored at -80°C for the long term.

2.2.3.2. Protein Quantification by BCA Assay

The concentrations of the lysates were quantified by Pierce™ BCA Protein Assay Kit according to the manufacturer's protocol (Intron Bio, South Korea). For the standards, absorbance values of eight different concentrations of albumin (2 mg/ml) between 0-15 ug were determined. 200 µl of BCA solution was prepared for each lysate in triplicate. 1 µl of the lysate and 24 µl of ddH₂O were

mixed with 200 μ l of BCA solution in a well in triplicate on 96-well plates. The optical density was measured at 562 nm by a spectrophotometer. For blank, only BCA and ddH₂O mixture was used. The mean of the absorbance values of the blank was subtracted from the mean of the absorbance values of each lysate. The unknown concentrations of the lysates were determined according to the equation, which was obtained by the absorbance values corresponding to the concentrations of the standards.

2.2.3.3. Western Blotting

10% resolving gel and 4% stacking gels were used for SDS-PAGE. The recipe for resolving or stacking gels is demonstrated in Table 2.1.

Table 2.1. Recipes for Resolving and Stacking Gels.

Components	Resolving Gel (10%)	Stacking Gel (4%)
Acrylamide/bisacrylamide (30% w/v)	3.3 mL	1.3 mL
TEMED	5 μ l	10 μ l
10% APS	50 μ l	50 μ l
Resolving Gel Buffer (pH=8.8)	2.5 mL	-
Stacking Gel Buffer (pH=6.8)	-	2.5 mL
ddH₂O	4.1 mL	6.1 mL
Total Volume	10 mL	10 mL

Loading samples were prepared with an appropriate amount (10-30 μ g as final concentration) of lysates and 1X laemmli buffer/ β -mercaptoethanol mixture. The loading samples were denatured

at 96°C for 10 minutes. Thus, 10-30 ug of proteins were loaded onto the gels. SDS-PAGE was conducted at 80-120V for around 100 minutes. Then, the gels were transferred to nitrocellulose membranes either at 250 mA for 150 minutes on ice or at 90 mA overnight at RT by wet transfer method. At the end of the wet transfer, the membranes were stained with Ponceau S for 5 minutes to verify the efficiency of the transfer, then washed with dH₂O. Next, the membranes were blocked with 5% milk solution or 5% BSA solution for an hour at RT. Then the membranes were blotted with proper primary antibodies overnight at 4°C. Then, the membranes were washed with 1X TBS-T for 5 minutes three times. After washing, the membranes were incubated with HRP-conjugated secondary antibodies for an hour at RT. Then, the membranes were washed with 1X TBS-T for 5 minutes three times. After the membranes were incubated with dH₂O for a few minutes, they were developed by incubating them with ECL solution for a minute in the dark, according to the manufacturer's protocol. The detection was conducted by Amersham Imager 600, and the densitometric analysis of the blots was done by ImageJ. The band densities of each protein were normalized to the loading control, and the band intensities of the phospho-proteins were also analyzed by normalizing them to the total proteins.

2.2.4. Immunofluorescence assay

LNCaP cells were seeded at a density of 1.5×10^5 on a coverslip in a 6-well plate. 24-hour post-seeding, the cells were treated with doxycycline with serum-reduced complete media (RPMI-1640 and 4% FBS Tet-free). At the end of three day-long treatment, the cells were washed once with 1X PBS and fixed with 4% PFA at RT for 15 minutes. Next, the cells were rewashed with 1X PBS and then washed with ddH₂O once. After the washing steps, the coverslips were dried. The coverslips containing fixed cells were mounted on the slides with 5-10 μ l of ProLong Gold

Antifade reagent with DAPI (Invitrogen, US) in the dark overnight at RT. Lastly, the images were observed with a Zeiss AX10 fluorescence microscope, and images were analyzed by ImageJ.

2.2.5. Cellular Proliferation Assays

Crystal violet assay and sulforhodamine (SRB) assay were used in this study.

2.2.5.1. Crystal Violet Assay

LNCaP cells were seeded at a density of 2.5×10^5 per well on a 12-well plate, or a density of 0.5×10^5 per well on a 6-well plate. 48 hours after cell seeding, the cells were treated with a selected drug with serum-reduced complete medium (RPMI-1640, 4% FBS, and an appropriate amount of drug of interest). When the control (non-treated) group of cells reached the confluency, the cells were fixed with 4% PFA for an hour at RT, or overnight at 4°C. Then, the cells were washed and stained with 0.4% crystal violet dye for at least an hour. After the crystal violet staining, the cells were gently washed twice with dH₂O. Next, the cells were air-dried under the fume hood at RT. After the cells were air-dried, the cells were incubated with the destaining solution for an hour on the shaker with mild agitation. Finally, 200 µl of 1:20 diluted destained solution from each condition and 200 µl of destaining solution as blank were put on a 96-well plate in triplicate and measured at 595 nm by the spectrophotometer. The average of the absorbance values of the blank was subtracted from the average of the absorbance values of each condition. Cell viability percentages were calculated by dividing the mean of the absorbance values of each condition by the mean of the absorbance values of the non-treated group and multiplying by 100.

2.2.5.2. Sulforhodamine (SRB) Assay

LNCaP cells were seeded at a density of 0.3×10^4 /well on a 96-well plate. 48-hour post-seeding, the cells were treated with a drug of interest with a serum-reduced complete medium for five days.

(RPMI-1640, 4% FBS (or tetracycline-free FBS for the Tet-on expression system) and proper amount of drug-of-interest). At the end of the experiment, the medium was discarded, and the cells were fixed with 10% trichloroacetic acid (TCA) for at least an hour at 4°C. Then, the cells were washed with dH₂O five times. The cells were stained with 0.4% SRB solution for 30 minutes at RT. After staining, the cells were washed with 1% acetic acid five times. Next, the cells were air-dried under the fume hood at RT. The cells were destained with 200 µl of non-buffered 10 mM Tris-base for 15 minutes on a shaker with mild agitation. Finally, the optical density was measured at 564 nm by spectrophotometer. The average of the absorbance values of the blank was subtracted from the average of the absorbance values of each condition. The percentages of the cell viability were calculated by dividing the mean of the absorbance values of each condition by the mean of the absorbance values of the non-treated group and multiplying by 100.

2.2.6. RT-qPCR

2.2.6.1. RNA Isolation

LNCaP cells were seeded at a density of 2×10^6 per 10-cm culture dish. On the following day, the cells were treated with the proper amount of doxycycline and incubated for three days at 37°C and 5% CO₂. Then, the cells were harvested, and RNA was isolated by using a NucleoSpin RNA Isolation kit according to the manufacturer's protocol (Macherey-Nagel, Germany). The cells were lysed by the provided lysis buffer. Then, the lysate was filtrated to bind RNA to the provided columns. The DNA was digested by a provided DNase. After a few washing steps and drying the columns, the RNA was eluted. RNA concentration was measured by NanoDrop, and the RNA samples were stored at -80°C.

2.2.6.2. cDNA Synthesis

RNA samples were converted to cDNA by employing the reverse transcription reaction by using Bio-Rad iScript cDNA Synthesis Kit according to the manufacturer's protocol (Bio-Rad, US). 1000 ng of total RNA was used for cDNA synthesis, the conditions of which were displayed in Table 2.2. At the end of the reaction, cDNA was diluted to 10 ng/ μ l with a 1:5 dilution rate and stored at -20°C.

Table 2.2. Conditions for cDNA Synthesis.

Component	Volume or Concentration
5X Reaction Mix	4 μ l
Reverse Transcriptase	1 μ l
RNA	1000 ng (1 μ g)
Nuclease-free H ₂ O	Complete to 20 μ l

2.2.6.2. qPCR and Analysis

qPCR reaction was conducted by using the SsoAdvanced Universal Inhibitor-Tolerant SYBR Green Supermix according to the manufacturer's protocol (Bio-Rad, US), which is displayed in Table 2.3. The thermal cycling protocol was conducted by Roche LightCycler 96 according to the manufacturer's protocol (Bio-Rad, US), which is displayed in Table 2.4. Relative mRNA expression was detected by utilizing the $2^{-\Delta\Delta CT}$ method to calculate the fold changes relative to the housekeeping gene (RPL19).

Table 2.3. Conditions for qPCR.

Component	Volume or Concentration
SsoAdvanced Universal Inhibitor-Tolerant	
SYBR Green Supermix (2X)	5 μ l
Forward Primer	250 nM
Reverse Primer	250 nM
cDNA Template	30 ng
Nuclease-free H ₂ O	Complete to 10 μ l

Table 2.4. Thermal Cycling Conditions for qPCR.

Step	Temperature	Duration	Cycle
Preincubation	98°C	150 s	1
2 Step Amplification	98°C	10 s	40
	60°C	30 s	
Melting	65°C	10 s	1
	95°C	300s	

2.2.7. Targeted Metabolomics

2.2.7.1. Sample Preparation

LNCaP cells were seeded at a confluency of 70% on 10 cm dishes. 48 hours later, the cells were treated with the proper amounts of doxycycline with serum-reduced complete medium (RPMI-1640, 2% FBS Tet-free, 1% pen/strep) and incubated for three days. Then the cells were harvested

by cell lifters and the pellets were collected after the centrifugation at 4000 rpm for 10 minutes at 4°C. The pellets were snap-frozen and stored at -80°C. Each biological replicate of LNCaP-PTEN cell variants had 5×10^6 cells for endogenous metabolite normalization. The experiments were repeated five times independently. The samples were sent to the Boğaziçi University for further mass spectrometry analysis with the collaboration of the laboratory of Prof. Berat Haznedaroğlu.

2.2.7.2. Mass Spectrometry and Analysis

Mass spectrometric analysis for targeted metabolomics was performed with the collaboration of the laboratory of Prof. Berat Haznedaroğlu at the Institute of Environmental Sciences at Boğaziçi University. Thermo Q Exactive™ mass spectrometer was used for the targeted metabolomics by utilizing the AbsoluteIDQ p400 HR kit (Biocrates, Austria). The LC-MS method detected amino acids and biogenic amines, whereas acylcarnitine, cholesteryl esters, glycerophospholipids, glycerides, sphingolipids, and sugar were detected by the FIA-MS method. The concentrations (μM) of the metabolites were quantitatively or relatively quantitatively determined according to the standards for each metabolite provided by the kit.

2.2.8. RNA-sequencing

2.2.8.1. Sample Preparation and Quality Control

LNCaP-rtTA-pRXTN, LNCaP-rtTA-pRXTN-PTEN-WT, C4-2-rtTA-pRXTN, C4-2-rtTA-pRXTN-PTEN-WT lines were seeded at a density of 2×10^6 on 10-cm plates. On the following day, the cells were treated with the proper amounts of doxycycline for three days with serum-reduced complete media (RPMI-1640, 4% FBS Tet-free) at 37°C and 5% CO₂. At the end of the experiment the cells were harvested by trypsinization, and RNA was isolated with the NucleoSpin RNA Isolation Kit according to the manufacturer's (Macherey-Nagel, Germany). The concentrations of

RNA samples were measured by NanoDrop, then the samples were stored at -80°C. Quality control of the RNA samples was conducted with Agilent RNA 6000 Nano kit by Agilent 2100 Bioanalyzer (Agilent Technologies, USA) to detect RNA concentration, RNA integrity number (RIN), and rRNA ratio for RNA sequencing. Each RNA sample had at least 100 ng/μl RNA, RIN > 9, and rRNA ratio > 1. The samples had two independent biological replicates.

2.2.8.2. RNA-seq analysis

The RNA samples were sent to Gen-Era Diagnostics for RNA sequencing and bioinformatic analysis. The company utilized the Illumina Stranded mRNA Prep kit (Cat. No. 20040534, Illumina, USA) for the enrichment of poly-A—mRNAs for next-generation sequencing. They performed purification, fragmentation, cDNA synthesis, RNase treatment, insertion of index sequencing, and final cDNA library generation. Before the sequencing, they checked the quality control of RNA and cDNA library with the Agilent DNA 1000 kit (Agilent Technologies, USA) by Bioanalyzer 2100 (Agilent Technologies, USA), and RNA qualities were validated. Illumina NovaSeq 6000 next-generation sequencing platform was used (Illumina, USA) to acquire 30 million paired-end 2x150 bp reads. Bioinformatical analysis was performed by Gen-Era Diagnostics. The FASTQC tool was used to control the quality of the obtained data. The low-quality reads and possible adaptor-index contaminations were trimmed by the Trimmomatic tool. After trimming, the alignment was performed by the HISAT2 tool based on the reference genome of *Homo Sapiens hg38*. The Ensembl dataset was used for the annotations and the Subread tool was used for the determination of the number of reads for each transcriptome element. Normalization and filtering of counts per gene were conducted by R:edgeR tool and the differentially expressed genes were determined by R:limma tool. The statistical analysis and

comparison between or within the sample groups and the data visualization were performed on R scripts.

2.2.9. Statistical Analysis

GraphPad Prism 9.2 was used for the statistical analysis of the experiments. Two-paired Student's t-test was performed to compare the means of two groups, or one-way ANOVA was utilized to detect significant differences of means among more than two groups for multiple comparisons.

ImageJ was used for the densitometric analysis of immunoblotting and quantification of GFP signals obtained from the group of cells during the immunofluorescence assay.

The statistical analysis, metabolite set enrichment analysis, or pathway analysis for the metabolomics data were conducted by MetaboAnalyst 5.0 (<https://www.metaboanalyst.ca>). For statistical analysis, the thresholds for fold change and p-value were set to 1.5 and 0.05, respectively. For quantitative metabolite set enrichment or pathway analysis, the SMPDB (Small Molecule Pathway Database), KEGG database, or the HMDB (the Human Metabolome Database) was utilized via the MetaboAnalyst 5.0 online tool.

For combination treatment experiments, CDI (coefficient drug index) was calculated as the formula $CDI = AB/(A \times B)$. AB indicates the ratio of absorbance values of the combination treatment to the control group. A or B indicates the ratio of absorbance values of the drugs alone to the control. $CDI < 1$ refers to a synergism, $CDI = 1$ refers to an additive effect, and $CDI > 1$ refers to an antagonist effect between two drugs.

3. RESULTS

3.1. Introduction of Tet-on Gene Expression System to LNCaP Cell Lines

LNCaP is a PTEN-null, androgen-sensitive human prostate adenocarcinoma cell line, which was derived from the lymph node metastasis [62]. We created a dox-inducible system in LNCaP cells to re-express WT PTEN or various PTEN function mutants to investigate the impact of PTEN loss on the metabolome of metastatic prostate cancer cells upon PTEN loss. We first transduced LNCaP cells with rtTA plasmid (Tet-on gene expression system) and the cells were selected with geneticin (G418). Then LNCaP-rtTA cells were transduced with pRXTN plasmids containing Tet operator and encoding wild-type, protein phosphatase deficient (PTEN-Y138L), lipid phosphatase deficient (PTEN-G129E), or catalytically-inactive (PTEN-C124S) PTEN genes, separately (**Table 3.1**). The cells were selected with nourseothricin (NAT).

Table 3.1. Different PTEN functions expressed in dox-inducible LNCaP cells.

LNCaP PTEN Variants	Phenotype
LNCaP-rtTA-pRXTN (MOCK)	Empty vector (negative control)
LNCaP-rtTA-pRXTN-PTEN-WT	Wild type PTEN
LNCaP-rtTA-pRXTN-PTEN-Y138L	Protein phosphatase deficient, lipid phosphatase intact PTEN
LNCaP-rtTA-pRXTN-PTEN-G129E	Lipid phosphatase deficient, protein phosphatase intact PTEN
LNCaP-rtTA-pRXTN-PTEN-C124S	Catalytically inactive PTEN

LNCaP PTEN variants were treated with doxycycline in the range of 0.01-0.5 ug/ml, and PTEN expression was confirmed at the protein level (**Figure 3.1**). Each LNCaP PTEN variant had a relatively equal amount of PTEN expression, except the mock, which is a negative control. Our Tet-on gene expression system did not have any detectable leakage for PTEN expression. PTEN-WT or PTEN-Y138L expressing LNCaP cells had diminished phosphorylated AKT S473 protein

level. This is in line with the downregulation in the PI3K pathway since both cell lines have intact lipid phosphatase function of PTEN. AKT is known to be one of the first effector proteins in the pathway, of which phosphorylation at S473 and T308 levels can be downregulated by the functional lipid phosphatase activity of PTEN [63]. On the other hand, PTEN-G129E or PTEN-C124S expressing LNCaP cells had no effects on the expression levels of pAKT S473 or pAKT T308, since protein phosphatase or phosphatase-independent activities of PTEN do not have any impacts on AKT phosphorylation.

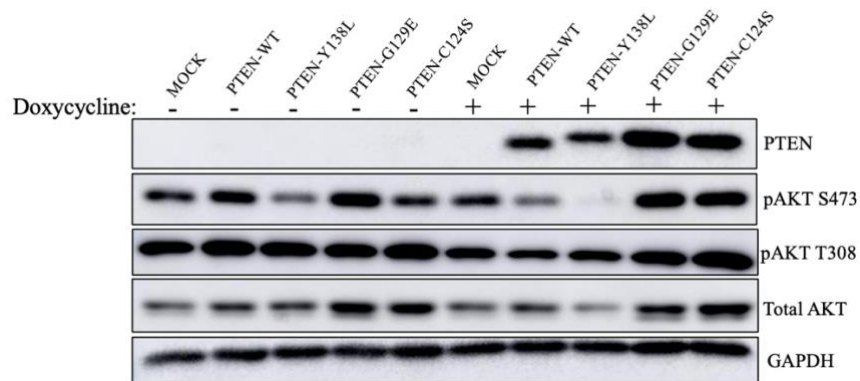


Figure 3.1. PTEN expression in dox-inducible LNCaP PTEN variants. Tet-on PTEN expression system was generated in LNCaP cell lines. The cells were induced with a range of 0.01-0.5 ug/ml doxycycline for three days. PTEN, pAKT S473, pAKT T308, and total AKT expression levels were detected. GAPDH was used as a loading control.

3.2. Confirmation of PTEN Functionality in LNCaP PTEN Variants

After we generated our dox-inducible LNCaP PTEN variants and confirmed PTEN expression in each variant, we wanted to verify PTEN functionality more directly in our system. PIP₃ on the cellular membrane, produced by PI3K, can recruit the proteins carrying a pleckstrin homology (PH) domain, such as AKT or PDK1 [64, p. 6]. In the presence of PTEN in the cells, PIP₃ can be dephosphorylated back to PIP₂, thus preventing downstream kinases carrying the PH domain from

being recruited to the cell membrane and reducing the activity of the PI3K/Akt pathway. Thus, we used a PIP₃ biosensor in LNCaP PTEN variants to further validate the PTEN functionality. Either dox-inducible PTEN-WT or PTEN-C124S expressing LNCaP cells were transduced with the pBabe-puro-PH^{Btk}-GFP plasmid encoding the pleckstrin homology (PH) domain of Bruton's tyrosine kinase (Btk) tagged with a green fluorescent protein (GFP), which was cloned in our laboratory. The transduced cells are denoted as PTEN-WT-PH^{Btk}-GFP or PTEN-C124S-PH^{Btk}-GFP in this study. After the cells were generated, we confirmed PH^{Btk}-GFP expression in the cells in the presence or absence of wild-type PTEN or catalytically-inactive PTEN (PTEN-C124S) (**Figure 3.2.A**). When the cells were induced with doxycycline, the cells started to express PTEN, and it did not affect the levels of PH^{Btk}-GFP fusion protein (**Figure 3.2.B**).

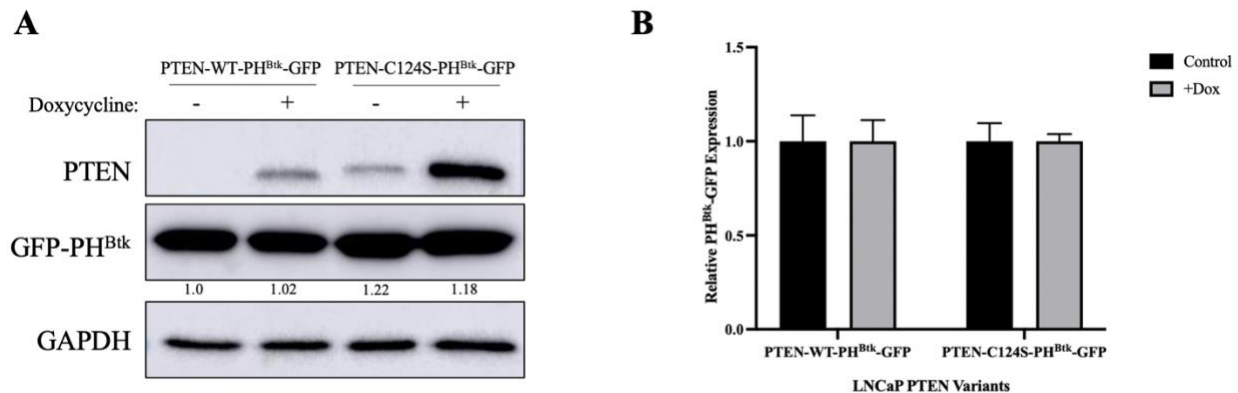


Figure 3.2. PH^{Btk}-GFP fusion protein expression in dox-inducible LNCaP PTEN variants.

The cells were induced with 1 µg/ml doxycycline for 72 hours. 15 µg of the lysates were subjected to western blot analysis. **A.** PTEN and GFP-PH^{Btk} expressions were detected with or without doxycycline induction. GAPDH was used as a loading control. The numbers depict the relative protein levels normalized to GAPDH. **B.** Quantification analysis of PH^{Btk}-GFP fusion protein expression level. The experiments were performed in

three biological replicates. Statistical significance was determined by Student's t-test, and no significance was detected. The error bars refer to the standard error means (SEM) in three independent experiments.

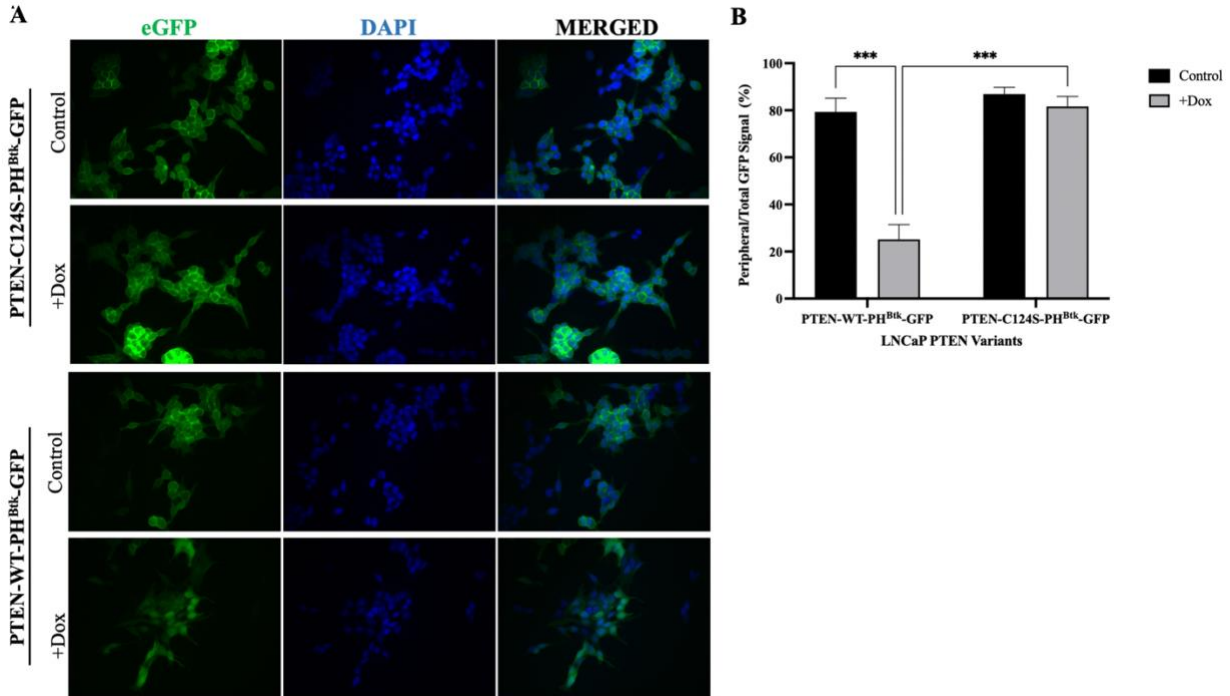


Figure 3.3. PH^{Btk}-GFP Reporter indicates membrane-bound PIP₃ abundance in LNCaP PTEN variants. **A.** Representative immunofluorescence images show PIP₃ abundance in the absence or presence of 1 μg/ml doxycycline in LNCaP PTEN variants. The representative image was taken with the fluorescent microscope at 40X magnification. **B.** Quantification of the peripheral GFP signals to the total GFP in the absence or presence of doxycycline in LNCaP PTEN variants expressing PH^{Btk}-GFP fusion protein (n=3, *** p<0.001). The experiments were repeated independently three times. Statistical significance was determined by two-way ANOVA for multiple comparisons. The error bars depict the standard error means (SEM) of three independent experiments.

To be able to observe PTEN functionality, we performed an immunofluorescence assay to detect the PIP₃ abundance in PH^{Btk}-GFP overexpressing LNCaP PTEN variants (**Figure 3.3**). When the cells were not induced with doxycycline, almost 80% of the cells had peripheral GFP signals, since

membrane-bound PIP₃ recruited PH^{Btk}-GFP fusion protein (**Figure 3.3.A**). In parallel with this, when PTEN-C124S-PH^{Btk}-GFP was induced with doxycycline, almost 80% of the cells also had a peripheral GFP signal, and since the cells had only catalytically inactive PTEN expression, it did not affect PIP₃ abundance on the membrane. However, as PTEN-WT-PH^{Btk}-GFP cells were induced with doxycycline, the peripheral GFP signal was significantly reduced compared to its counterpart control or that in dox-induced PTEN-C124S-PH^{Btk}-GFP (**Figure 3.3**). These results implicate that expression of wild-type PTEN in LNCaP-PTEN-WT-PH^{Btk}-GFP cells leads to dephosphorylation of membrane-bound PIP₃ back to PIP₂. Together with these findings, our PTEN functionality was confirmed in our dox-inducible LNCaP PTEN cellular model.

3.3. Determination of the Viability of Dox-inducible LNCaP PTEN variants

We wanted to detect the impact of wild-type or mutant PTEN on the viability of the dox-inducible LNCaP cells. LNCaP PTEN variants were induced with a range of 0.01-0.5 ug/ml doxycycline for 15 days. Upon doxycycline induction, the viability of PTEN-WT or PTEN-Y138L expressing LNCaP cells was significantly decreased (**Figure 3.4**). On the other hand, PTEN-G129E or PTEN-C124S expression did not alter the cellular viability in LNCaP cells compared to empty vector expressing LNCaP (MOCK) cells upon doxycycline treatment (**Figure 3.4**). The different proliferation states of dox-inducible LNCaP PTEN variants demonstrated that only lipid phosphatase function can negatively regulate the proliferation, as an antagonist of the PI3K/Akt pathway, while protein phosphatase or scaffold functions of PTEN have no significant impact on cellular viability.

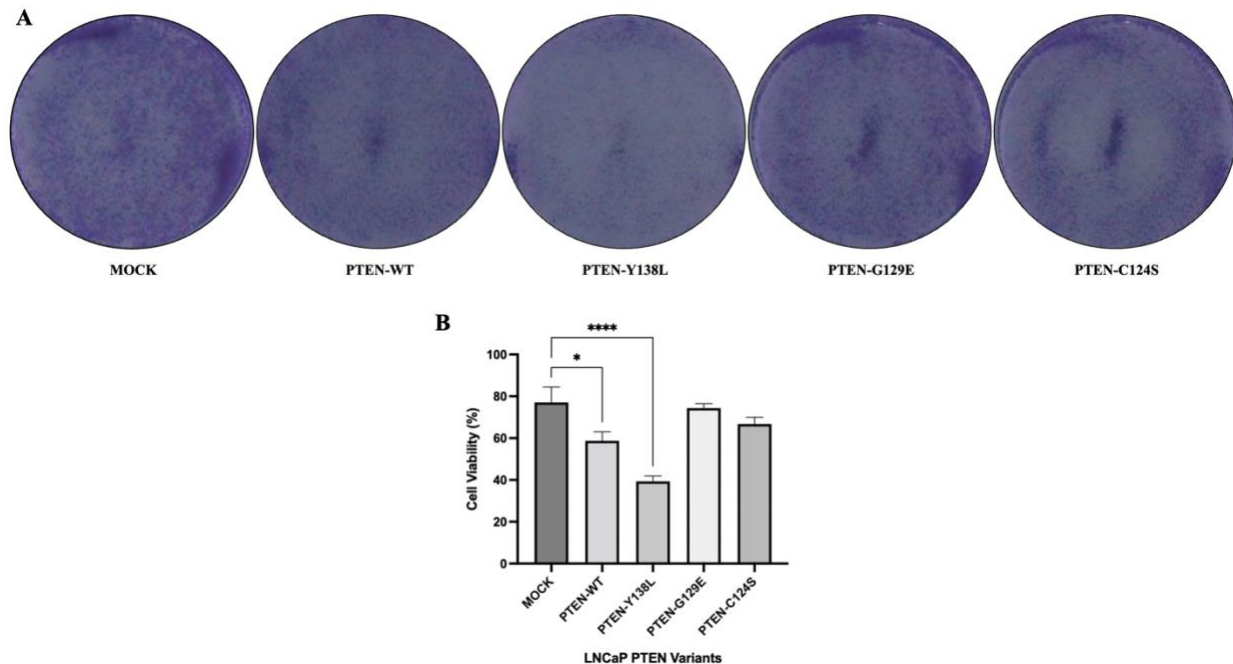


Figure 3.4. The lipid phosphatase function of PTEN diminishes the cellular viability in LNCaP cells. **A.** Crystal violet staining of dox-inducible LNCaP PTEN variants. The cells were induced with a range of 0.01-0.5 ug/ml doxycycline in serum-reduced media for 15 days. **B.** Quantification of cellular viability in percentage. Statistical significance was determined by one-way ANOVA for multiple comparisons to MOCK. The error bars depict standard error means (SEM) of two independent biological replicates (n=2, * p<0.05, **** p<0.0001).

3.4. Characterization of PI3K/PTEN/Akt pathway in LNCaP PTEN variants

We wanted to characterize the effects of the PTEN variants in the PI3K/Akt pathway in the dox-inducible LNCaP PTEN cells. Upon doxycycline induction, a relatively equal amount of PTEN expression in each variant, except MOCK, was detected (**Figure 3.5**). Since the phosphorylation of Akt is one of the earliest events in the activated PI3K pathway, the lipid phosphatase function of PTEN can directly modulate the activation of Akt by regulating PIP₃ abundance in the cell membrane [24]. As expected, the levels of phosphorylated Akt at the residues at S473 or T308 were significantly downregulated in wild-type or lipid phosphatase intact (PTEN-Y138L) PTEN

expressing LNCaP cells upon doxycycline treatment (**Figure 3.5.B**). However, there were no significant differences in the expression levels of pAKT at both residues in lipid phosphatase deficient (PTEN-G129E) or catalytically-inactive PTEN (PTEN-C124S) expressing LNCaP cells (**Figure 3.5.B**). We did not observe any statistically significant alterations in the expression of mTOR signaling proteins upon doxycycline induction, although phosphorylated mTOR S2481 or phosphorylated S6 S240/244 were slightly downregulated in PTEN-WT-, PTEN-Y138L- or PTEN-G129E-LNCaP cells. These findings demonstrated that activation of AKT through phosphorylation at serine or threonine residues can be directly regulated by the lipid phosphatase activity of PTEN, whereas the mTOR signaling pathway is not a direct effector of phosphatase-dependent or -independent functions of PTEN [65].

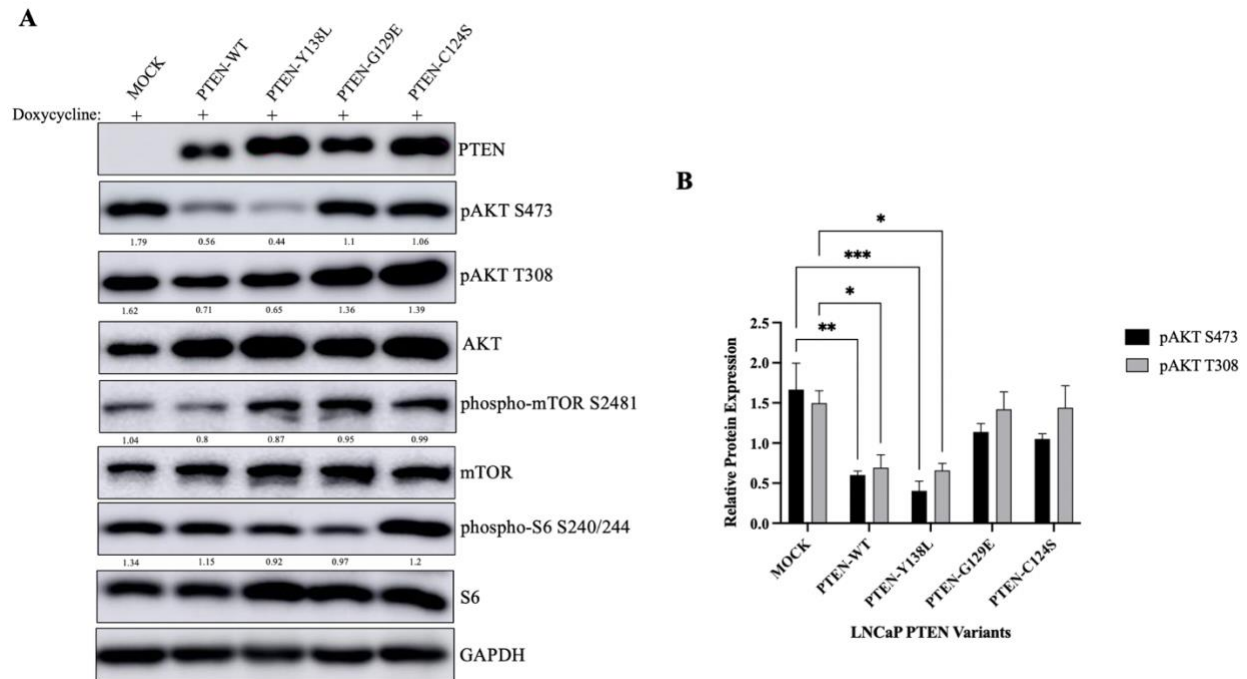


Figure 3.5. Characterization of PI3K/Akt pathway in dox-inducible LNCaP PTEN variants.

The cells were treated with a range of 0.01-0.5 ug/ml doxycycline in serum-reduced media for three days. 15 ug

of lysates were conducted for western blot analysis. **A.** PI3K/PTEN/Akt pathway substrates were detected upon doxycycline induction in LNCaP PTEN variants. The number under each phospho-protein blot depicts the relative expression level compared to their total proteins. GAPDH was used as a loading control. **B.** Quantification of western blot analysis. pAKT S473 or pAKT T308 proteins were normalized to the total AKT levels in the cells. Error bars show the standard error mean (SEM) of four independent. Statistical significance was determined by two-way ANOVA for multiple comparisons to MOCK experiments (n=4, * p<0.05, ** p<0.01, *** p<0.001).

3.5. Determination of the metabolome of LNCaP Cells upon different PTEN conditions

We wanted to identify the changes in the metabolome of the castration-naïve LNCaP cell line upon PTEN loss, thus we utilized a targeted metabolomics approach using Absolute*IDQ* p400 HR kit (Biocrates, Austria) according to the manufacturer's protocol with the collaboration of the group of Prof. Berat Haznedaroğlu (**Figure 3.6**).

We treated LNCaP cells with doxycycline in a range of 0,01-0,5 µg/ml for three days to re-express either wild-type or catalytically inactive PTEN (PTEN-C124S), or negative control (MOCK) in serum-reduced media. At the end of doxycycline treatments, the cells were harvested and 5x10⁶ cells from each variant were further analyzed in the metabolomics assay to provide metabolic standardization among them. Flow injection analysis was used to detect amino acids and biogenic amines, while LC-MS/MS was performed to detect the other metabolite groups. In total, 409 metabolites in 11 different metabolic classes were analyzed in each LNCaP PTEN variant (**Figure 3.7**).

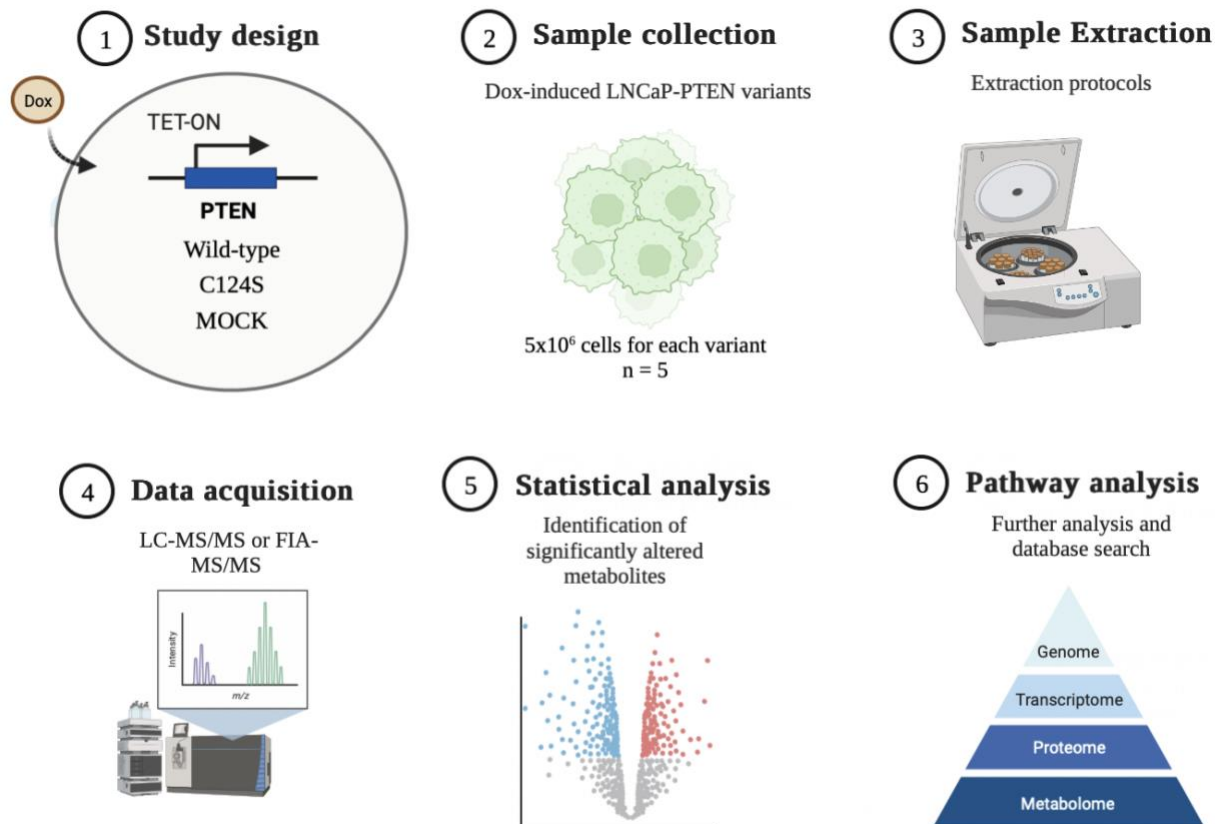


Figure 3.6. Workflow of targeted metabolomics. PTEN Tet-on expression system in LNCaP cells was created to re-express wild-type or catalytically inactive PTEN (PTEN-C124S) together with negative control (MOCK). The cells were induced with doxycycline in a range of 0.01-0.5 $\mu\text{g/ml}$ in low serum conditions (RPMI + 2% tet-free FBS + 1% pen/strep) for three days. 5×10^6 cells of each variant were conducted for mass spectrometry analysis with five independent biological replicates. Either FIA-MS/MS or LC-MS/MS were conducted to detect different metabolic classes. After the data acquisition, statistical analysis and pathway analysis were performed on MetaboAnalyst 5.0.

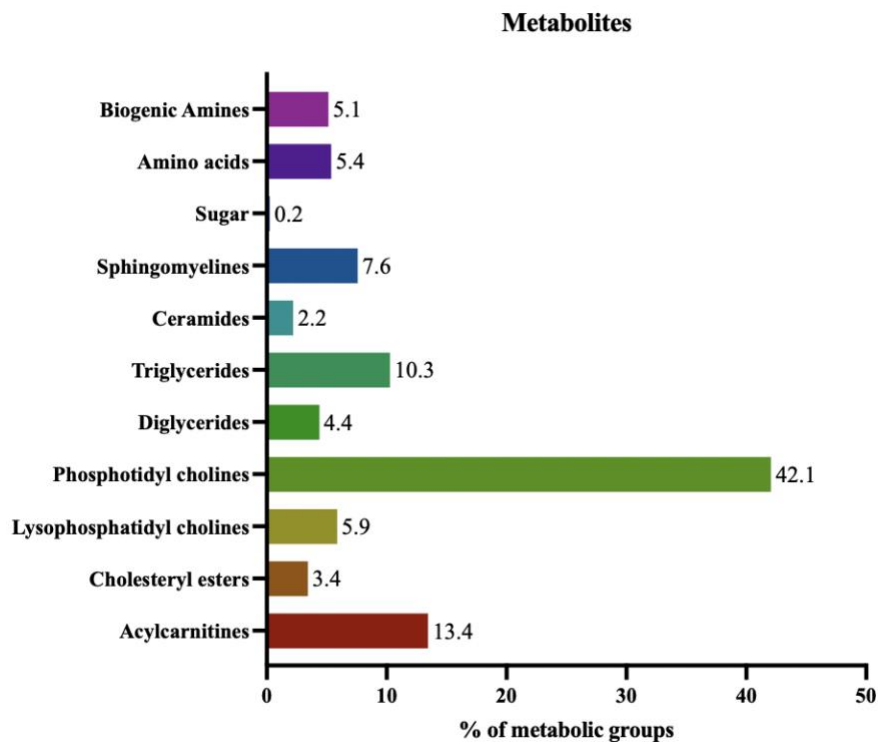


Figure 3.7. Distribution of detected metabolites based on their metabolic classes. The targeted metabolomics kit detected 409 metabolites in 11 metabolic classes in LNCaP PTEN variants. The annotated numbers indicate the percentage of the metabolic classes.

The metabolomics data identified 196 glycerophospholipids, 31 sphingomyelins, and 9 ceramide species. However, some of them were detected below the set confidence thresholds. Some species of glycerophospholipids or sphingolipids were found to be significantly upregulated, although some species of glycerophospholipids were found to be significantly downregulated in wild-type PTEN expressing cell lines in comparison to PTEN-null (MOCK) or PTEN-C124S LNCaP cell lines (**Figure 3.8**).

A

Metabolites	LNCaP		
	WT	C124S	WT vs C124S
LPC(16:0)	1,31	1,70	0,77
LPC(18:0)	1,23	2,04	0,60
PC(31:2)	1,55	1,47	1,06
PC(31:3)	1,82	3,16	0,89
PC(32:4)	NA	NA	0,61
PC(33:3)	1,66	1,90	0,88
PC(36:1)	1,02	0,51	1,99
PC(36:4)	1,52	0,89	1,70
PC(37:4)	1,11	0,54	2,06
PC(37:6)	2,03	1,42	1,43
PC(38:2)	0,87	0,53	1,64
PC(38:3)	1,23	0,77	1,60
PC(38:4)	1,36	0,76	1,79
PC(40:2)	0,64	0,47	1,37
PC(40:3)	0,81	0,49	1,66
PC(40:4)	1,11	0,58	1,91
PC(40:5)	0,97	0,62	1,57
PC(40:8)	1,65	1,47	1,12
PC(40:9)	1,94	2,18	0,89
PC(42:5)	0,83	0,57	1,46
PC(42:6)	1,27	0,77	1,66
PC-O(30:0)	1,42	1,82	0,78
PC-O(32:2)	1,54	1,02	1,51
PC-O(32:3)	2,02	1,70	1,18
PC-O(33:3)	2,64	2,59	1,02
PC-O(34:2)	1,52	1,23	1,23
PC-O(34:3)	2,33	1,67	1,39
PC-O(34:4)	1,13	1,61	0,70
PC-O(36:1)	2,03	1,15	1,76
PC-O(36:3)	1,63	1,33	1,22
PC-O(36:4)	1,91	1,18	1,62
PC-O(36:6)	2,01	1,40	1,44
PC-O(38:4)	2,19	1,82	1,20
PC-O(38:5)	1,98	1,47	1,35
PC-O(38:6)	1,86	NA	NA
PC-O(40:7)	1,73	1,18	1,46

B

Metabolites	LNCaP		
	WT	C124S	WT vs C124S
Cer(42:2)	1,27	0,81	1,57
SM(32:1)	1,63	1,28	1,57
SM(36:1)	2,32	2,13	1,09
SM(38:1)	1,56	0,96	1,63
SM(38:2)	2,52	1,81	1,39
SM(40:1)	1,26	0,69	1,81
SM(40:2)	n.s	n.s	2,8
SM(41:2)	1,84	1,51	1,22
SM(42:2)	1,76	0,96	1,83
SM(42:3)	1,96	1,2	1,64
SM(43:1)	4,36	3,44	1,27

Figure 3.8. Selected metabolite quantifications for LNCaP cells expressing wildtype PTEN or PTEN-C124S upon doxycycline induction. The first and second columns show the metabolic classes and the species respectively. The third and fourth columns depict the fold changes in metabolite concentrations in wild-type PTEN or PTEN-C124S mutant LNCaP cells relative to MOCK control, while the fifth column shows the fold changes in metabolite concentrations in WT-PTEN-LNCaP cells relative to PTEN-C124S-LNCaP cells. Yellow-filled boxes refer to the downregulation of metabolites ($FC < 1/1.5$, $p < 0.05$); red-filled boxes refer to the upregulation of metabolites ($FC > 1.5$, $p < 0.05$), and the bold greens refer to either upregulation or downregulation of the metabolites with narrowly missing significance ($FC < 1/1.5$ or $FC > 1.5$, $0.05 < p < 0.1$). All variants of each cell line have at least 3 biological replicates ($3 < n < 5$). Statistical analysis of the data was performed on MetaboAnalyst 5.0 and Prism 9.2 (FC = fold change, NA = not assigned, LPC = lysophosphatidylcholine, PC = phosphatidylcholine, PC-O = glycerophosphocholine, Cer = ceramide, SM = sphingomyelin).

Several glycerophosphocholine species including PC-O(36:4), PC-O(36:6), or PC-O(38:5) were detected to be significantly upregulated in WT-PTEN re-expressed LNCaP cells relative to LNCaP-MOCK cells. Besides, PC-O(36:4) was found to be nearly significantly upregulated in WT-PTEN-expressing LNCaP cells relative to PTEN-C124S-expressing LNCaP cells. PC(36:4) is also found to be significantly upregulated in WT-PTEN-LNCaP cells relative to MOCK or PTEN-C124S-LNCaP cells (**Figure 3.8.A**). Similarly, phosphatidylcholines like PC(38:4), and PC(42:6) were found to be significantly upregulated in WT-PTEN-LNCaP cells in comparison with PTEN-C124S-LNCaP cells. Moreover, PC(37:4) and PC(40:4) were significantly upregulated in WT-PTEN-LNCaP cells relative to PTEN-C124S-LNCaP cells, while it was also nearly significantly downregulated in PTEN-C124S-LNCaP cells in comparison to LNCaP-MOCK (**Figure 3.8.A**). However, there were also some phosphatidylcholine species such as PC(40:2), which were significantly downregulated both in WT-PTEN or PTEN-C124S-LNCaP cells. PC(40:3) and PC(40:5) were also found to be downregulated significantly in PTEN-C124S-LNCaP cells, even though we did not observe any significant changes in WT-PTEN-LNCaP cells (**Figure 3.8.A**).

Ceramides, which are the central molecules of sphingolipid metabolism, and sphingomyelins produced from ceramides were also identified as significantly altered in LNCaP cells. We found that cer(42:2) was nearly significantly upregulated in WT-PTEN LNCaP relative to PTEN-C124S-LNCaP cells, although upregulation in WT-PTEN versus MOCK was not significant and below the foldchange threshold ($FC < 1.5$, $p > 0.05$) (**Figure 3.8.B**). SM(36:1), SM(41:2), and SM(42:2) were detected significantly upregulated upon WT-PTEN re-expression. Besides, SM(40:2) and SM(42:2) were also found to be significantly increased in WT-PTEN LNCaP cells in comparison to PTEN-C124S-LNCaP cells (**Figure 3.8.B**). However, SM(38:2) species were found to be

significantly upregulated both in WT-PTEN or PTEN-C124S-LNCaP cells (**Figure 3.8.B**). These findings imply that most of the glycerophospholipid and sphingolipid species were regulated in PTEN-replete LNCaP cells via PTEN phosphatase function, mostly upregulated, although only a few glycerophospholipid species indicate the phosphatase-independent function of PTEN may also regulate lipid abundance in LNCaP cells.

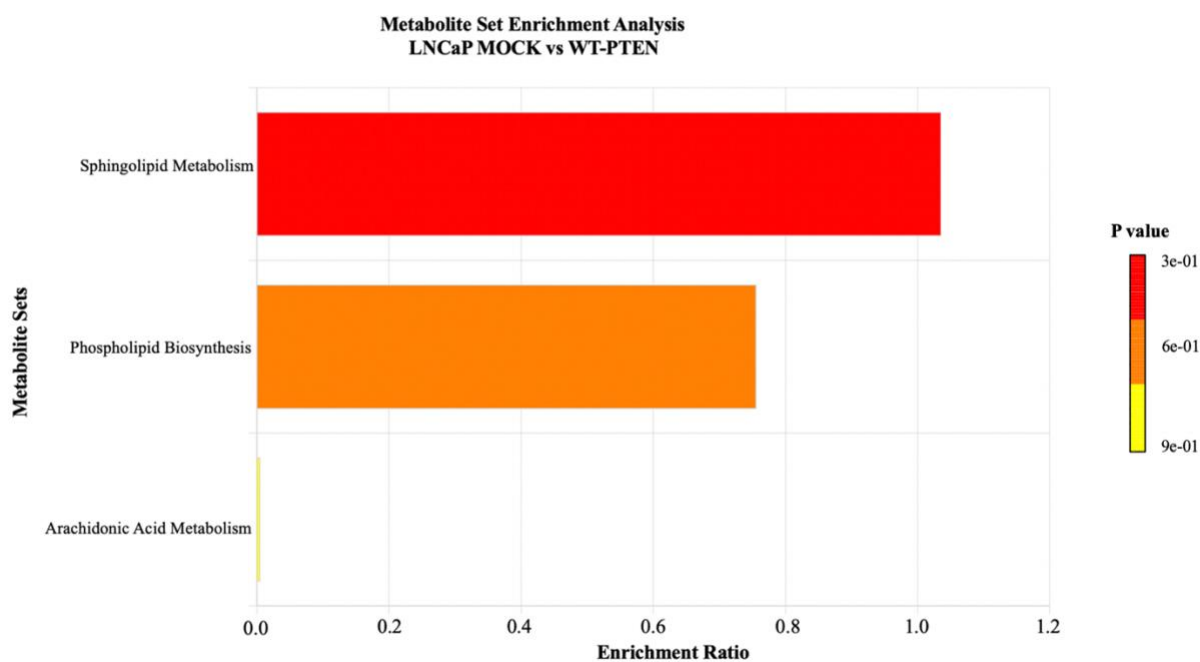


Figure 3.9. Metabolite Set Enrichment Analysis in PTEN-null vs PTEN-replete LNCaP cells.

Metabolite set enrichment analysis was performed on the glycerophospholipids and sphingolipids by MetaboAnalyst 5.0. Quantitative enrichment analysis shows the correlation between the metabolite concentrations and the clinical outcome based on the Small Molecule Pathway Database (SMPDB) metabolite library (99 metabolite sets based on normal human metabolic pathways).

Next, we performed a metabolite set enrichment analysis to understand the regulation of these lipid species in PTEN null and replete backgrounds (**Figure 3.9**). Since prostate cancer harbors mostly homozygous PTEN deletions compared to point mutations in its catalytic domain [16], we only focused on the PTEN loss vs wild-type PTEN re-expression comparisons in our study. Therefore, the metabolite set enrichment analysis was conducted in PTEN-null (MOCK) or PTEN-replete (WT-PTEN-expressing) LNCaP cells. We found that sphingolipid metabolism is the most enriched pathway among glycerophospholipids and sphingolipids (**Figure 3.9**). Although the enrichment was not significant because only four sphingomyelin species had significant upregulation in WT-PTEN-LNCaP cells, our metabolomics data revealed that all the detected sphingomyelin species, except Cer(34:1), were increased in WT-PTEN-LNCaP cells compared to MOCK (**Figure 3.8.B, Figure 3.10**).

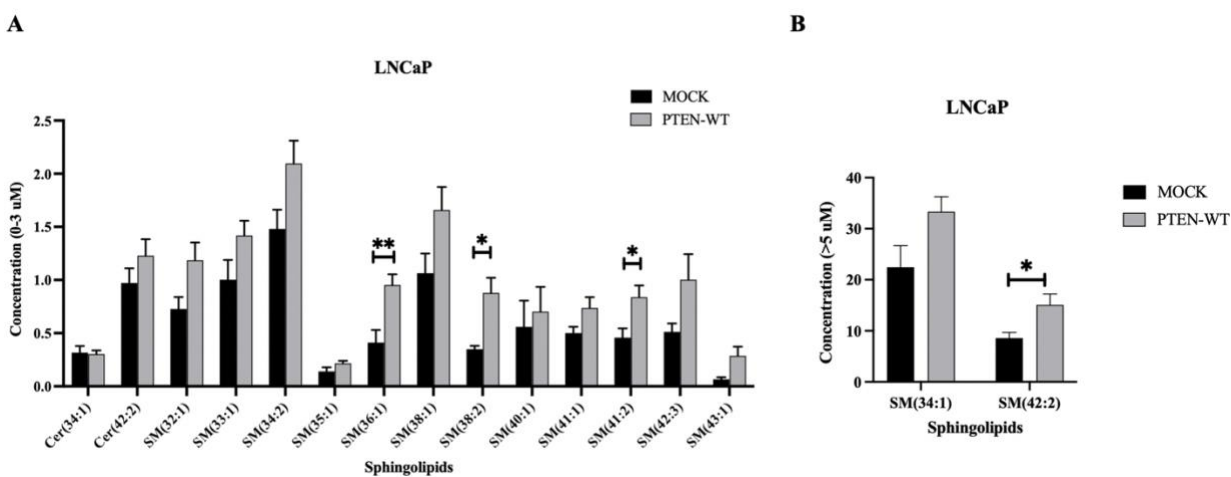


Figure 3.10. The concentrations of sphingolipids decrease in LNCaP cells upon PTEN loss.

Targeted metabolomics determined the abundance of sphingolipid species in PTEN-null (MOCK) and PTEN-replete (PTEN-WT) LNCaP cells. **A**. Sphingolipid species whose concentrations were smaller than 3 µM. **B**. Sphingolipid species whose concentrations were greater than 5 µM. Statistical significance was determined by

the Student's t-test. The error bars show the standard error mean (SEM) of at least three biological replicates ($3 < n < 5$, * $p < 0.05$, ** $p < 0.01$).

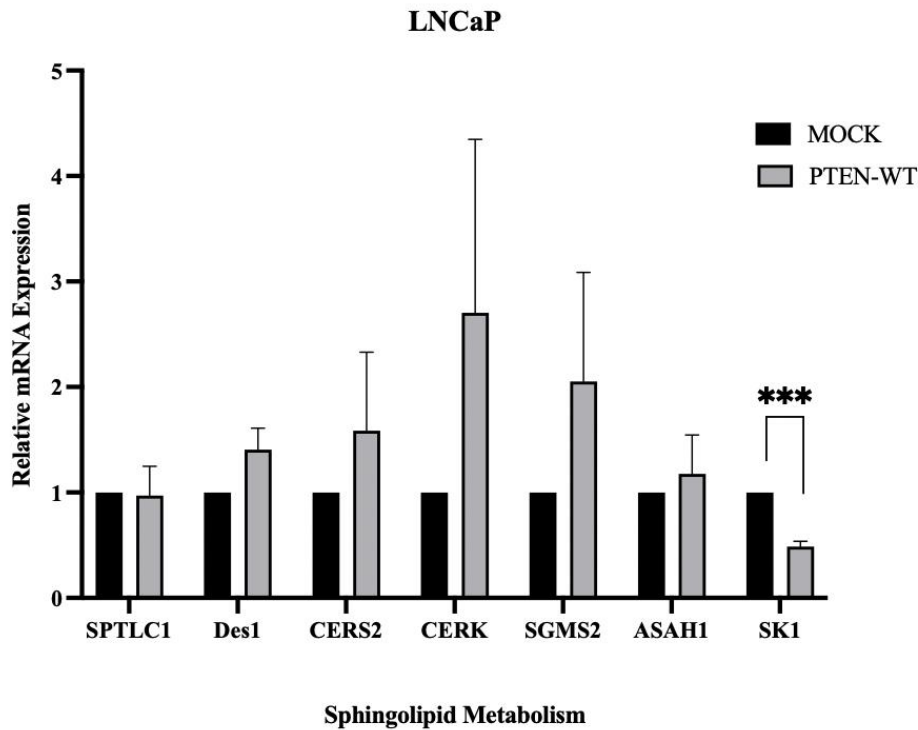


Figure 3.11. Relative mRNA expression levels of the genes in sphingolipid metabolism in PTEN-null and PTEN-replete LNCaP cells. LNCaP MOCK and LNCaP-PTEN-WT cells were induced with doxycycline in a range of 0.01 to 0.5 ug/ml for three days. RNA contents were extracted from the cells and RT-qPCR was conducted. RPL19 was used as a housekeeping gene. The fold change analysis was performed according to the $2^{-\Delta\Delta CT}$ method. Statistical significance was determined by multiple t-tests with a false discovery rate approach. The error bars show the SEM of three independent biological replicates ($n=3$, * $p < 0.05$, ** $p < 0.01$, *** $p < 0.001$).

We further investigated the regulation of the sphingolipid metabolism in WT-PTEN or empty vector (MOCK) expressing LNCaP cells using a transcriptomic approach. We analyzed the mRNA

expression levels of the genes involved in the sphingolipid metabolism by RT-qPCR analysis (**Figure 3.11**). We did not observe any significant difference in the mRNA levels of the genes involved in the *de novo* synthesis of ceramides, which are SPTLC1, DES1, and CERS2. We, however, observed an increase in CERK or SGMS2 mRNA expressions, which convert ceramides to ceramide-1-phosphate or sphingomyelin, respectively. The upregulation of SGMS2 enzyme in transcriptional levels upon PTEN re-expression in LNCaP cells is in parallel with our metabolomics data since we observed sphingomyelin upregulation in WT-PTEN expressing LNCaP cells (**Figure 3.8.B, Figure 3.10**). We also did not detect any significant differences in the acid ceramidase enzyme gene, ASAH1, upon PTEN repletion. Interestingly, we found the gene encoding the sphingosine kinase enzyme, SK1 (SPHK1), significantly downregulated upon wild-type PTEN expression in LNCaP cells. Sphingosine kinase phosphorylates sphingosine, which is produced from ceramide by ceramidases, to produce sphingosine-1-phosphate (S1P). Contrary to the proapoptotic and anti-survival roles of ceramides or sphingosines in cancer, sphingosine-1-phosphate is implicated to be an oncogenic metabolite by stimulating pro-survival signals in the cancer [53]. Hence, the downregulation in sphingosine kinase 1 mRNA levels in the presence of PTEN implies that PTEN may regulate sphingolipid metabolism by interfering with sphingosine kinase activity, switching the sphingolipid metabolism pathway to the direction of sphingomyelin synthesis in castration-naïve prostate cancer cells.

3.6. Identification of the Transcriptome Profile of Castration-Naïve and Castration-Resistant Prostate Cancer Cells

Since we found sphingolipid metabolism was enriched upon PTEN re-expression in LNCaP cells, we wanted to further verify how the genes of sphingolipid metabolism were regulated upon PTEN loss in metastatic prostate cancer cells. We wanted to reveal the transcriptome profiles of

castration-naïve LNCaP or castration-resistant C4-2 cells in the absence or presence of PTEN expression. We treated the cells with doxycycline in the range of 0.01-0.5 µg/ml for three days to re-express PTEN or empty vector as a negative control. Then, we extracted the RNA by using a NucleoSpin RNA extraction kit (Macherey-Nagel, Germany) according to the manufacturer’s protocol, and we verified the qualities by Agilent 2100 Bioanalyzer (Agilent Technologies, USA). We found RIN (RNA integrity number) greater than 9, ribosomal RNA (rRNA) ratio was found greater than 1.6. We prepared two biological replicates for PTEN-null or PTEN-replete conditions in LNCaP and C4-2 cells and sent our samples for RNA sequencing and subsequent bioinformatical analysis.

Firstly, we focused to investigate the transcriptomic changes in castration-naïve LNCaP cells upon PTEN loss. Our transcriptomics data revealed 1005 significantly upregulated and 1085 significantly downregulated genes in LNCaP cells upon PTEN loss based on the false discovery rate smaller than 0.05 (FDR < 0.05).

We detected ceramide kinase gene (CERK) was significantly downregulated upon PTEN loss in parallel with our qPCR findings (**Table 3.2, Figure 3.11**). We could not detect any significant differences in the other genes in sphingolipid metabolism in our transcriptomic data in LNCaP cells when we compared mock and WT-PTEN expressing conditions, even though we demonstrated sphingosine kinase 1 (SK1 or SPHK1) gene was significantly downregulated in WT-PTEN-LNCaP cells in our qPCR data (**Figure 3.11**).

Table 3.2. Significant DEGs in sphingolipid metabolism in LNCaP cells upon PTEN loss.

DEGs in Sphingolipid Metabolism	logFC	p-value	FDR
CERK	-1,40555	0	0,00033

Our analysis revealed that the most significantly upregulated pathways were ECM-receptor interaction, Ras signaling pathway, focal adhesion, cGMP-PKG signaling pathway, cell adhesion molecules, phospholipase D signaling pathway, axon guidance, PI3K/Akt signaling pathway and the cytokine-cytokine interaction in PTEN-null LNCaP cells compared to PTEN-replete condition (**Figure 3.12.A**). Some of the significantly differentially expressed genes associated with the most significantly upregulated pathways were common, like the genes encoding collagen, laminin, integrin subunits, insulin-like growth factor 1 receptor, PAK (P21-activated kinase), Ras, GPCRs, PI3Ks, PLC (phospholipase C), AC (adenylate cyclase), PLD (phospholipase D), FYN, semaphorins, smoothened, Wnt, CREB (cAMP response element-binding protein) and NFAT (nuclear factor of activated T cell).

Interestingly, the phospholipase D signaling pathway can mediate sphingolipid metabolism, sphingolipid signaling pathway, and glycerolipid metabolism. Phospholipase D (PLD) hydrolyzes the phosphodiester bond of phosphatidylcholine and generates phosphatidic acid (PA) [66]. Sphingosine kinase 1 is recruited to PA-enriched parts of the membrane, and directly interacts with PA [67]. Thus, PA production by upregulated PLD signaling can also activate SK1 activity. Our transcriptomics data suggests that the significant upregulation of the PLD2 gene and PLD signaling pathway in PTEN-null LNCaP cells may promote sphingosine kinase 1 activity to produce oncogenic metabolite, sphingosine-1-phosphate, to activate proliferation and survival of LNCaP cells upon PTEN deficiency.

We also utilized an online tool to analyze our transcriptomics data, which is the Qiagen RNA-sequencing analysis portal. We uploaded our FASTQC files to the portal and it automatically trimmed and aligned the raw counts based on the reference genome, Homo sapiens (GRCh38.103). Then we designed an experiment, where we compared the transcriptome of LNCaP-MOCK cells

with WT-PTEN-LNCaP cells. The tool was able to detect 36813 transcript reads in total, 1440 of which significantly differentially expressed genes in LNCaP-MOCK cells compared to WT-PTEN-LNCaP cells with a false discovery rate smaller than 0.05 ($FDR < 0.05$) and logarithmic fold changes greater than 2 or smaller than -2 ($\logFC < -2$ or $\logFC > 2$).

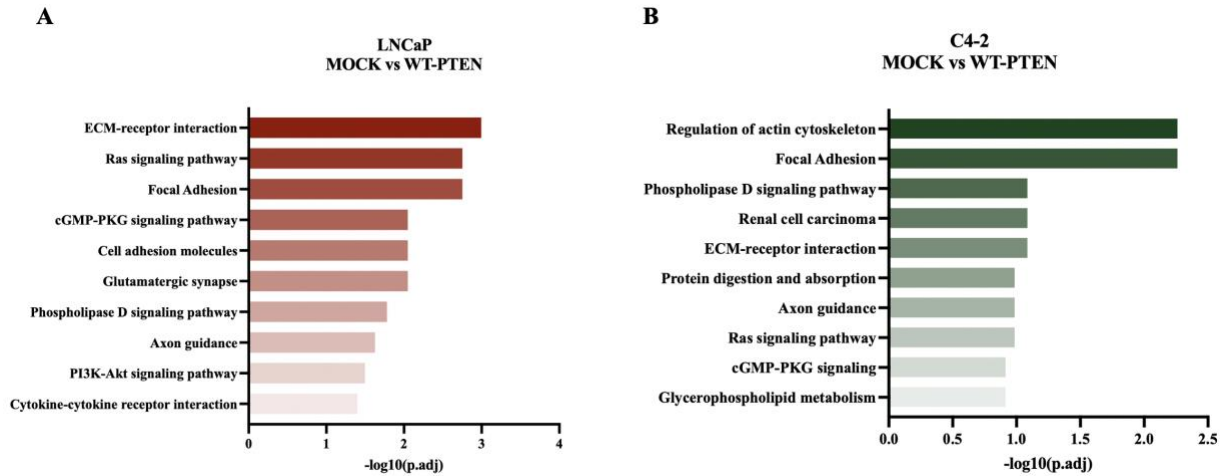


Figure 3.12. The most significantly upregulated pathways upon PTEN loss in metastatic prostate cancer cells. KEGG Pathway database was used for the pathway analysis in LNCaP (A) or C4-2 (B) cells upon PTEN loss (<https://www.kegg.jp>). The pathways were statistically tested according to the number of genes they have and the number of genes that overlapped in the pathway. The clusterProfiler::enrichKEGG package was used in the analysis. $-\log_{10}(p.adj)$ refers to the logarithmic adjusted p values, which were corrected by the Benjamini-Hochberg correction method.

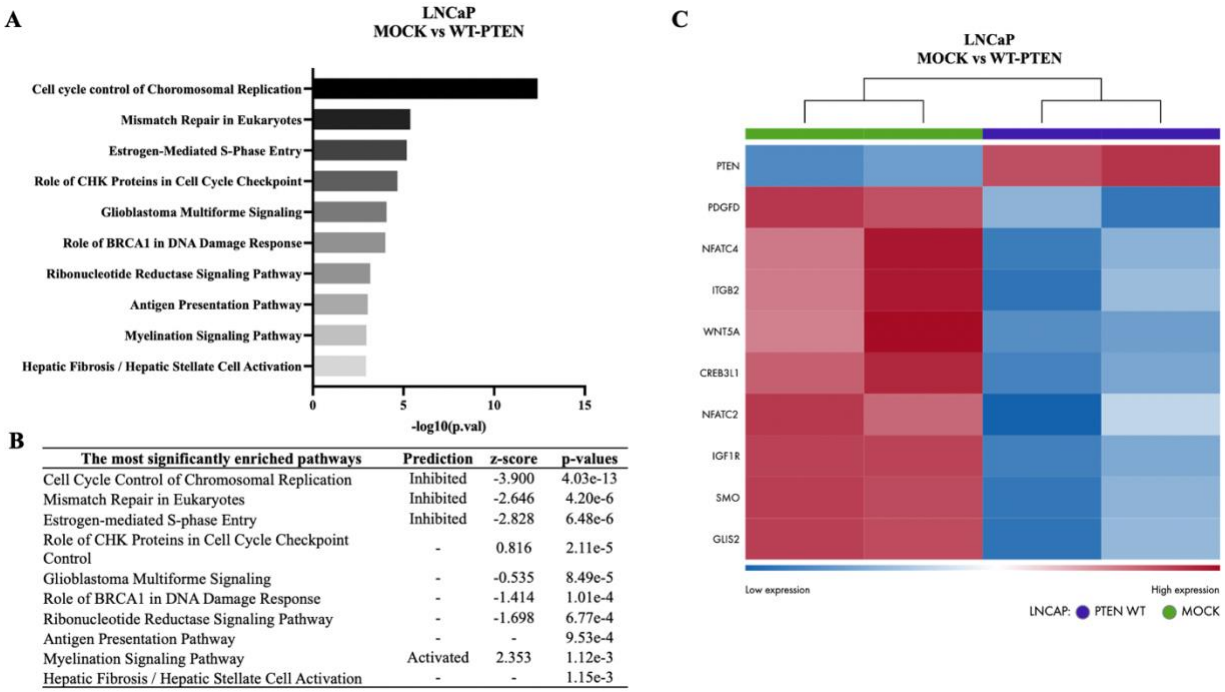


Figure 3.13. The most significantly enriched canonical pathways in LNCaP cells upon PTEN

loss. **A.** The most significantly enriched pathways in LNCaP cells upon PTEN loss were obtained from the Qiagen RNA-seq analysis portal 3.0.1 with the Qiagen IPA tool. Statistical significance was determined by using Fischer’s Exact test without applying any correction methods. The pathways were statistically tested according to the number of genes they have and the number of genes that overlapped in the pathway. **B.** The table shows the most significantly enriched pathways in LNCaP cells upon PTEN loss as in panel A, with their z-scores and p-values. Z-scores greater than 2 or smaller than -2 were considered significant and the activation or inhibition of the pathways was predictable. – depicts no prediction because of $-2 < z\text{-score} < 2$. **C.** The heatmap of significant DEGs involved in the myelination signaling pathway ($z\text{-score}=2.353$, $-\log_{10}(p.\text{val}) = 2.951$). Statistical significance for the DEGs was determined by using Benjamini-Hochberg multiple-testing correction method. The heatmap shows the genes overlapped with the myelination signaling pathway with $FDR < 0.05$, $FC < -2$, or $FC > 2$ (IPA = Ingenuity Pathway Analysis, DEG = differentially expressed genes, FC = foldchange).

We determined the 10 most significantly enriched pathways in LNCaP cells upon PTEN loss via the Qiagen RNA-seq analysis portal (**Figure 3.13.A**). The portal also allowed us to detect z-scores of the significantly regulated pathways together with raw p-values (**Figure 3.13.B**). We found that the myelination signaling pathway was activated in LNCaP cells upon PTEN loss. Cell cycle control of chromosomal replication, mismatch repair in eukaryotes, and estrogen-mediated S-phase entry pathway was found to be inhibited in LNCaP cells upon PTEN loss (**Figure 3.13.B**). The myelination signaling pathway, which is regulated by the crosstalk of Wnt/B-catenin, PI3K/Akt/mTOR, and Ras signaling pathways, is necessary for the myelination process of neuronal axons [68]. Myelin sheaths, which are yielded by oligodendrocytes, serve as insulating agents promoting the faster transmission of action potentials [68]. Human myelin is composed of 30% proteins and 70% lipids, which are cholesterols, cerebroside, ethanolamine phosphatides, lecithin, phosphatidylserine, phosphatidylinositol, and sphingomyelins [69]. Since our metabolomics data suggested an increase in sphingomyelin synthesis in WT-PTEN-LNCaP cells, it was compelling to investigate the significant upregulation in the myelination signaling pathway upon PTEN loss in LNCaP cells. We generated a heatmap displaying significant DEGs associated with the myelination signaling pathway on the Qiagen RNA-seq analysis portal (FDR < 0.05, logFC < -2, or logFC > 2) (**Figure 3.13.C**). We demonstrated significant PTEN overexpression in WT-PTEN-LNCaP cells at the transcriptomic level. However, platelet-derived growth factor D (PDGFD), NFATC4, NFATC2, ITGB2, WNT5A, CREB3L1, IGF1R, SMO, and GLIS2 were significantly downregulated in WT-PTEN expressing LNCaP cells (**Figure 3.13.C**). In our analysis, these genes, which were significantly upregulated upon PTEN loss in LNCaP cells, were implicated in cancer development and progression in previous studies. Interestingly, CREB3L1 was implicated as a pleiotropic gene that can either suppress metastasis or promote cancer

proliferation in different cancer types [70, p. 3], [71]. These results demonstrated that PTEN may negatively regulate the myelination signaling pathway to interfere with cancer progression and tumorigenesis.

Table 3.3. Significant DEGs in sphingolipid metabolism in C4-2 cells upon PTEN loss.

DEGs in Sphingolipid Metabolism	logFC	p-value	FDR
SPTLC2	-0,28324	0,00327	0,03241
SPTLC3	1,36877	0	0,00027
DEGS2	1,12107	0,00081	0,01229
ASAHI	-0,20935	0,00344	0,03339
CERK	1,06605	0	0,0001
SGMS1	-0,26607	0,00379	0,03583
SMPD4	-0,37179	0,00053	0,00924

Secondly, we focused to examine the transcriptomic changes in castration-resistant C4-2 cells upon PTEN loss. Our transcriptomics data revealed 1203 significantly upregulated and 1205 significantly downregulated genes in C4-2 cells upon PTEN loss based on the false discovery rate smaller than 0.05 (FDR < 0.05). We detected some genes involved in the *de novo* ceramide biosynthesis, such as SPTLC2, SPTLC3, or DEGS2 (DES2), were significantly differentially expressed in C4-2 cells upon PTEN loss (**Table 3.3**). Even though SPTLC2 was significantly downregulated upon PTEN loss, SPTLC3 and DEGS2 were significantly upregulated upon PTEN loss in C4-2 cells. Also, we detected the ASAHI gene involved in the salvage pathway, which hydrolyzes ceramides into sphingosine reciprocally, was significantly downregulated in C4-2 cells

upon PTEN loss. Furthermore, CERK was significantly upregulated upon PTEN loss, while SGMS1 and SMPD4 were significantly downregulated upon PTEN loss in C4-2 cells (**Table 3.3**). These results were in parallel with mRNA analysis of the genes involved in sphingolipid metabolism in C4-2 cells [72]. CERK and DEGS2 upregulations may imply that C4-2 cells tend to increase ceramide-1-phosphate abundance upon PTEN loss, while PTEN re-expression switches the pathway direction towards ceramide and sphingomyelin biosynthesis.

We revealed that the most significantly upregulated pathways were regulation of actin cytoskeleton, focal adhesion, phospholipase D signaling pathway, ECM-receptor interaction, axon guidance, Ras signaling pathway, and glycerophospholipid pathway upon PTEN loss in C4-2 cells (**Figure 3.12.B**). Some of the significantly differentially expressed genes associated with the most significantly upregulated pathways were common, like the genes encoding collagen, laminin, integrin subunits, IGF1R, PAK, Ras, Rac, GPCRs, PI3Ks, PLC, PLD, Fyn, CREB, and NFAT.

Interestingly, we detected a similar pattern in upregulated pathways and the differentially expressed genes associated with these pathways upon PTEN loss in LNCaP and C4-2 cells (**Figure 3.12**). We also detected phospholipase D signaling pathway upregulation together with glycerophospholipid metabolism upon PTEN loss in C4-2 cells (**Figure 3.12.B**). As explained above, the phospholipase D signaling pathway can mediate sphingolipid metabolism, sphingolipid signaling pathway, and glycerolipid metabolism, which is also intertwined with glycerophospholipid metabolism. However, the PLD1 gene, instead of PLD2, was found to be significantly upregulated in C4-2 cells upon PTEN loss. Our transcriptomics data suggests that the significant upregulation of the PLD1 gene and PLD signaling pathway in C4-2 cells upon PTEN loss may promote sphingosine kinase 1 activity to produce oncogenic metabolite, sphingosine-1-phosphate, to activate proliferation and survival of C4-2 cells upon PTEN deficiency.

As a third approach for our transcriptomics, we compared the transcriptome profiles of LNCaP as a castration-naïve prostate cancer cell and C4-2 as their castration-resistant derivatives. C4-2 cells were derived from LNCaP cells subcutaneous xenograft tumor of castrated mice, and it has bone metastasis characteristics and more tumorigenic capacity. LNCaP cells, which were isolated from a patient with lymph node metastases of prostate cancer, were injected into the nude mice subcutaneously, then the mice were castrated. And then, C4-2 cells were collected from the bone metastasis tumor of castrated nude mice. Even though C4-2 has AR gene and protein expressions as LNCaP has, it grows in an androgen-independent manner [73]. By comparing these two cells, we aimed to unravel the differences in transcriptomic regulation of metabolic genes and potential mechanisms underlying androgen dependency and castration resistance.

Our transcriptomics approach detected 5037 significantly upregulated and 5056 significantly downregulated genes in C4-2 cells compared to LNCaP cells based on a false discovery rate smaller than 0.05 (FDR < 0.05). Interestingly, we detected the most significantly upregulated pathway in C4-2 compared to LNCaP was sphingolipid metabolism (**Figure 3.14.A**). Significant DEGs associated with the sphingolipid metabolism pathway were mostly upregulated in C4-2 cells, except some isoforms of the enzymes encoding SMPD4 (sphingomyelin phosphodiesterase 4), PLPP4 (phospholipid phosphatase 2), SPHK2 (sphingosine kinase 2), and CERS2 (ceramide synthase 2) (**Figure 3.14.B**). We observed significant upregulation in the genes encoding enzymes of de novo synthesis of ceramides (SPTLCs, DEGS, CERSs), enzymes of the salvage pathway (ASAH1, ACER2, SPHK1, PLPPs), enzymes of sphingomyelin biosynthesis (SMGS2, SMPDs), ceramide kinase (CERK), the enzymes of biosynthesis of sulfoglycolipids (UGT8, GALC), and the enzymes of lactosylceramide biosynthesis (UGCG, ARSA, B4GALNT1) in C4-2 cells compared to LNCaP (**Figure 3.14.B**).

We also observed significant upregulations in ferroptosis, lysosome, peroxisome, calcium signaling pathway, PI3K/Akt/FoxO signaling pathway, and ECM-receptor interaction in C4-2 cells compared to LNCaP cells (**Figure 3.14.A**). Intriguingly, we found glycine, serine, and threonine metabolism pathway was also significantly upregulated in C4-2 cells (**Figure 3.14.A**). This pathway processes serine and glycine to generate important intermediate metabolites and bioactive precursors for protein and lipid synthesis for other pathways. Serine can also be further processed into 3-ketosphinganine through a condensation reaction by the SPT enzyme, which is the first step of the *de novo* synthesis of ceramides. These findings indicate that deregulated metabolic pathways may dictate tumorigenicity and/or therapy-responsiveness, e.g. androgen depletion therapy, in prostate cancer cells. Our results also suggest that sphingolipid metabolism is one of the most crucial pathways in prostate cancer cells, and castration resistance mechanisms may rely on the upregulation of the sphingolipid metabolism pathway or the upregulation of the downstream mechanisms of sphingolipid metabolism.

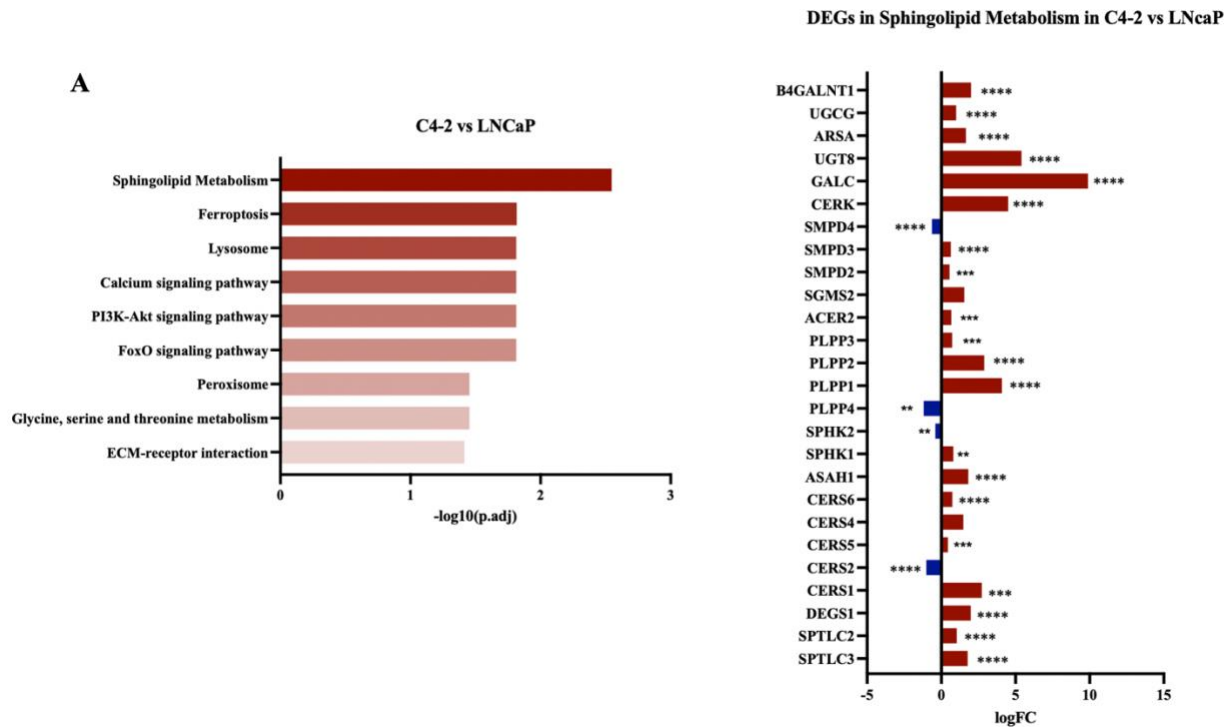
B

Figure 3.14. The most significantly upregulated pathways in C4-2 cells compared to LNCaP

cells. A. The most significantly upregulated pathways in C4-2 cells relative to LNCaP cells. KEGG Pathway database was used for the pathway analysis in LNCaP cells upon PTEN loss (<https://www.kegg.jp>). The pathways were statistically tested according to the number of genes they have and the number of genes that overlapped in the pathway. The clusterProfiler::enrichKEGG package was used in the analysis. $-\log_{10}(p.adj)$ refers to the logarithmic adjusted p values, which were corrected by the Benjamini-Hochberg correction method.

B. The bar plot shows significantly upregulated or downregulated DEGs in the sphingolipid metabolism pathway in C4-2 cells compared to LNCaP cells. Statistical significance reflects false discovery rates (p-values corrected by Benjamini-Hochberg multiple-testing correction method). Red bars on the right side of the logFC axis depict the significant upregulated DEGs, while blue bars on the left side of the logFC axis depict the significant downregulated DEGs (* $p < 0.05$, ** $p < 0.01$, *** $p < 0.001$, **** $p < 0.0001$, DEGs = differentially expressed genes, logFC = logarithmic fold changes).

3.7. Targeting Prostate Cancer Cells with Sphingolipid Metabolism Inhibitors

According to our metabolomics data, the sphingolipid metabolism pathway was detected as the most enriched pathway in both LNCaP (**Figure 3.9**) or C4-2 cells in the presence of exogenous PTEN expression [72]. Moreover, we also revealed that sphingolipid metabolism was significantly upregulated in C4-2 cells compared to LNCaP cells via transcriptomic profiling (**Figure 3.14**). Thus, we wanted to target sphingolipid metabolism in either castration-naïve LNCaP or castration-resistant C4-2 cells with appropriate inhibitors. We decided to target different enzymes acting on various steps of the de novo synthesis of ceramides or the salvage pathway of sphingolipid metabolism, such as dihydroceramide desaturase (DES), acid ceramidases, sphingosine kinases (SPHKs), and sphingosine-1-phosphate receptors (S1PR), thus we hypothesized inhibiting those branches of the pathway could switch on sphingomyelin synthesis or ceramide phosphorylation, as they did in our PTEN re-expressing cellular models via metabolomics approach (**Figure 3.9**, **Figure 3.10**).

We utilized three different inhibitors, which are opaganib (ABC294640), ARN14988, and fingolimod (FTY720), targeting SPHKs or DES, acid ceramidases (ASAH1), and sphingosine kinase/sphingosine-1-phosphate receptors, respectively. We found the viability responses of both LNCaP and C4-2 cells against indicated inhibitors at different concentrations (**Figure 3.15**). We found opaganib or ARN14988 were more effective on C4-2 cells, as they exhibited more sensitivity to those drugs (**Figure 3.15.A, B**), while LNCaP cells were more sensitive to fingolimod compared to C4-2 (**Figure 3.15.C**). We detected IC₅₀ values for each inhibitor. Half-maximal inhibitory concentrations were 5.6 μM for opaganib, 2.6 μM for ARN14988, and 1.37 μM for fingolimod in LNCaP cells, whereas 4.2 μM for opaganib, 0.33 μM for ARN14988 or 3.09 μM for fingolimod were the half-maximal inhibitory concentrations of C4-2 cells (**Figure 3.15**).

Differential responses to each drug suggest that LNCaP or C4-2 cells rely on separate branches of sphingolipid metabolism. We can speculate that C4-2 may rely on *de novo* synthesis of ceramides or sphingosine-1-phosphate production for proliferation, survival, or lipid and protein synthesis due to more pronounced sensitivity to opaganib and ARN14988 in C4-2, supported by the upregulated sphingolipid metabolism profile of C4-2 (**Figure 3.14**). This approach can be applied to target castration-resistant prostate cancer cells. However, castration-naïve prostate cancer cells may rely on sphingosine kinase activity, mostly S1PR activity, as fingolimod significantly decreased the viability of LNCaP cells more than it did in C4-2 cells (**Figure 3.15.C**). Besides, fingolimod had dramatic cytotoxic effects on both cells compared to other drugs.

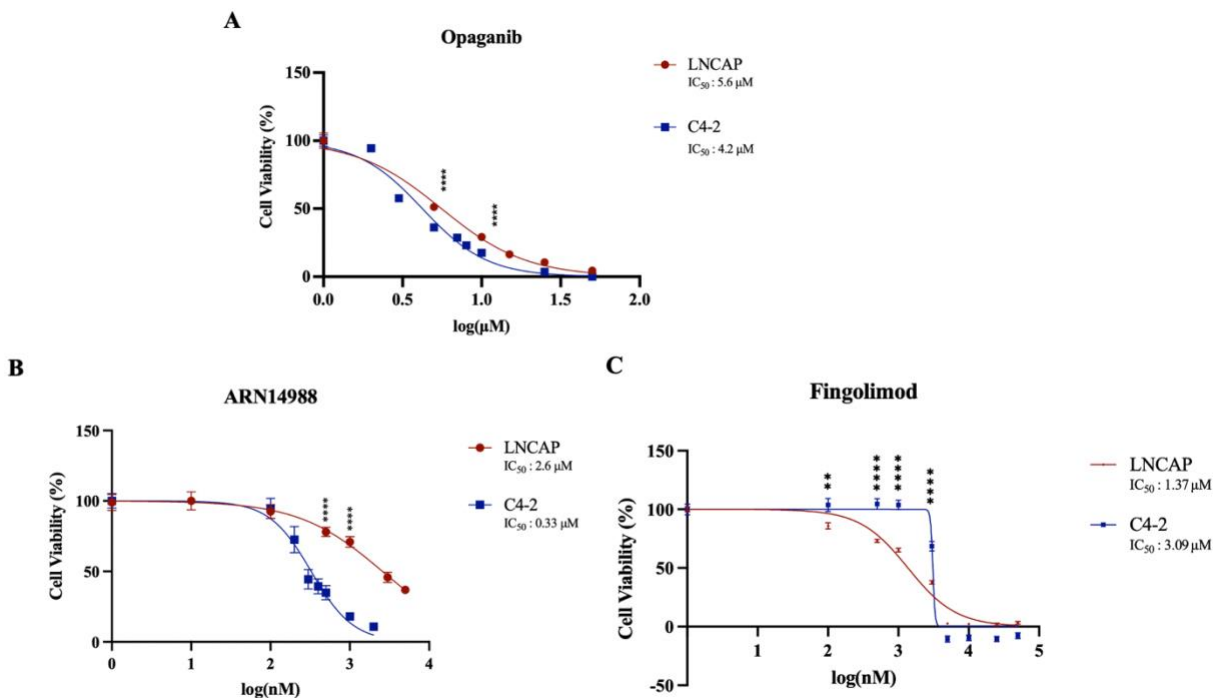


Figure 3.15. Dose-response curves of LNCaP or C4-2 cells for opaganib, ARN14988, and fingolimod. A, B. LNCaP or C4-2 cells were treated with increasing concentrations of opaganib or ARN14988 for 5 days in serum-reduced conditions. At the end of the treatment, cells were fixed with 4% PFA and crystal violet assays were conducted. The error bars depict the standard error means (SEM) of two independent

biological replicates [72]. **C.** LNCaP or C4-2 cells were treated with increasing concentrations of fingolimod for 5 days. At the end of the treatment, cells were fixed with 10% TCA and SRB assay was conducted. Statistical significance was determined by ordinary two-way ANOVA with Šidak's multiple comparison test. The error bars depict the standard error means (SEM) of three independent biological replicates (n=3, * p<0.05, ** p<0.01, *** p<0.001, **** p<0.0001).

3.8. Regulation of PI3K/Akt Pathway upon Sphingolipid Metabolism Inhibition in Castration-naïve Prostate Cancer Cells

Based on our RNA-seq and qPCR analyses demonstrating significant downregulation of the SPHK1 gene in PTEN-replete LNCaP cells together with the potent response of LNCaP cells to increasing doses of opaganib, we wanted to characterize the response of opaganib to castration-naïve LNCaP cells. Since opaganib is a dual inhibitor, targeting DES and SPHK in the sphingolipid metabolism [74], we wanted to determine the consequences of targeting the deregulated sphingolipid metabolism of LNCaP cells. We treated LNCaP cells with DMSO, 5 μ M (IC₅₀ value of LNCaP), and 10 μ M of opaganib for three days. Then we harvested the cells by counting the cells by dye exclusion trypan blue test (**Figure 3.16.A**). We demonstrated that around 50% of LNCaP cell viability was significantly reduced upon 5 μ M of opaganib treatment, and opaganib at 10 μ M significantly reduced the number of viable LNCaP cells by nearly 80% (**Figure 3.16.A**), consistent with the opaganib dose-response experiments in LNCaP cells (**Figure 3.15.A**). Then, we characterized the opaganib responses on MAPK (ERK) or PI3K/Akt pathways in LNCaP cells to understand the underlying mechanisms of opaganib potency. Even though we did not observe any significant change in phosphorylation of ERK levels in LNCaP cells upon different concentrations of opaganib treatments, we observed a general reduction in the activity of the PI3K/Akt pathway (**Figure 3.16.B, 3.16.C**). The levels of phosphorylated AKT S473 were

decreased upon opaganib treatment in a dose-dependent manner, but we did not observe a gradual reduction of the expression of other components in the PI3K pathway, instead, we detected almost equivalent amount of reduction in the expression levels of p110 β , phosphorylated PRAS40, phosphorylated mTOR, phosphorylated S6 or phosphorylated 4EBP1 (**Figure 3.16.B**). Interestingly, we also observed a more potent decrease in total proteins of the PI3K/Akt pathway, which indicates that opaganib treatment may affect the stability of the proteins involved in the mTOR signaling pathway, especially 4EBP1 (**Figure 3.16.C**). Interestingly, we also detected that inhibition of sphingolipid metabolism by opaganib treatment diminished the expression of SREBP2 in a dose-dependent manner, which is a sterol-regulatory element-binding protein encoded by the SREBF2 gene and modulates sterol-regulating genes in the cholesterol biosynthesis [75] (**Figure 3.16.D**). However, we observed the inverse effect on the SQLE expression upon opaganib treatment. SQLE, which is directly targeted and transcriptionally regulated by SREBP2, serves as a second-rate-limiting enzyme in the cholesterol biosynthesis pathway [76]. We demonstrated increased SQLE expression levels upon opaganib treatment in LNCaP cells (**Figure 3.16.D**). These findings suggested that SREBP2 can be directly targeted by opaganib treatment, possibly affecting the upstream effectors of the cholesterol pathway. Also,

possible feedback regulations activated by the decrease of SREBP2 might increase SQLE expression.

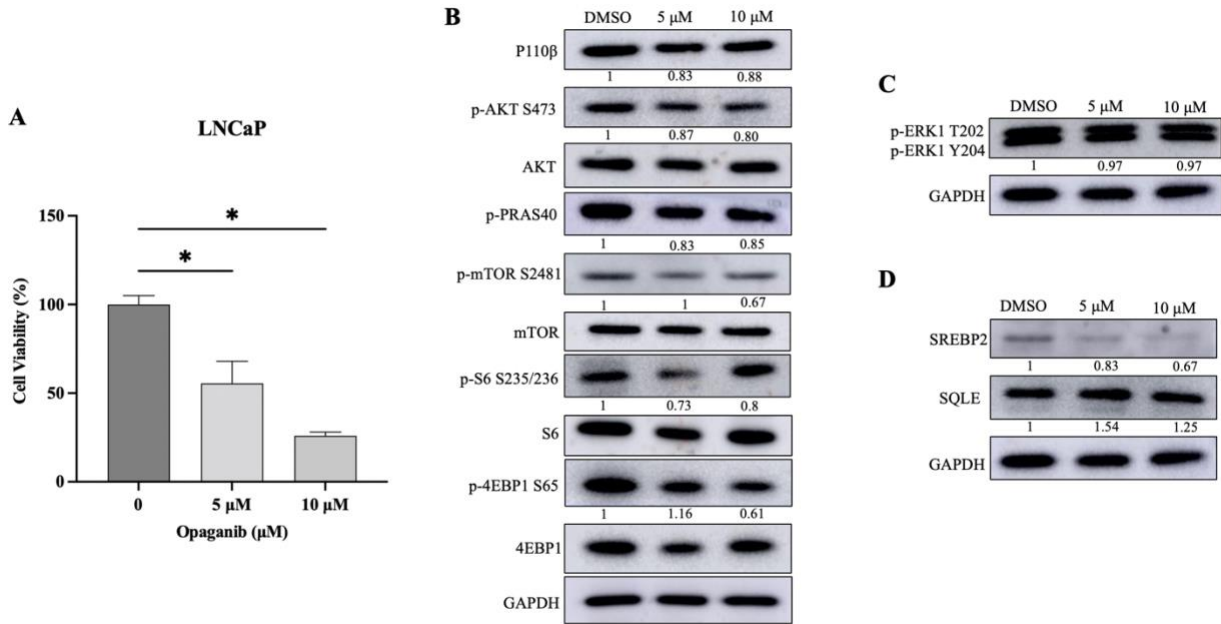


Figure 3.16. Opaganib inhibits LNCaP proliferation by downregulating the PI3K/Akt pathway. The cells were treated with either DMSO, 5 μM or 10 μM opaganib for 72 hours with serum-reduced media. 15 μg of the lysates were subjected to western blot analysis. **A.** Cell viability was assessed by trypan blue exclusion test while harvesting the cells. Statistical significance was determined by an ordinary one-way ANOVA test. Error bars depict standard error means of two repeating and independent cell counting (* p<0.05). **B.** Protein expression profiles of the PI3K/Akt pathway components upon opaganib treatment. The number under each phospho-protein blot depicts the relative expression level compared to their total proteins. GAPDH was used as a loading control. **C.** Protein expression profiles of the components of Ras signaling pathway upon opaganib treatment. The number under phospho-protein blot depicts the relative expression level compared to their total proteins. GAPDH was used as a loading control. **D.** Protein expression profiles of the components of cholesterol biosynthesis pathway upon opaganib treatment. The number under the protein blot depicts the relative expression level compared to the loading control. GAPDH was used as a loading control.

All in all, our metabolomics and transcriptomics approaches detected that sphingolipid metabolism was deregulated in PTEN-null metastatic prostate cancer cells. Rational treatment strategies including standalone or combinatorial treatments with sphingolipid metabolism inhibitors could be potent anti-cancer therapy options in metastatic and castration-resistant prostate cancer.

4. DISCUSSION

Prostate cancer is the second leading cause of death and the most diagnosed cancer type among men globally. Surgery, hormone therapy alone, or along with chemotherapy and radiation are the initial treatment options for prostate cancer. Since androgens are the main fuel for prostate cancer development and progression, androgen deprivation therapy (ADT) by surgery or anti-androgen administration, is the initial approach to treat prostate cancer [77]. Even though these treatment options are primarily effective, prostate cancer can still progress by acquiring resistance against androgen ablation conditions, and it becomes more aggressive, develops castration resistance, and has an androgen-independent progression [78]. Thus, the treatment options become dramatically restricted, leading to higher lethality in metastatic and castration-resistant prostate cancer. Therefore, it is crucial to reveal the underlying mechanisms of castration resistance and aberrant androgen signaling activity against androgen depletion for more effective and approachable treatments.

PI3K/Akt pathway is one the most important and frequently mutated pathways in prostate cancer. It regulates proliferation, anti-apoptotic and pro-survival signals, migration, and invasion, as well as cellular metabolism. It mediates the metabolic needs of cancer cells by upregulating nutrient uptake and promoting aerobic glycolysis, nucleotide synthesis, and lipid synthesis [79]. PTEN, which is a negative regulator of the PI3K/Akt pathway, is a very frequently mutated tumor

suppressor gene in prostate cancer. PTEN dephosphorylates membrane-bound PIP3 to convert it to PIP2, thus downregulating the activity of PI3K and the downstream mediators' [37]. Inactivation of PTEN occurs at the initial stages of the malignancy of prostate cancer (Robinson et al., 2015). Previous reports showed the consequences of PTEN loss for metabolic rewiring in cancer, such as increasing lipid biosynthesis by upregulating the activity of SREBPs in prostate cancer and promoting the Warburg effect or nucleotide synthesis [17]. As a result, PI3K/Akt activating mutations in prostate cancer, along with homozygous PTEN loss, can substantially deregulate metabolic pathways, promoting prostate cancer growth and progression. In this study, we wanted to identify metabolomic alterations directly affected by PTEN-loss in the metastatic and castration-naïve prostate cancer cell, LNCaP. Moreover, we also aimed to understand the transcriptomic regulations of the metabolome of both castration-naïve and castration-resistant prostate cancer cells in the absence and the presence of PTEN expression.

We generated a doxycycline-inducible Tet-on PTEN expression system to introduce either wild-type, only lipid phosphatase mutant, only protein phosphatase mutant, or catalytically inactive PTEN into LNCaP cells. Thus, we were able to observe the direct consequences of PTEN loss in this cellular model of prostate cancer. Using a Tet-on system, we also ruled out the likelihood of LNCaP cells adapting to stable exogenous PTEN expression. After we generated a Tet-on PTEN expression system in LNCaP cells, we also confirmed that our system did not have PTEN expression leakage in the absence of doxycycline (**Figure 3.1**). We determined that wild-type PTEN or PTEN-Y138L expressing LNCaP cells downregulated the expression levels of pAKT S473 or pAKT T308. Akt is one of the first effectors in the PI3K/Akt pathway, so mainly lipid phosphatase activity of PTEN diminishes AKT phosphorylation by antagonizing PI3K function [65]. Further, we confirmed the functionality of PTEN in our system by utilizing the PIP3

biosensor, and by performing immunofluorescence assays (**Figure 3.2, Figure 3.3**). There were significantly fewer peripheral GFP signals in wild-type PTEN-expressing LNCaP cells upon doxycycline induction, whereas catalytically inactive PTEN-expressing LNCaP cells (PTEN-C124S) upon doxycycline treatment had strong peripheral GFP signals. These results strongly suggest that membrane-bound PIP3 was successfully dephosphorylated by PTEN phosphatase function as expected [64], while catalytically inactive PTEN failed to do so.

We demonstrated the effects of different PTEN functions on LNCaP cell viability (**Figure 3.4**). We observed a significant reduction in viability in WT-PTEN-LNCaP or PTEN-Y138L-LNCaP cells in parallel with the previous findings showing the negative impacts of PTEN lipid phosphatase function on cancer cell proliferation [80]. We have also shown protein phosphatase function or the phosphatase-independent function of PTEN does not have any impact on cellular viability because PTEN lipid phosphatase function is primarily the negative regulator of the PI3K/Akt pathway.

During characterizing the impacts of wild-type or functional mutants of PTEN on the PI3K/Akt pathway, we demonstrated significant downregulation of AKT phosphorylation at the S473 or T308 residues in WT-PTEN-LNCaP or PTEN-Y138L-LNCaP cells upon doxycycline induction (**Figure 3.5**). There was no change in the phosphorylation levels of Akt in the cells expressing either only protein phosphatase or catalytically inactive PTEN. We did not observe any significant changes in the phosphorylation levels of mTOR signaling components, such as phospho-mTOR S2481 or phospho-S6 S240/244, upon re-expression of either wild-type or different PTEN functional mutants. mTOR signaling pathway has different upstream regulators in addition to the PI3K/Akt signaling, e.g. MAPK signaling, Wnt signaling, and growth factors such as amino acids, glucose, or varying oxygen availability [81]. Thus, PTEN re-expression of any functional variants

in LNCaP did not overcome the impacts of other upstream regulators to control mTOR signaling. Furthermore, we did not observe any significant alterations in the expression of PI3K/Akt pathway components in PTEN-G129E-LNCaP or PTEN-C124S-LNCaP cells upon doxycycline induction, which explains that protein phosphatase or phosphatase-inactive PTEN do not affect the PI3K/Akt pathway and cell proliferation in a noticeable way (**Figure 3.4, Figure 3.5**).

We performed targeted metabolomics to reveal deregulated metabolites upon PTEN deficiency in castration-naïve LNCaP cells. Metabolic rewiring is one of the hallmarks of cancer cells, thus it is crucial to interrogate the impact of deregulated metabolic pathways and target them to prevent cancer development. We unveiled significant alterations in some metabolites constituting glycerophospholipids or sphingolipids in WT-PTEN-LNCaP, C124S-PTEN-LNCaP, or negative control (MOCK) cells (**Figure 3.8**). Homozygous loss of PTEN alleles or PTEN phosphatase inactivation are the most frequent PTEN alterations in prostate cancer, therefore we studied those events in greater detail with our cellular models.

Some glycerophospholipid species were significantly upregulated in WT-PTEN-LNCaP cells compared to empty vector control or catalytically inactive PTEN expressing (C124S-PTEN) LNCaP cells (**Figure 3.8.A**). It demonstrated that the phosphatase activity of PTEN predominantly affected glycerophospholipid metabolism rather than its phosphatase-independent functions. However, only one glycerophosphocholine species (PC-O(32:3)) was detected as significantly upregulated in both wild-type or catalytically-inactive PTEN-expressing LNCaP cells (**Figure 3.10.A**). On the other hand, one phosphocholine (PC(40:2)) species was significantly downregulated in both WT-PTEN or C124S-PTEN-LNCaP cells, and two other phosphocholine species (PC(40:3), PC(40:5)) were downregulated only in C124S-PTEN-LNCaP cells compared to the negative control (**Figure 3.10.A**). These results might imply that PTEN phosphatase-

independent function may be important to modulate the abundance of specific phosphocholine species. Hence, loss of PTEN function may rewire glycerophospholipid metabolism in castration-naïve LNCaP cells to meet cancerous demands, mostly by downregulating the levels of certain glycerophospholipid metabolites.

We also detected significant changes in sphingolipids in the presence of wild-type PTEN in LNCaP cells (**Figure 3.8.B**). Almost all the sphingolipid species, except Cer(34:1), were increased in WT-PTEN-LNCaP cells compared to negative control and catalytically-inactive PTEN variant. Some of the sphingomyelin upregulation in WT-PTEN-LNCaP cells were statistically significant, whereas few of them were nearly significantly upregulated in the WT-PTEN-LNCaP cells. We observed only one sphingomyelin species (SM(38:2)) was significantly upregulated both in WT-PTEN or C124S-PTEN-LNCaP cells compared to their negative control (**Figure 3.8.B**). These findings showed that, primarily, PTEN phosphatase function may be crucial for the upregulation of sphingomyelins. Sphingomyelin synthases (SGMSs) can produce sphingomyelins and DAGs from ceramides and phosphatidylcholines [50]. A significant increase in some sphingomyelin species may result in a decrease in ceramides. Along these lines, our results yielded a lower limit of quantification of the concentration of ceramides in LNCaP cells. These findings suggested that PTEN re-expression increases sphingomyelin abundance in LNCaP cells.

To further understand these alterations upon PTEN re-expression in LNCaP cells, we did perform metabolite set enrichment analysis on glycerophospholipids and sphingolipids metabolite sets in WT-PTEN-LNCaP and LNCaP-MOCK via MetaboAnalyst 5.0 MSEA tool. At this point, we eliminated C124S-PTEN-LNCaP cells from the analysis because homozygous PTEN deletion is clinically more frequent in prostate cancer than point mutation in its phosphatase domain of PTEN. MSEA demonstrated that sphingolipid metabolism was the most enriched pathway among

glycerophospholipids, and sphingolipids based on their abundances in WT-PTEN-LNCaP and LNCaP-MOCK (**Figure 3.9**). Although enrichment in sphingolipid metabolism was not statistically significant, our previous findings displayed significant enrichment in sphingolipid metabolism in C4-2 cells upon PTEN re-expression [72]. Therefore, we decided to further interrogate the possible and potential alterations in sphingolipid metabolism in castration-naïve LNCaP cells.

We detected the relative mRNA expression levels of the genes involved in sphingolipid metabolism in PTEN-null and PTEN-replete LNCaP cells to compare the regulation of sphingolipid metabolism at the transcriptional level (**Figure 3.11**). In parallel with our metabolomics data, we found upregulation of the *SGMS2* gene, which synthesizes sphingomyelins, in PTEN-replete condition relative to its PTEN-null counterpart. However, we did not observe any significant changes in the genes encoding enzymes in the *de novo* synthesis of ceramides, which are *SPTLC1*, *DES1*, *CERS2*, or *ASAH1* gene, which is an acid ceramidase converting ceramides to sphingosine. It may imply that PTEN does not affect the *de novo* biosynthesis of ceramides to stimulate anti-proliferative signals in castration-naïve prostate cancer cells. However, we cannot rule out the involvement of PTEN in regulating the activity of these enzymes at the translational level. Interestingly, we detected significant downregulation in the *SPHK1* gene upon PTEN re-expression in LNCaP cells. Sphingosine kinases phosphorylate sphingosine to yield sphingosine-1-phosphate (S1P), which is indicated as an oncogenic metabolite by transducing pro-survival signals and promoting proliferation, growth, and migration. It suggests that PTEN may regulate sphingosine kinase mRNA expression, thereby regulating sphingosine kinase activity in prostate cancer cells.

We also detected that the ceramide kinase gene (CERK), phosphorylating ceramides and yielding to ceramide-1-phosphate (C1P), was upregulated in PTEN-replete LNCaP cells. Although C1P has been indicated as a pro-proliferative metabolite in cancer, a recent study demonstrated CERK is one of the AR-repressed genes. It was also shown that an anti-androgen treatment by Enzalutamide (MDV3100) on prostate cancer cells or castrated mouse models enhanced C1P abundance [82], [83]. Furthermore, PTEN can negatively regulate AR signaling by directly interacting with AR and blocking its nuclear translocation, in turn, leading to AR protein degradation [84]. These findings may explain how PTEN re-expression in LNCaP cells upregulated the CERK gene, demonstrated by mRNA analysis and transcriptomics approach (**Figure 3.11, Table 3.1**).

Regarding qPCR experiments, the standard error means could be stemmed from the experimental mistakes, inconsistencies between biological replicates, and low abundance of the assigned genes in LNCaP cells as they also were not detected as significantly differentially expressed genes by RNA-sequencing analysis.

Moreover, we also performed transcriptomics in castration-resistant C4-2 cells to reveal the transcriptional differences between PTEN-null and PTEN-replete conditions (**Figure 3.12.B, Table 3.3**). Interestingly, we detected that CERK gene expression was significantly upregulated upon PTEN loss in C4-2, the opposite of the pattern in LNCaP (**Table 3.2, Table 3.3**). In C4-2 cells, PTEN re-expression could downregulate C1P abundance by inhibiting the pro-survival activity of CERK. Since C4-2 are androgen-independent and castration-resistant prostate cancer cells, PTEN re-expression may affect ceramide metabolism independent of AR-signaling. We also observed that the genes involved in the *de novo* biosynthesis of ceramides were significantly upregulated and the sphingomyelin synthase gene with sphingomyelin phosphodiesterase was

significantly downregulated in C4-2 cells upon PTEN loss (**Table 3.3**). These findings were in parallel with the mRNA analysis of C4-2 cells upon PTEN re-expression [72]. Collectively, our transcriptomics analysis suggests that the re-expression of PTEN in C4-2 cells might lean towards sphingomyelin biosynthesis because of the ceramide accumulation.

The most significantly commonly upregulated pathways upon PTEN loss in metastatic prostate cancer cells were found to be the ECM-interaction, focal adhesion, Ras signaling pathway, phospholipase D signaling pathway, cGMP-PKG signaling pathway, PI3K/Akt signaling pathway and axon guidance (**Figure 3.12**). These findings demonstrate that loss of tumor-suppressor PTEN activity upregulated the genes associated with migratory-related pathways in line with its known functions. It also shows that since PTEN loss occurs at the initial stage of prostate cancer, mechanisms related to castration resistance in metastatic prostate cancer cells might not be affected by PTEN deficiency. On the other hand, upregulation in SGMS gene expression and sphingomyelin biosynthesis in PTEN re-expressed LNCaP or C4-2 cells may affect the migratory profiles of these cells. A previous study demonstrated that sphingomyelin enrichment driven by SGMS enzymes downregulated CXCR4 dimerization by changing the lipid rafts, thereby CXCR4/CXCL12 signaling-induced migration in the MEF cells [85]. In parallel with these findings and based on our transcriptomic data, we infer that upregulation of the SGMS gene and sphingomyelin species upon PTEN re-expression may lead to diminishing the migration pathways by possibly downregulating ACKR3 (CXCR7) gene expression in LNCaP and C4-2 cells. Because ACKR3, which we detected significantly upregulated upon PTEN loss in LNCaP and C4-2 cells, is known to dimerize with CXCR4 to induce CXCL12-mediated migration in the nasopharyngeal carcinoma [86]. Hence, a decrease in sphingomyelin caused by PTEN loss may lead to changes in the compositional variabilities of lipid rafts in the membrane, increasing the ACKR3/CXC12-

induced migration. This may also explain the upregulation of the cytokine-cytokine interaction pathway upon PTEN loss in LNCaP (**Figure 3.12.A**).

For further examination of our transcriptomics findings in LNCaP cells upon PTEN loss, we utilized the Qiagen RNA-seq analysis portal. We detected the 10 most significantly enriched pathways upon PTEN loss in our cellular models (**Figure 3.13.A**). The pathway analysis was based on Ingenuity Pathway Analysis (IPA) database by Qiagen; thus, we observed slightly different annotations of the most enriched pathways compared to our initial analysis. We observed that cell cycle control of chromosomal replication and mismatch repair in eukaryotes were also significantly enriched and predicted to be inhibited upon PTEN loss in LNCaP cells, which is consistent with the tumor suppressor function of PTEN. Interestingly, we determined that the myelination signaling pathway was significantly enriched and predicted to be activated upon PTEN loss in LNCaP (**Figure 3.13.B**). The myelination signaling is made up of PI3K/Akt signaling, the Wnt/ β -catenin signaling, and Ras signaling pathways and it leads to myelination of the neuronal axons [68]. Some of the constituents of myelin sheaths are the sphingomyelins [69]. Thus, we focused on the significant differentially expressed genes involved in the myelination signaling pathway and found significant upregulations in the genes encoding platelet-growth factors, integrin subunits, insulin growth factor-like receptor 1, Wnt signaling proteins, non-classical GPCR smoothed and cAMP-responsive element-binding protein 3 like 1, all of which is indicated to act as oncogenic roles in cancer cells. Interestingly, our transcriptomics analysis in C4-2 cells upon PTEN loss also revealed significant upregulations of those genes which were also associated with the significantly upregulated pathways in C4-2 cells upon PTEN loss (**Figure 3.12.B**).

For instance, NFAT (nuclear factor of activated T cells) is a transcription factor, including four different calcium-regulated members, which are NFATC1, NFATC2, NFATC3, and NFATC4. NFAT genes are also involved in axon guidance and cGMP-PKG signaling pathways, promoting axon outgrowth and transcription of hypertrophic response genes, respectively [87]. A recent study demonstrated that NFATC2 promoted epithelial-mesenchymal transition in melanoma cells [88]. Besides, another study revealed that the NFATC1 member of the NFAT family functions as an oncogene in prostate tumorigenesis by stimulating downstream oncogene expressions and inhibiting senescence that is driven by PTEN loss [89]. Our analysis supported the NFAT family's oncogenic actions in LNCaP. PTEN-loss-induced NFAT genes may promote EMT by upregulating migratory pathways in LNCaP cells upon PTEN loss. Interestingly, we also detected significant upregulation in the NFATC2 gene upon PTEN loss in C4-2 cells. Hence, the NFAT transcription factor family may be important to induce PTEN-loss responses in metastatic prostate cancer cells, especially to stimulate migration.

The final approach of our transcriptomics was to compare PTEN-null castration-resistant C4-2 and PTEN-null castration-naïve LNCaP cells. C4-2 is a subline of LNCaP cell, which is derived from LNCaP xenograft tumors of castrated mice. C4-2 is derived from bone metastatic prostate cancer and has higher tumorigenic activity compared to LNCaP. Even though both cell lines have AR gene expression, C4-2 has androgen-independent growth and castration resistance [73]. We aimed to reveal the transcriptional alterations underlying the castration-resistance mechanism. Interestingly, we detected that the most significantly upregulated pathway is sphingolipid metabolism (**Figure 3.14.A**) and CERK is one of the most upregulated genes in C4-2 cells compared to LNCaP (**Figure 3.14.B**). Our analyses suggest that the acquisition of castration resistance in metastatic prostate cancer cells may rely on deregulation in sphingolipid metabolism

and the CERK gene may be the key regulator determining this switch since it is an AR-repressed and PTEN-regulated gene. Additionally, we also detected that glycine, serine, and threonine metabolism was significantly upregulated in C4-2 cells compared to LNCaP (**Figure 3.14.A**). This pathway uses serine to make intermediate metabolites and building blocks for making proteins and fats. Serine is also utilized by SPTLC, the first enzyme in *de novo* ceramide biosynthesis, in the condensation reaction with palmitoyl-CoA to yield 3-ketosphinganine. Upregulation of sphingolipid metabolism, as well as serine metabolism, may highlight the possible mechanisms leading to higher tumorigenicity, androgen independence, and castration resistance in metastatic prostate cancer cells. It is tempting to suggest that castration resistance in prostate cancer may rely on the upregulation of the sphingolipid metabolism pathway or the upregulation of its crosstalk mechanisms.

Based on our high throughput data, we wanted to target the sphingolipid metabolism pathway in metastatic prostate cancer cells. We used opaganib, ARN14988, and fingolimod to inhibit different steps of the sphingolipid metabolism in LNCaP and C4-2 cells. We observed each standalone treatment of metastatic prostate cancer cells was effective (**Figure 3.15**). We detected more sensitivity in C4-2 cells against opaganib and ARN14988 treatments, whereas LNCaP cells exhibited more sensitivity against fingolimod. Fingolimod (FTY720) is a sphingosine 1 kinase inhibitor and it is also an FDA-approved oral administration drug for multiple sclerosis treatment [90]. In the last two decades, studies showed that fingolimod has also anti-cancer effects, which can induce apoptosis and inhibit proliferation, angiogenesis, and metastasis in prostate cancer [91]–[93]. Fingolimod is a sphingosine analog that can be phosphorylated by sphingosine kinases, and phosphorylated fingolimod can bind to sphingosine-1-phosphate receptors (S1PRs) and act as an antagonist of S1PR and inhibit downstream signaling in sphingolipid metabolism regulated

GPCRs [94]. Our dose-response experiments showed that LNCaP cells were more sensitive to treatment with fingolimod, even though both types of cells died when treated with more than 3 μ M of fingolimod (**Figure 3.15.C**). LNCaP may rely on sphingosine kinase 1 activity more than sphingosine kinase 2, as we detected significant downregulation of SPHK1 in the presence of PTEN. It may be suggested that LNCaP may rely on sphingosine kinase 1 enzyme activity more than C4-2.

Opananib is a dual inhibitor, targeting DES and SPHK2 enzymes in sphingolipid metabolism. It inhibits the S1P generation and its further downstream effects [45]. Phase II trials of opananib are currently in progress for mCRPC patients [95]. Even though SPHK2 gene expression was significantly downregulated in C4-2 cells compared to LNCaP (**Figure 3.14.B**), C4-2 was found to be more sensitive to opananib treatment. Yet, opananib also blocks DES activity, whose mRNA expression levels were significantly upregulated in C4-2 cells (**Figure 3.14.B**). However, catalytic activity regulations of sphingosine kinase 1 or 2 in C4-2 and LNCaP would also explain the effects of opananib and fingolimod. Lastly, ARN14988 is an ASAH1 inhibitor, which is an acid ceramidase in the salvage pathway of sphingolipid metabolism. Our findings suggested that ARN14988 is the most potent inhibitor hindering the proliferation of castration-resistant C4-2 cells (**Figure 3.15.B**). On the other hand, we detected more cytostatic effects of ARN14988 on LNCaP cells. Our transcriptomics data detected that ASAH1 gene expression was significantly upregulated in C4-2 cells compared to LNCaP. It may explain why castration-resistant C4-2 cells may rely more on the ASAH1 gene's activities than castration-naïve LNCaP as they exhibit increased sensitivity to ARN14988 treatments. Interestingly, we observed significant downregulation in ASAH1 expression upon PTEN loss in C4-2 cells. Targeting ASAH1 in castration-resistant prostate cancer may have more potential to inhibit pro-survival activities. A

recent study found that the capacity of melanoma cells to generate cancer-initiating cells upon ASAH1 depletion was lost [96]. It suggests that ARN14988 treatment targeting ASAH1 in metastatic prostate cancer would be promising to overcome the castration resistance mechanisms and increase overall survival.

We continued to investigate the sphingolipid metabolism inhibitor responses on castration-naïve LNCaP cells. We aimed to resolve the mechanism underlying opaganib responses on cell viability. We determined a downregulation of the PI3K/Akt pathway, but not the MAPK pathway, upon treatment of LNCaP cells with two different concentrations of opaganib (**Figure 3.16.B, 3.16.C**). The reason that opaganib reduces the proliferation of LNCaP cells might be due to the downregulation of the PI3K/Akt pathway and the decreased stability of proteins involved in the mTOR signaling. Interestingly, we detected a dose-dependent downregulation in SREBP2 protein expression, while an upregulation in SQLE expression (**Figure 3.16.D**). SREBP2 might be affected by opaganib treatment, although the upregulation in SQLE expression might be regulated by feedback mechanisms to compensate for the cholesterol levels. Higher doses of opaganib treatment might overcome SQLE expression in longer treatment conditions. Nevertheless, our findings suggested possible regulations of lipid homeostasis by inhibiting sphingolipid metabolism via SREBP2-regulated mechanisms.

To sum up, we demonstrated that sphingolipid metabolism is deregulated upon PTEN loss in metastatic prostate cancer cells. Additionally, the sphingolipid metabolism may regulate the mechanism of androgen independence and castration resistance in prostate cancer cells. It is crucial to target sphingolipid metabolism with standalone or combinatory treatment strategies, especially with androgen deprivation therapies.

5. CONCLUSION AND FUTURE PERSPECTIVES

In this study, we aimed to illustrate the metabolomic and transcriptomic changes associated with PTEN loss and castration resistance in advanced-stage prostate cancers. We detected a significant increase in some sphingomyelin and glycerophospholipid species in PTEN-replete LNCaP cells and showed that these changes mostly depend on the catalytic activity of PTEN. We performed metabolite set enrichment analysis in PTEN-null or PTEN-replete LNCaP cells and it revealed that the sphingolipid metabolism pathway is reprogrammed upon PTEN loss in castration-naïve LNCaP cells. We further investigated transcriptomic alterations in LNCaP and C4-2 cells upon PTEN re-expression by performing RT-qPCR and RNA-sequencing. We correlated that the increase in sphingomyelin species in PTEN-replete conditions results from the upregulation in the sphingomyelin synthase gene expression in PTEN-replete LNCaP cells. mRNA and transcriptomics analysis also demonstrated a significant increase in ceramide kinase expression in PTEN-replete LNCaP cells. On the other hand, we observed a significant decrease in sphingosine kinase gene expression upon PTEN re-expression. Our results implicate that PTEN re-expression in LNCaP cells causes sphingomyelin and ceramide-1-phosphate accumulation by directing the sphingolipid metabolism pathway toward sphingomyelin production. Further investigations are needed to uncover the detailed mechanistic relationship between PTEN and sphingolipid metabolism, to understand how PTEN leads to an increase in sphingomyelin abundance and whether PTEN is one of the interaction partners of the enzymes involved in sphingolipid metabolism. When we targeted sphingosine kinase activity in LNCaP cells by opaganib treatment, we detected downregulation of the PI3K/Akt pathway as well as SREBP2 protein expression. The diverse effects of sphingolipid metabolism inhibitors could be studied in more detail at

transcriptional and translational levels. Sphingolipid inhibitors' mode of action on cancer cell viability should be investigated further either in standalone or combinatorial trials.

Furthermore, we inspected transcriptomic differences between castration-naïve and castration-resistant prostate cancer cells. We reported that the most significantly upregulated pathway in castration-resistant cells compared to castration-naïve cells is the sphingolipid metabolism. Additionally, upon treatment with various sphingolipid biosynthesis inhibitors, we found a trend toward increased sensitivity in castration-resistant prostate cancer cells. We speculated that castration-resistant prostate cancer cells rely on sphingolipid metabolism more than castration-naïve prostate cancer cells do. For further confirmation of our results, chIP-sequencing would be performed to reveal AR-regulated sphingolipid metabolism genes in metastatic prostate cancer cells. Proteomics studies could be helpful to resolve the relationship between AR-signaling and the sphingolipid metabolism pathway if one may regulate the other. Since sphingolipid metabolism inhibitors work better on prostate cancer cells that are resistant to castration, it would be a good idea to use these inhibitors to improve the effectiveness of anti-androgen drugs both in vitro and in vivo by using them in combination with other drugs.

6. BIBLIOGRAPHY

- [1] R. J. Rebello *et al.*, “Prostate cancer,” *Nat. Rev. Dis. Primer*, vol. 7, no. 1, p. 9, Feb. 2021, doi: 10.1038/s41572-020-00243-0.
- [2] S. Sandhu, C. M. Moore, E. Chiong, H. Beltran, R. G. Bristow, and S. G. Williams, “Prostate cancer,” *The Lancet*, vol. 398, no. 10305, pp. 1075–1090, Sep. 2021, doi: 10.1016/S0140-6736(21)00950-8.

- [3] D. Robinson *et al.*, “Integrative Clinical Genomics of Advanced Prostate Cancer,” *Cell*, vol. 162, no. 2, p. 454, Jul. 2015, doi: 10.1016/j.cell.2015.06.053.
- [4] E. S. Antonarakis, A. J. Armstrong, S. M. Dehm, and J. Luo, “Androgen receptor variant-driven prostate cancer: clinical implications and therapeutic targeting,” *Prostate Cancer Prostatic Dis.*, vol. 19, no. 3, pp. 231–241, Sep. 2016, doi: 10.1038/pcan.2016.17.
- [5] S. C. Chan and S. M. Dehm, “Constitutive activity of the androgen receptor,” *Adv. Pharmacol. San Diego Calif*, vol. 70, pp. 327–366, 2014, doi: 10.1016/B978-0-12-417197-8.00011-0.
- [6] T. van der Steen, D. J. Tindall, and H. Huang, “Posttranslational modification of the androgen receptor in prostate cancer,” *Int. J. Mol. Sci.*, vol. 14, no. 7, pp. 14833–14859, Jul. 2013, doi: 10.3390/ijms140714833.
- [7] S. M. G. Espiritu *et al.*, “The Evolutionary Landscape of Localized Prostate Cancers Drives Clinical Aggression,” *Cell*, vol. 173, no. 4, pp. 1003–1013.e15, May 2018, doi: 10.1016/j.cell.2018.03.029.
- [8] M. Korpál *et al.*, “An F876L mutation in androgen receptor confers genetic and phenotypic resistance to MDV3100 (enzalutamide),” *Cancer Discov.*, vol. 3, no. 9, pp. 1030–1043, Sep. 2013, doi: 10.1158/2159-8290.CD-13-0142.
- [9] Y. Yan and H. Huang, “Interplay Among PI3K/AKT, PTEN/FOXO and AR Signaling in Prostate Cancer,” in *Prostate Cancer: Cellular and Genetic Mechanisms of Disease Development and Progression*, S. M. Dehm and D. J. Tindall, Eds. Cham: Springer International Publishing, 2019, pp. 319–331. doi: 10.1007/978-3-030-32656-2_14.

- [10] B. S. Carver *et al.*, “Reciprocal Feedback Regulation of PI3K and Androgen Receptor Signaling in PTEN-Deficient Prostate Cancer,” *Cancer Cell*, vol. 19, no. 5, pp. 575–586, May 2011, doi: 10.1016/j.ccr.2011.04.008.
- [11] J. Yang, J. Nie, X. Ma, Y. Wei, Y. Peng, and X. Wei, “Targeting PI3K in cancer: mechanisms and advances in clinical trials,” *Mol. Cancer*, vol. 18, no. 1, p. 26, Feb. 2019, doi: 10.1186/s12943-019-0954-x.
- [12] Iksen, S. Pothongrisit, and V. Pongrakhananon, “Targeting the PI3K/AKT/mTOR Signaling Pathway in Lung Cancer: An Update Regarding Potential Drugs and Natural Products,” *Molecules*, vol. 26, no. 13, 2021, doi: 10.3390/molecules26134100.
- [13] M.-M. Georgescu, “PTEN Tumor Suppressor Network in PI3K-Akt Pathway Control,” *Genes Cancer*, vol. 1, no. 12, pp. 1170–1177, Dec. 2010, doi: 10.1177/1947601911407325.
- [14] J. Armenia *et al.*, “The long tail of oncogenic drivers in prostate cancer,” *Nat. Genet.*, vol. 50, no. 5, pp. 645–651, May 2018, doi: 10.1038/s41588-018-0078-z.
- [15] Y.-R. Lee, M. Chen, and P. P. Pandolfi, “The functions and regulation of the PTEN tumour suppressor: new modes and prospects,” *Nat. Rev. Mol. Cell Biol.*, vol. 19, no. 9, pp. 547–562, Sep. 2018, doi: 10.1038/s41580-018-0015-0.
- [16] A. Liu, Y. Zhu, W. Chen, G. Merlino, and Y. Yu, “PTEN Dual Lipid- and Protein-Phosphatase Function in Tumor Progression,” *Cancers*, vol. 14, no. 15, 2022, doi: 10.3390/cancers14153666.
- [17] C.-Y. Chen, J. Chen, L. He, and B. L. Stiles, “PTEN: Tumor Suppressor and Metabolic Regulator,” *Front. Endocrinol.*, vol. 9, p. 338, Jul. 2018, doi: 10.3389/fendo.2018.00338.

- [18] C. B. Knobbe, V. Lapin, A. Suzuki, and T. W. Mak, “The roles of PTEN in development, physiology and tumorigenesis in mouse models: a tissue-by-tissue survey,” *Oncogene*, vol. 27, no. 41, pp. 5398–5415, Sep. 2008, doi: 10.1038/onc.2008.238.
- [19] A. D. Cristofano, P. Kotsi, Y. F. Peng, C. Cordon-Cardo, K. B. Elkon, and P. P. Pandolfi, “Impaired Fas Response and Autoimmunity in *Pten*^{+/-} Mice,” *Science*, vol. 285, no. 5436, pp. 2122–2125, Sep. 1999, doi: 10.1126/science.285.5436.2122.
- [20] A. D. Cristofano, B. Pesce, C. Cordon-Cardo, and P. P. Pandolfi, “Pten is essential for embryonic development and tumour suppression,” *Nat. Genet.*, vol. 19, no. 4, pp. 348–355, Aug. 1998, doi: 10.1038/1235.
- [21] A. Alimonti *et al.*, “Subtle variations in Pten dose determine cancer susceptibility,” *Nat. Genet.*, vol. 42, no. 5, pp. 454–458, May 2010, doi: 10.1038/ng.556.
- [22] A. Ortega-Molina *et al.*, “Pten Positively Regulates Brown Adipose Function, Energy Expenditure, and Longevity,” *Cell Metab.*, vol. 15, no. 3, pp. 382–394, Mar. 2012, doi: 10.1016/j.cmet.2012.02.001.
- [23] A. H. Berger, A. G. Knudson, and P. P. Pandolfi, “A continuum model for tumour suppression,” *Nature*, vol. 476, no. 7359, pp. 163–169, Aug. 2011, doi: 10.1038/nature10275.
- [24] T. Tu, J. Chen, L. Chen, and B. L. Stiles, “Dual-Specific Protein and Lipid Phosphatase PTEN and Its Biological Functions,” *Cold Spring Harb. Perspect. Med.*, vol. 10, no. 1, p. a036301, Jan. 2020, doi: 10.1101/cshperspect.a036301.
- [25] T. Gu, Z. Zhang, J. Wang, J. Guo, W. H. Shen, and Y. Yin, “CREB Is a Novel Nuclear Target of PTEN Phosphatase,” *Cancer Res.*, vol. 71, no. 8, pp. 2821–2825, Apr. 2011, doi: 10.1158/0008-5472.CAN-10-3399.

- [26] M. Tamura, J. Gu, K. Matsumoto, S. Aota, R. Parsons, and K. M. Yamada, “Inhibition of Cell Migration, Spreading, and Focal Adhesions by Tumor Suppressor PTEN,” *Science*, vol. 280, no. 5369, pp. 1614–1617, Jun. 1998, doi: 10.1126/science.280.5369.1614.
- [27] H. Y. K. Yip *et al.*, “Control of Glucocorticoid Receptor Levels by PTEN Establishes a Failsafe Mechanism for Tumor Suppression,” *Mol. Cell*, vol. 80, no. 2, pp. 279–295.e8, Oct. 2020, doi: 10.1016/j.molcel.2020.09.027.
- [28] S. Zhang *et al.*, “Combating trastuzumab resistance by targeting SRC, a common node downstream of multiple resistance pathways,” *Nat. Med.*, vol. 17, no. 4, pp. 461–469, Apr. 2011, doi: 10.1038/nm.2309.
- [29] W. H. Shen *et al.*, “Essential role for nuclear PTEN in maintaining chromosomal integrity,” *Cell*, vol. 128, no. 1, pp. 157–170, Jan. 2007, doi: 10.1016/j.cell.2006.11.042.
- [30] O. Gimm *et al.*, “Differential nuclear and cytoplasmic expression of PTEN in normal thyroid tissue, and benign and malignant epithelial thyroid tumors,” *Am. J. Pathol.*, vol. 156, no. 5, pp. 1693–1700, May 2000, doi: 10.1016/S0002-9440(10)65040-7.
- [31] Y. Lindsay *et al.*, “Localization of agonist-sensitive PtdIns(3,4,5)P₃ reveals a nuclear pool that is insensitive to PTEN expression,” *J. Cell Sci.*, vol. 119, no. Pt 24, pp. 5160–5168, Dec. 2006, doi: 10.1242/jcs.000133.
- [32] J. Lyu *et al.*, “The protein phosphatase activity of PTEN is essential for regulating neural stem cell differentiation,” *Mol. Brain*, vol. 8, pp. 26–26, Apr. 2015, doi: 10.1186/s13041-015-0114-1.
- [33] A. Papa *et al.*, “Cancer-Associated PTEN Mutants Act in a Dominant-Negative Manner to Suppress PTEN Protein Function,” *Cell*, vol. 157, no. 3, pp. 595–610, Apr. 2014, doi: 10.1016/j.cell.2014.03.027.

- [34] M. Shimobayashi and M. N. Hall, “Making new contacts: the mTOR network in metabolism and signalling crosstalk,” *Nat. Rev. Mol. Cell Biol.*, vol. 15, no. 3, pp. 155–162, Mar. 2014, doi: 10.1038/nrm3757.
- [35] M. G. Vander Heiden, L. C. Cantley, and C. B. Thompson, “Understanding the Warburg Effect: The Metabolic Requirements of Cell Proliferation,” *Science*, vol. 324, no. 5930, pp. 1029–1033, May 2009, doi: 10.1126/science.1160809.
- [36] R. J. DeBerardinis *et al.*, “Beyond aerobic glycolysis: transformed cells can engage in glutamine metabolism that exceeds the requirement for protein and nucleotide synthesis,” *Proc. Natl. Acad. Sci. U. S. A.*, vol. 104, no. 49, pp. 19345–19350, Dec. 2007, doi: 10.1073/pnas.0709747104.
- [37] T. Jamsapishvili *et al.*, “Clinical implications of PTEN loss in prostate cancer,” *Nat. Rev. Urol.*, vol. 15, no. 4, pp. 222–234, Apr. 2018, doi: 10.1038/nrurol.2018.9.
- [38] R. Zoncu, A. Efeyan, and D. M. Sabatini, “mTOR: from growth signal integration to cancer, diabetes and ageing,” *Nat. Rev. Mol. Cell Biol.*, vol. 12, no. 1, pp. 21–35, Jan. 2011, doi: 10.1038/nrm3025.
- [39] L. Eguez *et al.*, “Full intracellular retention of GLUT4 requires AS160 Rab GTPase activating protein,” *Cell Metab.*, vol. 2, no. 4, pp. 263–272, Oct. 2005, doi: 10.1016/j.cmet.2005.09.005.
- [40] J. T. Wong *et al.*, “Pten (phosphatase and tensin homologue gene) haploinsufficiency promotes insulin hypersensitivity,” *Diabetologia*, vol. 50, no. 2, pp. 395–403, Feb. 2007, doi: 10.1007/s00125-006-0531-x.

- [41] M. Chen *et al.*, “An aberrant SREBP-dependent lipogenic program promotes metastatic prostate cancer,” *Nat. Genet.*, vol. 50, no. 2, pp. 206–218, Feb. 2018, doi: 10.1038/s41588-017-0027-2.
- [42] T. Porstmann *et al.*, “PKB/Akt induces transcription of enzymes involved in cholesterol and fatty acid biosynthesis via activation of SREBP,” *Oncogene*, vol. 24, no. 43, pp. 6465–6481, Sep. 2005, doi: 10.1038/sj.onc.1208802.
- [43] A. Zabala-Letona *et al.*, “Erratum: Corrigendum: mTORC1-dependent AMD1 regulation sustains polyamine metabolism in prostate cancer,” *Nature*, vol. 554, no. 7693, pp. 554–554, Feb. 2018, doi: 10.1038/nature25470.
- [44] Y. A. Hannun and L. M. Obeid, “Principles of bioactive lipid signalling: lessons from sphingolipids,” *Nat. Rev. Mol. Cell Biol.*, vol. 9, no. 2, pp. 139–150, Feb. 2008, doi: 10.1038/nrm2329.
- [45] B. Ogretmen, “Sphingolipid metabolism in cancer signalling and therapy,” *Nat. Rev. Cancer*, vol. 18, no. 1, pp. 33–50, Jan. 2018, doi: 10.1038/nrc.2017.96.
- [46] B. Ogretmen and Y. A. Hannun, “Biologically active sphingolipids in cancer pathogenesis and treatment,” *Nat. Rev. Cancer*, vol. 4, no. 8, pp. 604–616, Aug. 2004, doi: 10.1038/nrc1411.
- [47] K. A. Dressler, S. Mathias, and R. N. Kolesnick, “Tumor Necrosis Factor- α Activates the Sphingomyelin Signal Transduction Pathway in a Cell-Free System,” *Science*, vol. 255, no. 5052, pp. 1715–1718, Mar. 1992, doi: 10.1126/science.1313189.
- [48] C. Voelkel-Johnson, J. S. Norris, and S. White-Gilbertson, “Interdiction of Sphingolipid Metabolism Revisited: Focus on Prostate Cancer,” in *Advances in Cancer Research*, vol. 140, Elsevier, 2018, pp. 265–293. doi: 10.1016/bs.acr.2018.04.014.

- [49] A. H. Janneh and B. Ogretmen, “Targeting Sphingolipid Metabolism as a Therapeutic Strategy in Cancer Treatment,” *Cancers*, vol. 14, no. 9, p. 2183, Apr. 2022, doi: 10.3390/cancers14092183.
- [50] K. Huitema, J. van den Dikkenberg, J. F. H. M. Brouwers, and J. C. M. Holthuis, “Identification of a family of animal sphingomyelin synthases,” *EMBO J.*, vol. 23, no. 1, pp. 33–44, Jan. 2004, doi: 10.1038/sj.emboj.7600034.
- [51] D. S. Wijesinghe, N. F. Lamour, A. Gomez-Munoz, and C. E. Chalfant, “Ceramide Kinase and Ceramide-1-Phosphate,” in *Methods in Enzymology*, vol. 434, Elsevier, 2007, pp. 265–292. doi: 10.1016/S0076-6879(07)34015-9.
- [52] G. D’Angelo *et al.*, “Vesicular and non-vesicular transport feed distinct glycosylation pathways in the Golgi,” *Nature*, vol. 501, no. 7465, pp. 116–120, Sep. 2013, doi: 10.1038/nature12423.
- [53] P. Grbčić and M. Sedić, “Sphingosine 1-Phosphate Signaling and Metabolism in Chemoprevention and Chemoresistance in Colon Cancer,” *Molecules*, vol. 25, no. 10, p. 2436, May 2020, doi: 10.3390/molecules25102436.
- [54] W. Huang *et al.*, “Sphingosine-1-phosphate phosphatase 2 promotes disruption of mucosal integrity, and contributes to ulcerative colitis in mice and humans,” *FASEB J.*, vol. 30, no. 8, pp. 2945–2958, Aug. 2016, doi: 10.1096/fj.201600394R.
- [55] T. H. Beckham, J. C. Cheng, S. T. Marrison, J. S. Norris, and X. Liu, “Chapter One - Interdiction of Sphingolipid Metabolism to Improve Standard Cancer Therapies,” in *Advances in Cancer Research*, vol. 117, J. S. Norris, Ed. Academic Press, 2013, pp. 1–36. doi: 10.1016/B978-0-12-394274-6.00001-7.

- [56] M. Eto *et al.*, “C16 ceramide accumulates following androgen ablation in LNCaP prostate cancer cells,” *The Prostate*, vol. 57, no. 1, pp. 66–79, Sep. 2003, doi: 10.1002/pros.10275.
- [57] J. C. Cheng *et al.*, “Radiation-induced acid ceramidase confers prostate cancer resistance and tumor relapse,” *J. Clin. Invest.*, vol. 123, no. 10, pp. 4344–4358, Oct. 2013, doi: 10.1172/JCI64791.
- [58] A. E. Mahdy *et al.*, “Acid Ceramidase Upregulation in Prostate Cancer Cells Confers Resistance to Radiation: AC Inhibition, a Potential Radiosensitizer,” *Mol. Ther.*, vol. 17, no. 3, pp. 430–438, Mar. 2009, doi: 10.1038/mt.2008.281.
- [59] C. McNair *et al.*, “Cell cycle-coupled expansion of AR activity promotes cancer progression,” *Oncogene*, vol. 36, no. 12, pp. 1655–1668, Mar. 2017, doi: 10.1038/onc.2016.334.
- [60] T. H. Beckham, J. C. Cheng, P. Lu, S. T. Marrison, J. S. Norris, and X. Liu, “Acid Ceramidase Promotes Nuclear Export of PTEN through Sphingosine 1-Phosphate Mediated Akt Signaling,” *PLoS ONE*, vol. 8, no. 10, p. e76593, Oct. 2013, doi: 10.1371/journal.pone.0076593.
- [61] G. D’Angelo, S. Moorthi, and C. Luberto, “Chapter Three - Role and Function of Sphingomyelin Biosynthesis in the Development of Cancer,” in *Advances in Cancer Research*, vol. 140, C. E. Chalfant and P. B. Fisher, Eds. Academic Press, 2018, pp. 61–96. doi: 10.1016/bs.acr.2018.04.009.
- [62] M. A. Castanares *et al.*, “Characterization of a novel metastatic prostate cancer cell line of LNCaP origin: Characterization of JHU-LNCaP-SM,” *The Prostate*, vol. 76, no. 2, pp. 215–225, Feb. 2016, doi: 10.1002/pros.23115.

- [63] L. Bu *et al.*, “PTEN suppresses tumorigenesis by directly dephosphorylating Akt,” *Signal Transduct. Target. Ther.*, vol. 6, no. 1, p. 262, Jul. 2021, doi: 10.1038/s41392-021-00571-x.
- [64] Q. Jiang *et al.*, “S6K1-mediated phosphorylation of PDK1 impairs AKT kinase activity and oncogenic functions,” *Nat. Commun.*, vol. 13, no. 1, p. 1548, Mar. 2022, doi: 10.1038/s41467-022-28910-8.
- [65] L. Bu *et al.*, “PTEN suppresses tumorigenesis by directly dephosphorylating Akt,” *Signal Transduct. Target. Ther.*, vol. 6, no. 1, p. 262, Jul. 2021, doi: 10.1038/s41392-021-00571-x.
- [66] E. Haas and D. W. Stanley, “Phospholipase D,” in *xPharm: The Comprehensive Pharmacology Reference*, Elsevier, 2007, pp. 1–4. doi: 10.1016/B978-008055232-3.60544-6.
- [67] C. Delon *et al.*, “Sphingosine Kinase 1 Is an Intracellular Effector of Phosphatidic Acid,” *J. Biol. Chem.*, vol. 279, no. 43, pp. 44763–44774, Oct. 2004, doi: 10.1074/jbc.M405771200.
- [68] J. M. Gaesser and S. L. Fyffe-Maricich, “Intracellular signaling pathway regulation of myelination and remyelination in the CNS,” *Exp. Neurol.*, vol. 283, pp. 501–511, Sep. 2016, doi: 10.1016/j.expneurol.2016.03.008.
- [69] R. H. Q. Pierre Morell, “Characteristic Composition of Myelin,” in *Basic Neurochemistry: Molecular, Cellular and Medical Aspects*, 6th edition., 1999.
- [70] P. Mellor, L. Deibert, B. Calvert, K. Bonham, S. A. Carlsen, and D. H. Anderson, “CREB3L1 Is a Metastasis Suppressor That Represses Expression of Genes Regulating Metastasis, Invasion, and Angiogenesis,” *Mol. Cell. Biol.*, vol. 33, no. 24, pp. 4985–4995, Dec. 2013, doi: 10.1128/MCB.00959-13.

- [71] Z. Yan, Y. Hu, Y. Zhang, Q. Pu, L. Chu, and J. Liu, “Effects of endoplasmic reticulum stress-mediated CREB3L1 on apoptosis of glioma cells,” *Mol. Clin. Oncol.*, vol. 16, no. 4, p. 83, Feb. 2022, doi: 10.3892/mco.2022.2516.
- [72] T. B. Gungul, “Targeted metabolomics revealed a key metabolic reprogramming in cholesterol biosynthesis pathway upon PTEN re-expression in PTEN-null, metastatic and castration-resistant prostate cancer,” Master’s thesis, Bilkent University, Ankara, 2022.
- [73] C. Cai, D. C. Portnoy, H. Wang, X. Jiang, S. Chen, and S. P. Balk, “Androgen Receptor Expression in Prostate Cancer Cells Is Suppressed by Activation of Epidermal Growth Factor Receptor and ErbB2,” *Cancer Res.*, vol. 69, no. 12, pp. 5202–5209, Jun. 2009, doi: 10.1158/0008-5472.CAN-09-0026.
- [74] M. Sheridan and B. Ogretmen, “The Role of Ceramide Metabolism and Signaling in the Regulation of Mitophagy and Cancer Therapy,” *Cancers*, vol. 13, no. 10, p. 2475, May 2021, doi: 10.3390/cancers13102475.
- [75] L. Xue *et al.*, “Targeting SREBP-2-Regulated Mevalonate Metabolism for Cancer Therapy,” *Front. Oncol.*, vol. 10, p. 1510, Aug. 2020, doi: 10.3389/fonc.2020.01510.
- [76] Y. Zou, H. Zhang, F. Bi, Q. Tang, and H. Xu, “Targeting the key cholesterol biosynthesis enzyme squalene monooxygenase for cancer therapy,” *Front. Oncol.*, vol. 12, p. 938502, Aug. 2022, doi: 10.3389/fonc.2022.938502.
- [77] F. Chen and X. Zhao, “Prostate Cancer: Current Treatment and Prevention Strategies,” *Iran. Red Crescent Med. J.*, vol. 15, no. 4, pp. 279–284, Apr. 2013, doi: 10.5812/ircmj.6499.
- [78] C. Dai, H. Heemers, and N. Sharifi, “Androgen Signaling in Prostate Cancer,” *Cold Spring Harb. Perspect. Med.*, vol. 7, no. 9, p. a030452, Sep. 2017, doi: 10.1101/cshperspect.a030452.

- [79] E. C. Lien, C. A. Lyssiotis, and L. C. Cantley, “Metabolic Reprogramming by the PI3K-Akt-mTOR Pathway in Cancer,” in *Metabolism in Cancer*, vol. 207, T. Cramer and C. A. Schmitt, Eds. Cham: Springer International Publishing, 2016, pp. 39–72. doi: 10.1007/978-3-319-42118-6_3.
- [80] J. Wu, H. Gao, W. Ge, and J. He, “Over expression of PTEN induces apoptosis and prevents cell proliferation in breast cancer cells,” *Acta Biochim. Pol.*, Dec. 2020, doi: 10.18388/abp.2020_5371.
- [81] S. Sengupta, T. R. Peterson, and D. M. Sabatini, “Regulation of the mTOR Complex 1 Pathway by Nutrients, Growth Factors, and Stress,” *Mol. Cell*, vol. 40, no. 2, pp. 310–322, Oct. 2010, doi: 10.1016/j.molcel.2010.09.026.
- [82] L. Camacho, A. Ouro, A. Gomez-Larrauri, A. Carracedo, and A. Gomez-Muñoz, “Implication of Ceramide Kinase/C1P in Cancer Development and Progression,” *Cancers*, vol. 14, no. 1, p. 227, Jan. 2022, doi: 10.3390/cancers14010227.
- [83] L. Camacho *et al.*, “Identification of Androgen Receptor Metabolic Correlome Reveals the Repression of Ceramide Kinase by Androgens,” *Cancers*, vol. 13, no. 17, p. 4307, Aug. 2021, doi: 10.3390/cancers13174307.
- [84] H.-K. Lin, Y.-C. Hu, D. K. Lee, and C. Chang, “Regulation of Androgen Receptor Signaling by PTEN (Phosphatase and Tensin Homolog Deleted on Chromosome 10) Tumor Suppressor through Distinct Mechanisms in Prostate Cancer Cells,” *Mol. Endocrinol.*, vol. 18, no. 10, pp. 2409–2423, Oct. 2004, doi: 10.1210/me.2004-0117.
- [85] S. Asano *et al.*, “Regulation of Cell Migration by Sphingomyelin Synthases: Sphingomyelin in Lipid Rafts Decreases Responsiveness to Signaling by the CXCL12/CXCR4 Pathway,” *Mol. Cell. Biol.*, vol. 32, no. 16, pp. 3242–3252, Aug. 2012, doi: 10.1128/MCB.00121-12.

- [86] N. Qiao, L. Wang, T. Wang, and H. Li, “Inflammatory CXCL12-CXCR4/CXCR7 axis mediates G-protein signaling pathway to influence the invasion and migration of nasopharyngeal carcinoma cells,” *Tumor Biol.*, vol. 37, no. 6, pp. 8169–8179, Jun. 2016, doi: 10.1007/s13277-015-4686-2.
- [87] M. Kanehisa, M. Furumichi, Y. Sato, M. Kawashima, and M. Ishiguro-Watanabe, “KEGG for taxonomy-based analysis of pathways and genomes,” *Nucleic Acids Res.*, p. gkac963, Oct. 2022, doi: 10.1093/nar/gkac963.
- [88] V. Perotti *et al.*, “An actionable axis linking NFATc2 to EZH2 controls the EMT-like program of melanoma cells,” *Oncogene*, vol. 38, no. 22, pp. 4384–4396, May 2019, doi: 10.1038/s41388-019-0729-2.
- [89] K. R. Manda *et al.*, “NFATc1 promotes prostate tumorigenesis and overcomes PTEN loss-induced senescence,” *Oncogene*, vol. 35, no. 25, pp. 3282–3292, Jun. 2016, doi: 10.1038/onc.2015.389.
- [90] R. M. Allam *et al.*, “Fingolimod interrupts the cross talk between estrogen metabolism and sphingolipid metabolism within prostate cancer cells,” *Toxicol. Lett.*, vol. 291, pp. 77–85, Jul. 2018, doi: 10.1016/j.toxlet.2018.04.008.
- [91] C.-W. Chua *et al.*, “Suppression of Androgen-Independent Prostate Cancer Cell Aggressiveness by FTY720: Validating Runx2 as a Potential Antimetastatic Drug Screening Platform,” *Clin. Cancer Res.*, vol. 15, no. 13, pp. 4322–4335, Jul. 2009, doi: 10.1158/1078-0432.CCR-08-3157.
- [92] S. Permpongkosol *et al.*, “Anticarcinogenic effect of FTY720 in human prostate carcinoma DU145 cells: Modulation of mitogenic signaling, FAK, cell-cycle entry and apoptosis,” *Int. J. Cancer*, vol. 98, no. 2, pp. 167–172, Mar. 2002, doi: 10.1002/ijc.10178.

- [93] C. Zhou, M.-T. Ling, T. Kin-Wah Lee, K. Man, X. Wang, and Y.-C. Wong, “FTY720, a fungus metabolite, inhibits invasion ability of androgen-independent prostate cancer cells through inactivation of RhoA-GTPase,” *Cancer Lett.*, vol. 233, no. 1, pp. 36–47, Feb. 2006, doi: 10.1016/j.canlet.2005.02.039.
- [94] C. White, H. Alshaker, C. Cooper, M. Winkler, and D. Pchejetski, “The emerging role of FTY720 (Fingolimod) in cancer treatment,” *Oncotarget*, vol. 7, no. 17, pp. 23106–23127, Apr. 2016, doi: 10.18632/oncotarget.7145.
- [95] O. Kucuk *et al.*, “Phase II trial of opaganib in patients with metastatic castration-resistant prostate cancer progressing on abiraterone or enzalutamide (NCT04207255).,” *J. Clin. Oncol.*, vol. 39, no. 6_suppl, pp. TPS191–TPS191, Feb. 2021, doi: 10.1200/JCO.2021.39.6_suppl.TPS191.
- [96] M. Lai *et al.*, “Complete Acid Ceramidase ablation prevents cancer-initiating cell formation in melanoma cells,” *Sci. Rep.*, vol. 7, no. 1, p. 7411, Aug. 2017, doi: 10.1038/s41598-017-07606-w.

7. APPENDIX

7.1. COPYRIGHT PERMISSIONS

Copyrights for Figure 1.1:

SPRINGER NATURE LICENSE
TERMS AND CONDITIONS

Jan 03, 2023

This Agreement between Bilkent University -- Irmak Kaysudu ("You") and Springer Nature ("Springer Nature") consists of your license details and the terms and conditions provided by Springer Nature and Copyright Clearance Center.

License Number	5459290397143
License date	Dec 31, 2022
Licensed Content Publisher	Springer Nature
Licensed Content Publication	Nature Reviews Disease Primers
Licensed Content Title	Prostate cancer
Licensed Content Author	Richard J. Rebello et al
Licensed Content Date	Feb 4, 2021
Type of Use	Thesis/Dissertation
Requestor type	academic/university or research institute
Format	print and electronic
Portion	figures/tables/illustrations
Number of figures/tables/illustrations	1
High-res required	no
Will you be translating?	no
Circulation/distribution	1 - 29
Author of this Springer Nature content	no
Title	M.Sc. student
Institution name	Bilkent University
Expected presentation date	Jan 2023

Copyrights for Figure 1.4:

SPRINGER NATURE LICENSE
TERMS AND CONDITIONS

Jan 03, 2023

This Agreement between Bilkent University -- Irmak Kaysudu ("You") and Springer Nature ("Springer Nature") consists of your license details and the terms and conditions provided by Springer Nature and Copyright Clearance Center.

License Number	5459281000977
License date	Dec 31, 2022
Licensed Content Publisher	Springer Nature
Licensed Content Publication	Nature Reviews Urology
Licensed Content Title	Clinical implications of PTEN loss in prostate cancer
Licensed Content Author	Tamara Jamaspishvili et al
Licensed Content Date	Feb 20, 2018
Type of Use	Thesis/Dissertation
Requestor type	academic/university or research institute
Format	print and electronic
Portion	figures/tables/illustrations
Number of figures/tables/illustrations	1
High-res required	no
Will you be translating?	no
Circulation/distribution	1 - 29
Author of this Springer Nature content	no
Title	M.Sc. student
Institution name	Bilkent University
Expected presentation date	Jan 2023

Copyrights for Figure 1.2 and Figure 1.5:

“All MDPI journals are Open Access and subject to the Creative Commons Attribution License (CC BY). The CC BY permits unrestricted use, distribution, and reproduction of the material in any medium, even commercially, provided the original work is properly cited.

<https://creativecommons.org/licenses/by/4.0/>

<https://creativecommons.org/licenses/by/4.0/legalcode>”

Copyrights for Figure 1.3:

Permission is granted for the use of Fig 3, p.6 in the article detailed below for inclusion in this master's thesis only. Complete reference and copyright to Cold Spring Harbor Laboratory Press are included in the figure legend.

Name: Irmak Kaysudu
Company/Institution: Bilkent University
Library Address:
Library Address (line 2):
City:
State (US and Canada):
Country:
Zip:
Title: M.Sc. student
Lab/Department:
Phone:
Fax:
Email: irmakkaysudu@gmail.com
Title of Publication: Identification and targeting of deregulated metabolic pathways in metastatic prostate cancer cells
Authors/Editors: Taojian Tu, Jingyu Chen, Lulu Chen, Bangyan L. Stiles
Date of Publication: 2020
Publisher: Cold Spring Harbor Perspectives in Medicine
Title of CSHLP Journal/Book: Dual-specific Protein and Lipid Phosphatase PTEN and its Biological Functions
Title of Article/Chapter:
CSHL Authors/Editors:
Page Numbers: 6
Figure Numbers: 3
Figure Page Numbers:
Copyright Date:
Language:
Territory:
Format:
Additional comments:

ipaddress: 176.041.030.208
Default Footer
Default Footer - line2